

THE HABITABILITY OF PROXIMA CENTAURI B I: EVOLUTIONARY SCENARIOS

RORY BARNES^{1,2,3}, RUSSELL DEITRICK^{1,2}, RODRIGO LUGER^{1,2}, PETER E. DRISCOLL^{4,2}, THOMAS R. QUINN^{1,2}, DAVID P. FLEMING^{1,2}, BENJAMIN GUYER^{1,2}, DIEGO V. McDONALD^{1,2}, VICTORIA S. MEADOWS^{1,2}, GIADA ARNEY^{1,2}, DAVID CRISP^{5,2}, SHAWN D. DOMAGAL-GOLDMAN^{6,2}, DANIEL FOREMAN-MACKEY^{1,7}, NATHAN A. KAIB⁸, ANDREW LINCOWSKI^{1,2}, JACOB LUSTIG-YAEGER^{1,2}, EDDIE SCHWIETERMAN^{1,2}

Draft version March 7, 2018

ABSTRACT

We analyze the evolution of the potentially habitable planet Proxima Centauri b to identify environmental factors that affect its long-term habitability. We consider physical processes acting on size scales ranging from the galactic to the stellar system to the planet’s core. We find that there is a significant probability that Proxima Centauri has had encounters with its companion stars, Alpha Centauri A and B, that are close enough to destabilize an extended planetary system. If the system has an additional planet, as suggested by the discovery data, then it may perturb planet b’s eccentricity and inclination, possibly driving those parameters to non-zero values, even in the presence of strong tidal damping. We also model the internal evolution of the planet, evaluating the roles of different radiogenic abundances and tidal heating and find that magnetic field generation is likely for billions of years. We find that if planet b formed *in situ*, then it experienced 169 ± 13 million years in a runaway greenhouse as the star contracted during its formation. This early phase could remove up to 5 times as much water as in the modern Earth’s oceans, possibly producing a large abiotic oxygen atmosphere. On the other hand, if Proxima Centauri b formed with a substantial hydrogen atmosphere (0.01 – 1% of the planet’s mass), then this envelope could have shielded the water long enough for it to be retained before being blown off itself. After modeling this wide range of processes we conclude that water retention during the host star’s pre-main sequence phase is the biggest obstacle for Proxima b’s habitability. These results are all obtained with a new software package called `VPLANET`.

1. INTRODUCTION

The discovery of Proxima Centauri b, hereafter Proxima b, revealed the closest possible exoplanet and one of the most observationally accessible planets orbiting a late-type M dwarf host. Very little is currently known about Proxima b and its environment, but the planet is likely terrestrial and receives an incident flux that places it in the “habitable zone” (HZ) (Kasting et al. 1993; Selsis et al. 2007; Kopparapu et al. 2013). Although it does not transit (Kipping et al. 2017), its proximity and favorable star-planet contrast ratio make Proxima b an exciting target in the near term for phase curve observations with JWST (Turbet et al. 2016; Kreidberg & Loeb 2016; Meadows et al. 2018), and for early direct imaging characterization efforts, especially with ground-based Extremely Large Telescopes (Meadows et al. 2018). Modifications to instrumentation on the Very Large Telescope (VLT) may combine high-contrast imaging with high-resolution spectroscopy to enable the search for O₂ in Proxima b’s atmosphere in the next few years (Lovis

et al. 2017).

The interpretation of these spectra require a firm understanding of the history of Proxima b and its host system. Proxima b exists in an environment that is significantly different from Earth and has likely experienced different phenomena that could preclude or promote the development of life. When viewed across interstellar distances, biology is best understood as a planetary process: life is a global phenomenon that alters geochemical and photochemical processes (Lovelock 1965). Unambiguous spectroscopic indicators of life, *i.e.* biosignatures, can only be identified if the abiotic processes on a planet are understood – no single feature in a spectrum is a “smoking gun” for life. A robust detection of extraterrestrial life requires that all plausible non-biological sources for an observed spectral feature can be ruled out. This requirement is a tall order in light of the expected diversity of terrestrial exoplanets in the galaxy and the plethora of mechanisms capable of mimicking biosignatures (Schwieterman et al. 2016; Meadows 2017). With these challenges in mind, Proxima b may still offer the best opportunity to search for unequivocal signs of life beyond the Solar System.

In this study, we leverage the known (but sparse) data on Proxima b and its host system to predict the range of evolutionary pathways that the planet may have experienced. As we show below, many evolutionary histories are possible and depend on factors ranging from the cooling rate of b’s core to the orbital evolution of the stellar system through the Milky Way galaxy, and everything in between. The evolution of Proxima b, and by extension its potential habitability, depends on physical processes that tend to be studied by scientists from different fields,

¹ Astronomy Department, University of Washington, Box 951580, Seattle, WA 98195

² NASA Astrobiology Institute – Virtual Planetary Laboratory Lead Team, USA

³ E-mail: rory@astro.washington.edu

⁴ Department of Terrestrial Magnetism, Carnegie Institution for Science, Washington, DC

⁵ Jet Propulsion Laboratory, California Institute of Technology, M/S 183-501, 4800 Oak Grove Drive, Pasadena, CA 91109

⁶ Planetary Environments Laboratory, NASA Goddard Space Flight Center, 8800 Greenbelt Road, Greenbelt, MD 20771

⁷ NASA Sagan Fellow

⁸ Department of Physics and Astronomy, University of Oklahoma, 440 W. Brooks St, Norman, OK 73019

such as geophysics and astrophysics. However, for the purpose of interpreting Proxima b, these divisions must be overcome. A critical examination of the potential habitability of Proxima b necessitates a cohesive model that can fold in the impact of the many factors that shape its evolutionary history. Our examination of Proxima b will draw on simple, but realistic, models that have been developed in the fields of geophysics, planetary science, atmospheric science and astrophysics. From this synthesis, we identify numerous opportunities and obstacles for life to develop on Proxima b, as well as numerous possible uninhabitable states. These calculations lay a foundation for future interpretation of spectroscopic observations, which are explored in the companion paper (Meadows et al. 2018). Additionally, many of the principles described are relevant to any potentially habitable planet orbiting low mass stars, such as TRAPPIST-1 d–f (Gillon et al. 2017) and LHS 1140 b (Dittman et al. 2017).

This paper is organized as follows. In § 2 we review the observational data on the system and the immediate implications for habitability. In § 3 we describe models to simulate the evolution of the system, with a focus on habitability. In this section we introduce a new software package, *VPLANET*, which couples physical models of planetary interiors, atmospheres, spins and orbits, stellar evolution, and galactic effects. In § 4 we present results of these models. An exhaustive analysis of all histories is too large to present here, so we only present suites for phenomena that are well-constrained and/or have a large impact on habitability. In § 5 we discuss the results and identify additional observations that could improve modeling efforts and connect our results to the companion paper (Meadows et al. 2018). Finally, in § 6 we draw our conclusions.

2. OBSERVATIONAL CONSTRAINTS

In this section we review known features of the triple star system Alpha Centauri (hereafter α Cen) of which Proxima Centauri is likely a third member. This star system has been studied carefully for centuries as it is the closest to the Sun. We will first review the direct observational data, then we will make inferences from those data, and finally we qualitatively consider how these data constrain the possibility for life to exist on Proxima b, which guide the quantitative modeling described in the subsequent sections. Transit searches have failed to turn up definitive evidence of one (Kipping et al. 2017; Li et al. 2017; Liu et al. 2018).

2.1. Properties of the Proxima Planetary System

Very little data exist for Proxima b. The radial velocity data reveal a planet with a minimum mass m of $1.27 M_{\oplus}$, an orbital period P of 11.186 days, and an orbital eccentricity e less than 0.35 (Anglada-Escudé et al. 2016). Aside from the orbital phase, these data are the extent of the direct observational data on the planet, but even the minimum mass relies on uncertain estimates of the mass of the host star, described below.

Proxima b may not be the only planet orbiting Proxima Centauri. The Doppler data suggest the presence of another planetary mass companion with an orbital period near 215 days, but it is not definitive yet (Anglada-Escudé et al. 2016; Damasso & Del Sordo 2017). If

present, the second planet has a projected mass of $\lesssim 10 M_{\oplus}$, consistent with previous non-detections (Endl & Kürster 2008; Barnes et al. 2014; Lurie et al. 2014). Recent ALMA observations have revealed a dust disk located from $\sim 1\text{--}4$ AU (Anglada et al. 2017), which is significantly farther out than the putative second planet. The orbital eccentricity and its relative inclination to Proxima b’s orbit are also unknown, but as described below, could take any value that permits dynamical stability of planet b and the dust belt. Additionally, lower mass and/or more distant planetary companions could also be present in the system.

2.2. Properties of the Host Star

As Proxima Centauri is the closest star to the Sun, it has been studied extensively since its discovery 100 years ago (Innes 1915). It has a radius R_* of $0.14 R_{\odot}$, a temperature T_{eff} of 3050 K, a luminosity L_* of $0.00165 L_{\odot}$ (Demory et al. 2009; Boyajian et al. 2012), and a rotation period P_* of 83 days (Benedict et al. 1998). Anglada-Escudé et al. (2016) find a spectral type of M5.5V. Wood et al. (2001) searched for evidence of stellar winds, but found none, indicating mass loss rates \dot{M}_* less than 20% of our Sun’s, *i.e.* $< 4 \times 10^{-15} M_{\odot}/\text{yr}$. Proxima Centauri possesses a much larger magnetic field ($B \sim 600$ G) than our Sun ($B = 1$ G) (Reiners & Basri 2008), but somewhat low compared to the majority of low mass stars.

Like our Sun, Proxima Centauri’s luminosity varies slowly with time due to starspots (Benedict et al. 1993). HST observations of Proxima Centauri found variations up to 70 milli-magnitudes (mmag) in V (Benedict et al. 1998), which, if indicative of the bolometric luminosity (which is unlikely), corresponds to about a 17.5% variation, with a period of 83.5 days (*i.e.* the rotation period). Moreover, Benedict et al. (1998) found evidence for two discrete modes of variability, one lower amplitude mode ($\Delta V \sim 30$ mmag) with a period of ~ 42 days, and a larger amplitude mode ($\Delta V \sim 60$ mmag) with a period of 83 days. These periods are a factor of 2 apart, leading Benedict et al. (1998) to suggest that sometimes a large spot (or cluster of spots) is present on one hemisphere only, while at other times smaller spots exist on opposite hemispheres. Regardless, incident stellar radiation (“instellation”) variations of 17% could impact atmospheric evolution and surface conditions of a planet (the sun’s variation is of order 0.1% (Willson et al. 1981)).

Additionally, the magnetic field strength may vary with time. Cincunegui et al. (2007) monitored the Ca II H and K lines, which are indicators of chromospheric activity, as well as H α for 7 years and found modest evidence for a 442 day cycle in stellar activity. Their result has recently been corroborated by Wargelin et al. (2017), and modeled by Yadav et al. (2016). Although the strength of Proxima’s magnetic field at the orbit of planet b is uncertain, it could affect the stability of b’s atmosphere and potentially affect any putative life on b (Garraffo et al. 2016; Airapetian et al. 2017; Atri 2017).

Proxima Centauri is a known flare star (Shapley 1951)⁹ and indeed several flares were reported during the Pale

⁹ Although Shapley is the sole author of his 1951 manuscript, the bulk of the work was performed by two assistants, acknowledged only as Mrs. C.D. Boyd, and Mrs. V.M. Nail.

Red Dot campaign (Anglada-Escudé et al. 2016). Walker (1981) performed the first study of the frequency of flares as a function of energy, finding that high energy events ($\sim 10^{30}$ erg) occurred about once per day, while lower energy events ($\sim 10^{28}$ erg) occurred about once per hour. Numerous observational campaigns since then have continued to find flaring at about this frequency (Benedict et al. 1998; Anglada-Escudé et al. 2016; Davenport et al. 2016).

2.3. Properties of the Stellar System

Many of the properties of Proxima Centauri are inferred from its relationship to α Cen A and B, thus a discussion of the current knowledge of α Cen is warranted here. Proxima Centauri is $\sim 13,000$ AU from α Cen A and B, but all three have the same motion through the galaxy. The proper motion and radial velocity of the center of mass of α Cen A and B permit the calculation of the system’s velocity relative to the sun. Poveda et al. (1996) find the three velocities are $(U, V, W) = (-25, -2, 13)$ km/s for the center of mass. This velocity implies the system is currently moving in the general direction of the Sun, and is on a roughly circular orbit around the galaxy with an eccentricity of 0.07 (Allen & Herrera 1998).

A recent, careful analysis of astrometric and HARPS RV data by Pourbaix & Boffin (2016) found the masses of the two stars to be 1.133 and 0.972 M_{\odot} , respectively, with an orbital eccentricity of 0.52 and a period of 79.91 years. The similarities between both A and B and the Sun, as well as their low apparent magnitudes, has allowed detailed studies of their spectral and photometric properties. These two stars (as well as Proxima) form a foundation in stellar astrophysics, and hence a great deal is known about A and B. However, as we describe below, many uncertainties still remain regarding these two stars.

The spectra of α Cen A and B provide information about the stellar temperature, gravitational acceleration in the photosphere, rotation rate, and chemical composition. That these features can be measured turns out to be critical for our analysis of the evolution of Proxima b. Proxima Centauri is a low mass star with strong molecular absorption lines and non-local thermal equilibrium effects, which make it extraordinarily difficult to identify elemental abundances; its composition is far more difficult to measure than for G and K dwarfs like α Cen A and B (Johnson & Apps 2009). Recently, Hinkel & Kane (2013) completed a reanalysis of published compositional studies, rejecting the studies of Laird (1985) and Neuforge-Verheecke & Magain (1997) because they were too different from the other 5 they considered. Hinkel & Kane (2013) found the mean metallicity [Fe/H] of each of the two stars to be +0.28 and +0.31 and with a large spread of 0.16 and 0.11, respectively. While it is frustrating that different groups have arrived at significantly different iron abundances, it is certain the stars are more metal-rich than the Sun.

Hinkel & Kane (2013) go on to examine 21 other elements, including C, O, Mg, Al, Si, Ca, and Eu. These elements can be important for the bulk composition and/or are tracers of other species that are relevant to planetary processes. In nearly all cases, the relative abundance of these elements to Fe is statistically indistinguishable from the solar ratios. Exceptions are Na, Zn and Eu in

α Cen A, and V, Zn, Ba and Nd in α Cen B. The discrepancies between the two stars is somewhat surprising given their likely birth from the same molecular cloud. On the other hand, the high eccentricity of their orbit could point toward a capture during the open cluster phase (*e.g.* Malmberg et al. 2007). For all elements beside Eu, the elemental abundances relative to Fe are larger than in the Sun. In particular, it seems likely that the stars are significantly enriched in Zn.

α Cen A and B are large and bright enough for asteroseismic studies that can reveal physical properties and ages of stars to a few percent, for high enough quality data (Chaplin et al. 2014). Indeed, these two stars are central to the field of asteroseismology, and have been studied in exquisite detail (*e.g.* Bouchy & Carrier 2001, 2002). However, significant uncertainties persist in our understanding of these stars, despite all the observational advantages.

A recent study undertook a comprehensive Bayesian analysis of α Cen A with priors on radius, composition, and mass derived from interferometric, spectroscopic and astrometric measurements, respectively (Bazot et al. 2016). Their adopted metallicity constraint comes from Neuforge-Verheecke & Magain (1997) via Thoul et al. (2003), which was rejected by the Hinkel & Kane (2013) analysis. They also used an older mass measurement from Pourbaix et al. (2002), which is slightly smaller than the updated mass from Pourbaix & Boffin (2016). They then used an asteroseismic code to determine the physical characteristics of A. Although the mass of A is similar to the Sun at 1.1 M_{\odot} , the simulations of Bazot et al. (2016) found that α Cen A’s core lies at the radiative/convective boundary and the transition between pp- and CNO-dominated energy production chains in the core. Previous results found the age of α Cen A to be 4.85 Gyr with a convective core (Thévenin et al. 2002), or 6.41 Gyr without a convective core (Thoul et al. 2003). The ambiguity is further increased by uncertainty in the efficiency of the $^{14}\text{N}(p,\gamma)^{15}\text{O}$ reaction rate in the CNO cycle, and by the possibility of convective overshooting of hydrogen into the core. They also consider the role of “microscopic diffusion,” the settling of heavy elements over long time intervals. All these uncertainties prevent a precise and accurate measurement of α Cen A’s age. Combining the different model predictions and including 1σ uncertainties, the age of α Cen A is likely to be between 3.4 and 5.9 Gyr, with a mean of 4.78 Gyr.

α Cen B has also been studied via asteroseismology, but as with A, the results have not been consistent. Lundkvist et al. (2014) find a nominal age of 1.5 Gyr with “Asteroseismology Made Easy,” but with uncertainties in excess of 4 Gyr. The asteroseismic oscillations on B are much smaller than on A, which make analyses more difficult (*see, e.g., Carrier & Bourban 2003*), leading to the large uncertainty. Combining studies of A and B, we must conclude that the ages of the two stars are uncertain by at least 25%. Given the difficulty in measuring B’s asteroseismic pulsations, we will rely on A’s asteroseismic data and assume the age of A and B (and Proxima) to be $4.8_{-1.4}^{+1.1}$ Gyr.

2.4. Inferences from the Observational Data

Because Proxima b was discovered indirectly, its properties and evolution depend critically on our knowledge of the host star’s properties. Although many properties of Proxima Centauri are known, the mass M_{Prox} , age, and composition are not. The spectra and luminosity suggest the mass of Proxima is $\sim 0.12 M_{\odot}$ (Delfosse et al. 2000). If we adopt this value, then the semi-major axis of b’s orbit is 0.0485 AU and the planet receives 65% of the instellation Earth receives from the Sun (Anglada-Escudé et al. 2016). Note that Sahu et al. (2014) suggested that Proxima’s proper motion sent it close enough to two background stars for the general relativistic deflection of their light by Proxima to be detectable with HST and should allow the determination of M_{Prox} to better than 10%, but those results are not yet available.

Additional inferences rely on the assumption that Proxima formed with the α Cen binary. The similarities in the proper motion and parallax between Proxima and α Cen immediately led to speculation as to whether the stars are “physically connected or members of the same drift” (Voûte 1917), *i.e.* are they bound or members of a moving group? If Proxima is just a random star in the solar neighborhood, Matthews & Gilmore (1993) concluded that the probability that Proxima would appear so close to α Cen is about 1 in a million, suggesting it is very likely the stars are somehow associated with each other. Using updated kinematic information, Anosova et al. (1994) concluded that Proxima is not bound, but instead part of a moving group consisting of about a dozen stellar systems. Wertheimer & Laughlin (2006)’s reanalysis found that the observational data favor a configuration that is at the boundary between bound and unbound orbits. However, their best fit bound orbit is implausibly large as the semi-major axis is 1.31 pc, *i.e.* larger than the distance from Earth to Proxima. Matvienko & Orlov (2014) also failed to unequivocally resolve the issue, and concluded that RV precision of better than 20 m/s is required to determine if Proxima is bound, which should be available in the data from Anglada-Escudé et al. (2016). Most recently, Kervella et al. (2017) improved upon previous RV measurements and found a probability of 4×10^{-8} that Proxima is *not* gravitationally bound to α Cen, and obtained a reasonable best fit orbit ($a = 8700_{-0.4}^{+0.7}$ AU, $e = 0.5_{-0.09}^{+0.08}$), and that Proxima is currently near apoastron.

Regardless of whether or not Proxima is bound to α Cen, the very low probability that the stars would be so close to each other strongly supports the hypothesis that the stars formed in the same star cluster. We will assume that they are associated and have approximately equal ages and similar compositions. An age near 5 Gyr for Proxima is also consistent with its slow rotation period and relatively modest activity levels and magnetic field (Reiners & Basri 2008).

Planet formation around M dwarfs is still relatively understudied. Few observations of disks of M dwarfs exist (*e.g.* Hernández et al. 2007; Williams & Cieza 2011; Luhman 2012; Downes et al. 2015), but these data point to a wide range of lifetimes for the gaseous disks of 1–15 Myr. This timescale is likely longer than the time to form terrestrial planets in the HZs of late M dwarfs (Raymond et al. 2007; Lissauer 2007), and hence Proxima b may

have been fully formed before the disk dispersed. For Proxima, the lifetime of the protoplanetary disk is unknown, and could have been altered by the presence of α Cen A and B, so any formation pathway or evolutionary process permitted within this constraint is plausible (Coleman et al. 2017; Alibert & Benz 2017).

The radial velocity data combined with M_{Prox} only provide a minimum mass for the planet, but significantly larger planet masses are geometrically unlikely, and very large masses can be excluded because they would incite detectable astrometric signals (note that the minimum mass solution predicts an astrometric orbit of the star of ~ 1 microsecond of arc), or would be detectable via direct imaging (Mesa et al. 2017). Assuming the probability distribution of Proxima b’s orbital plane is isotropic, there is a 50% chance that its mass is $< 2.84 M_{\oplus}$ (Luger et al. 2017). Bixel & Apai (2017) convolve planet occurrence rates for M dwarfs and mass-radius relationships from *Kepler* (Dressing & Charbonneau 2013; Weiss & Marcy 2014; Rogers 2015) to arrive at mass and radius estimates of $1.63_{-0.72}^{+1.66} M_{\oplus}$ and $1.07_{-0.31}^{+0.38} R_{\oplus}$, respectively, and that there is at least an 80% probability the planet is rocky. However, even at the minimum mass, we cannot exclude the possibility that Proxima b possesses a significant hydrogen envelope, and is better described as a “mini-Neptune,” which is unlikely to be habitable (but see Pierrehumbert & Gaidos 2011).

If non-gaseous, the composition is still highly uncertain and depends on the unknown formation process. Several possibilities exist according to recent theoretical studies: 1) the planet formed *in situ* from local material; 2) the planet formed at a larger semi-major axis and migrated in while Proxima still possessed a protoplanetary disk; or 3) an instability in the system occurred that impulsively changed b’s orbit. For case 1, the planet may be depleted in volatile material (Raymond et al. 2007; Lissauer 2007; Coleman et al. 2017), but could still initially possess a significant water reservoir (Ciesla et al. 2015; Mulders et al. 2015; Alibert & Benz 2017). For case 2, the planet would have likely formed beyond the snow line and hence could initially be very water-rich (Carter-Bond et al. 2012). Such a formation-then-migration scenario may be likely as previous studies of *in situ* planet formation about M dwarfs have found it is difficult to form Earth-mass and greater planets (Raymond et al. 2007). For case 3, the planet could be formed either volatile-rich or poor depending on its initial formation location as well as the details of the instability, such as the frequency of impacts that occurred in its aftermath. We conclude that all options are possible given the data and for simplicity will assume the planet is Earth-like in composition. If we adopt the minimum mass from Anglada-Escudé et al. (2016) as a fiducial, the silicate planet scaling law of Sotin et al. (2007), and then the radius of a $1.27 M_{\oplus}$ planet is $1.07 R_{\oplus}$, assumptions consistent with Bixel & Apai (2017).

2.5. Implications for Proxima b’s Evolution and Habitability

Given the above observations and their immediate implications, this planet may be able to support life. All life on Earth requires three basic ingredients: Water, energy, and the bioessential elements C, H, O, N, S and

P. Additionally, these ingredients must be present in an environment that is stable in terms of temperature, pressure, and pH for long periods of time. Proxima b clearly receives significant energy from its host star, and the bioessential elements are some of the most common in the galaxy. Thus, we assume that liquid water is the limiting factor for Proxima b to be habitable, and we adopt a working definition of “habitable” to be that the planet has liquid surface water.

Proxima’s luminosity and effective temperature combined with b’s orbital semi-major axis place the planet in the HZ of Proxima and nearly in the same relative position of Earth in the Sun’s HZ in terms of instellation. Specifically, the planet receives about 65% of Earth’s instellation, which, due to the redder spectrum of Proxima, places b comfortably in the “conservative” HZ of Kopparapu et al. (2013). Even allowing for observational uncertainties, Anglada-Escudé et al. (2016) find that the planet is in this conservative HZ.

However, its habitability depends on many more factors than just the instellation. The planet must form with sufficient water and maintain it over the course of the system’s age. Additionally, even if water is present, the evolution and potential habitability of Proxima b depends on many other factors involving stellar effects, the planet’s internal properties, and the gravitational influence of the other members of the stellar system.

The host star is about 10 times smaller and less massive than the Sun, the temperature is about half that of the Sun, and the luminosity is just 0.1% that of the Sun. These differences are significant and can have a profound effect on the evolution of Proxima b. Low mass stars can take billions of years to begin fusing hydrogen into helium in their cores, and the star’s luminosity can change dramatically during that time. Specifically, the star contracts at roughly constant temperature and so the star’s luminosity drops with time. For the case of Proxima, this stage lasted ~ 1 Gyr (Baraffe et al. 2015) and hence Proxima b could have spent significant time interior to the HZ. This “pre-main sequence” (pre-MS) phase could either strip away a primordial hydrogen atmosphere to reveal a “habitable evaporated core” (Luger et al. 2015), or, if b formed as a terrestrial planet with abundant water, it could desiccate that planet during an early runaway greenhouse phase and build up an oxygen-dominated atmosphere (Luger & Barnes 2015). Thus, the large early luminosity of the star could either help or hinder b’s habitability.

Low mass stars also show significant activity, *i.e.* flares, coronal mass ejections, and bursts of high energy radiation (*e.g.* West et al. 2008). This activity can change the composition of the atmosphere through photochemistry, or even completely strip the atmosphere away (Raymond et al. 2008). The tight orbit of Proxima b places it at risk of atmospheric stripping by these phenomena. A planetary magnetic field could increase the probability of atmospheric retention by deflecting charged particles, or it could decrease it by funneling high energy particles into the magnetic poles and provide enough energy to drive atmospheric escape (Strangeway et al. 2010). Either way, knowledge of the frequency of flaring and other high energy events, as well as of the likelihood that Proxima b possesses a magnetic field, would be invaluable information in assessing the longevity of Proxima

b’s atmosphere.

The close-in orbit also introduces the possibility that tidal effects are significant on the planet. Tides can affect the planet in five ways. First, they could cause the rotation rate to evolve to a frequency that is equal to or similar to the orbital frequency, a process typically called tidal locking (Dole 1964; Kasting et al. 1993; Barnes 2017), or into a spin-orbit resonance or other super-synchronous state (Ribas et al. 2016; Zanazzi & Lai 2017). Second, they can drive the planet’s obliquity ψ to zero or 180° , such that the planet has no seasons (Heller et al. 2011). Third, they can cause the orbital eccentricity to change, usually (but not always) driving the orbit toward a circular shape (Darwin 1880; Ferraz-Mello et al. 2008; Barnes 2017). Fourth, they can cause frictional heating in the interior, known as tidal heating (Peale et al. 1979; Jackson et al. 2008a; Barnes et al. 2013). Finally, they can cause the semi-major axis to decay as orbital energy is transformed into frictional heat, possibly pulling a planet out of the HZ (Barnes et al. 2008). Except in extreme cases, these processes are unlikely to sterilize a planet, but they can profoundly affect the planet’s evolution (Driscoll & Barnes 2015).

Many researchers have concluded that tidally locked planets of M dwarfs are unlikely to support life because their atmospheres would freeze out on the dark side (Kasting et al. 1993). However, numerous follow-up calculations have shown that tidal locking is not likely to result in uninhabitable planets (Joshi et al. 1997; Pierrehumbert 2011; Wordsworth et al. 2011; Yang et al. 2013; Shields et al. 2016; Kopparapu et al. 2016). These models all find that winds are able to transport heat to the back side of the planet for atmospheres larger than about 0.3 bars. Even below 0.3 bar, it may be possible for ocean currents to transport sufficient energy to ameliorate the temperature difference (Yang et al. 2014). In fact, synchronous rotation may actually allow habitable planets to exist closer to the host star because cloud coverage develops at the sub-stellar point and increases the planetary albedo (Yang et al. 2013). Thus, tidal locking may increase a planet’s potential to support life. Turbet et al. (2016) find with 3-D models that Proxima b could be habitable regardless of its current spin state.

Although the abundances of elements relative to iron in α Cen A and B, and, by assumption Proxima, are similar to the Sun’s, there is no guarantee that the abundance pattern is matched in Proxima b. Planet formation is often a stochastic process and composition depends on the impact history of a given world. The planet could have formed near its current location, which would have been relatively hot early on and the planet could be relatively depleted in volatiles (Raymond et al. 2007; Mulders et al. 2015). These studies may even overestimate volatile abundances as they ignored the high luminosities that late M dwarfs have during planet formation. Alternatively, the planet could have formed beyond the snow line and migrated in either while the gas disk was still present, or later during a large scale dynamical instability. In those cases, the planet could be volatile-rich.

If the abundances of Proxima are indeed similar to α Cen A and B, then the depletion of Eu in α Cen A is of note as it is often a tracer of radioactive material like ^{232}Th and ^{238}U (Young et al. 2014). These isotopes are primary drivers of the internal energy of Earth, and

hence if they are depleted in Proxima b, its internal evolution could be markedly different than Earth’s. However, since no depletion is observed in α Cen B, it is far from clear that such a depletion exists. One interesting radiogenic possibility is that the planet formed within 1 Myr (Raymond et al. 2007), then ^{26}Al could still provide energy to the planet’s interior, possibly altering the planet’s thermal evolution. Hence any prediction of b’s evolution should also consider its role.

The presence of additional planets can change the orbit and obliquity of planet b through gravitational perturbations. These interactions can change the orbital angular momentum of b and drive oscillations in the eccentricity e , the inclination i , longitude of periastron ϖ , and longitude of ascending node Ω . Changes in inclination can lead to changes in ψ as the planet’s rotational axis is likely fixed in inertial space, except for precession caused by the stellar torque, while the orbital plane precesses. These variations can significantly affect climate evolution and possibly even the planet’s potential to support life (Armstrong et al. 2014).

If Proxima is bound to α Cen A and B, then perturbations by passing stars and torques by the galactic tide can cause drifts in Proxima’s orbit about A and B (Kaib et al. 2013). During epochs of high eccentricity, Proxima may swoop so close to A and B that their gravity is able to disrupt Proxima’s planetary system. This could have occurred at any time in Proxima’s past and can lead to a total rearrangement of the system. Thus, should additional planets exist in the Proxima planetary system, these could be present on almost any orbit consistent with the dust ring, possibly with large eccentricities and large mutual inclinations relative to b’s orbital plane (e.g. Barnes et al. 2011). The dust ring could even be a result of a recent collision between bodies orbiting Proxima that were destabilized by a recent encounter between Proxima and α Cen A and B.

The inferred metallicity of Proxima Centauri is quite high for the solar neighborhood, which has a mean of -0.11 and standard deviation of 0.18 (Allende Prieto et al. 2004). Indeed, recent simulations of stellar metallicity distributions in the galaxy find that at the sun’s galactic radius R_{gal} of ~ 8 kpc, stars cannot form with $[\text{Fe}/\text{H}] > +0.15$ (Loebman et al. 2016). The discrepancy can be resolved by invoking radial migration (Sellwood & Binney 2002), in which stars on nearly circular orbits are able to ride corotation resonances with spiral arms either inward and outward. Loebman et al. (2016) find that with migration, the metallicity distribution of stars in the Sloan Digital Sky Survey III’s Apache Point Observatory Galactic Evolution Experiment (Hayden et al. 2015) is reproduced. Furthermore, Loebman et al. find that stars in the solar neighborhood with $[\text{Fe}/\text{H}] > +0.25$ must have formed at $R_{gal} < 4.5$ kpc. Similar conclusions were reached in an analysis of the RAVE survey by Kor-dopatis et al. (2015). We conclude that this system has migrated outward at least 3.5 kpc, but probably more. As the surface density scale length of the galaxy is ~ 2.5 kpc, this implies that the density of stars at their formation radius was at least 5 times higher than at the Sun’s current Galactic radius.

The observed and inferred constraints for the evolution of Proxima b are numerous, and the plausible range of evolutionary pathways is diverse. The proximity of two

solar-type stars complicates the dynamics, but allows the extension of their properties to Proxima Centauri. In the next sections we apply quantitative models of the processes described in this section to the full stellar system in order to explore the possible histories of Proxima b in detail. The outcomes of these histories serve as a foundation for the modeling efforts in Paper II (Meadows et al. 2018).

3. MODELS

In this section we describe the models we use to consider the evolution and potential habitability of Proxima b. We generally use published models that are common in different disciplines of science. Although the models come from disparate sources, we have compiled them all into a new software program called `VPLANET`. This code is designed to simulate planetary system evolution, with a focus on habitability. The problem of habitability is interdisciplinary, but we find it convenient to break the problem down into more manageable chunks, which we call “modules,” which are incorporated when applicable. At this time, `VPLANET` consists of simple models that are all representable as sets of ordinary differential equations. Below we describe qualitatively the modules and direct the reader to the references for the quantitative description. We then briefly describe how `VPLANET` unifies these modules and integrates the system forward.

3.1. Stellar Evolution: *STELLAR*

Of the many stellar evolutionary tracks available in the literature (e.g. Baraffe et al. 1998; Dotter et al. 2008; Baraffe et al. 2015), we find that the Yonsei-Yale tracks for low-mass stars (Spada et al. 2013) provide the best match to the stellar parameters of Proxima Centauri. We selected the $[\text{Fe}/\text{H}] = +0.3$ track with mixing length parameter $\alpha_{\text{MLT}} = 1.0$ and linearly interpolated between the $0.1 M_{\odot}$ and $0.15 M_{\odot}$ tracks to obtain a track at $M_{\text{Prox}} = 0.12 M_{\odot}$. While these choices yield a present-day radius within 1σ of $0.1410 \pm 0.0070 R_{\odot}$ (Demory et al. 2009; Boyajian et al. 2012), the model predicts a luminosity L_{\star} at $t = 4.78$ Gyr that is $\sim 20\%$ higher than the value reported in Demory et al. (2009) (a $\sim 2.2\sigma$ discrepancy). Such a discrepancy is not unexpected, given both the inaccuracies in the evolutionary models for low mass stars and the large intrinsic scatter of the luminosity and radius of M dwarfs at fixed mass and metallicity, likely due to unmodeled magnetic effects (Spada et al. 2013). Moreover, the large uncertainties in the age, mass, and metallicity of Proxima Centauri (§2) further contribute to the inconsistency.

Nevertheless, since we are concerned with the present-day habitability of Proxima b, it is imperative that our model match the present-day luminosity of its star. We therefore scale the Yonsei-Yale luminosity track down to match the observed value, adjusting the evolution of the effective temperature to be consistent with the radius evolution (which we do not change). We note that this choice results in a *lower* luminosity for Proxima Centauri at all ages, which yields conservative results (“optimistic” in terms of habitability) for the total amount of water lost from the planet (§4.4). Moreover, this adjustment likely has a smaller effect on our results than the large uncertainties on the properties of the star and the planet.

We also model the fiducial evolution of the XUV luminosity of the star as in Luger & Barnes (2015). We use the power-law of Ribas et al. (2005) with power law exponent $\beta = -1.23$, a saturation fraction $L_{\text{xuv}}/L_{\text{bol}} = 10^{-3}$ and a saturation time of 1 Gyr. These choices yield a good match to the present-day value, $L_{\text{xuv}}/L_{\text{bol}} = 2.83 \times 10^{-4}$ (Boyajian et al. 2012).

We use the fiducial L_{\star} and L_{xuv} evolution tracks discussed above to obtain the evolution of Proxima b’s water content (§3.2). Although this procedure yields the maximum likelihood estimate of the planet’s present-day water content conditioned on our assumptions, the large uncertainties associated with each of the parameters in our model result in even larger uncertainties on our result. To account for this, we run a suite of Markov Chain Monte Carlo (MCMC) simulations conditioned on the observational uncertainties associated with the model parameters to derive posterior probability distributions for Proxima b’s water content and other quantities of interest. We discuss this procedure in detail in §4.4.

In Fig. 1 we plot the evolution of the stellar luminosity, XUV luminosity, and radius as a function of time from $t_0 = 1$ Myr to the mean system age of 4.78 Gyr. We show the mean tracks (solid red lines) along with 100 samples randomly drawn from the posterior distributions of our MCMC runs (black lines). The present-day values are indicated by the dashed red lines, with 1σ uncertainties shaded. Note the long (~ 1 Gyr) pre-MS phase studied by Luger & Barnes (2015), and the high XUV luminosity during the first several 100 Myr.

3.2. Atmospheric Escape: *ATMESC*

We model atmospheric escape under the energy-limited (Watson et al. 1981; Erkaev et al. 2007) and diffusion-limited (Hunten 1973) parameterizations, closely following Luger et al. (2015) and Luger & Barnes (2015). We refer the reader to those papers for a detailed description of the equations and methodology. In this section we outline the main adaptations and improvements to the models therein.

We model both the escape of hydrogen from a putative thin primordial envelope and the escape of hydrogen and oxygen from photolysis of water during an early runaway greenhouse. As in Luger & Barnes (2015), we set water escape rates to zero once the planet enters the HZ, since the establishment of a cold trap should limit the availability of water in the upper atmosphere. We further assume that if Proxima b forms with a hydrogen envelope, it must be completely lost before water can escape, given the expected large diffusive separation between light H atoms and heavy H_2O molecules. We shut off hydrodynamic escape at 1 Gyr, the approximate time at which the star reaches the main sequence, to account for the transition to ballistic escape predicted by Owen & Mohanty (2016). We assume fiducial XUV escape efficiencies ϵ_{xuv} for hydrogen and water of 0.15 but also consider values ranging down to 0.01. Finally, for hydrogen-rich cases, we use the radius evolution tracks for super-Earths of Lopez et al. (2012) and Lopez & Fortney (2014); when no envelope is present, we use the terrestrial mass-radius relation of Sotin et al. (2007) to compute the planet’s radius.

The rate of escape of a steam atmosphere closely de-

pends on the fate of photolytically-produced oxygen. We compute the hydrodynamic drag on oxygen atoms using the formalism of Hunten et al. (1987) to obtain oxygen escape rates, tracking the buildup of O_2 in the atmosphere. As in Tian (2015) and Schaefer et al. (2016), we account for the increasing mixing ratio of O_2 at the base of the hydrodynamic flow, which slows the escape of hydrogen. Tian (2015) finds that as oxygen becomes the dominant species in the upper atmosphere, the Hunten et al. (1987) formalism predicts that an oxygen-dominated flow can rapidly lead to the loss of all O_2 from planets around M dwarfs. However, because an oxygen atom’s mass, m_{O} , is larger than a hydrogen’s, m_{H} , hydrodynamic oxygen-dominated escape requires exospheric temperatures $\sim m_{\text{O}}/m_{\text{H}} = 16$ times higher than that for a hydrogen-dominated flow, which is probably unrealistic for Proxima b. Following the prescription of Schaefer et al. (2016), we therefore shut off oxygen escape once its mixing ratio exceeds $X_{\text{O}} = 0.6$, switching to the diffusion-limited escape rate of hydrogen. Finally, as in Luger & Barnes (2015), we also consider the scenario in which sinks at the surface are efficient enough to remove O_2 from the atmosphere at the rate at which it is produced, resulting in an atmosphere that never builds up substantial amounts of oxygen. Recently, Schaefer et al. (2016) used a magma ocean model to calculate the rate of O_2 absorption by the surface, showing that final atmospheric O_2 pressures may range from zero to hundreds or even thousands of bars for the hot Earth GJ 1132b. Our two scenarios (no O_2 sinks and efficient O_2 sinks) should therefore bracket the atmospheric evolution of Proxima b.

We caution, finally, that the energy-limited formalism we adopt here is a very approximate description of the escape of an atmosphere to space. The heating of the upper atmosphere that drives hydrodynamic escape is strongly wavelength dependent and varies with both the composition and the temperature structure of the atmosphere. Moreover, line cooling mechanisms such as recombination radiation scale nonlinearly with the incident flux. Nonthermal escape processes, such as those controlled by magnetic fields, flares, and/or coronal mass ejections, lead to further departures from the simple one-dimensional energy-limited escape rate. Nevertheless, several studies show that for small planets the escape rate does indeed scale with the stellar XUV flux and inversely with the gravitational potential energy of the gas (e.g., Lopez et al. 2012; Lammer et al. 2013; Owen & Wu 2013, 2017) and that $\epsilon_{\text{xuv}} \approx 0.1$ is a reasonable median value that predicts the correct escape fluxes within a factor of a few. Since presently we have no information about Proxima b’s atmospheric composition, we choose to employ the energy-limited approximation and fold all of our uncertainty regarding the physics of the escape process into the XUV escape efficiency ϵ_{xuv} , which we vary between 0.01 and 0.15. This is roughly the range of escape efficiencies predicted by Bolmont et al. (2017) for the XUV fluxes received by Proxima b between its formation and the present day and should thus bracket reasonable escape rates for Proxima b.

3.3. Tidal Evolution: *EQTIDE*

To model the tidal evolution of the Proxima system, we will use a simple, but commonly-used model called

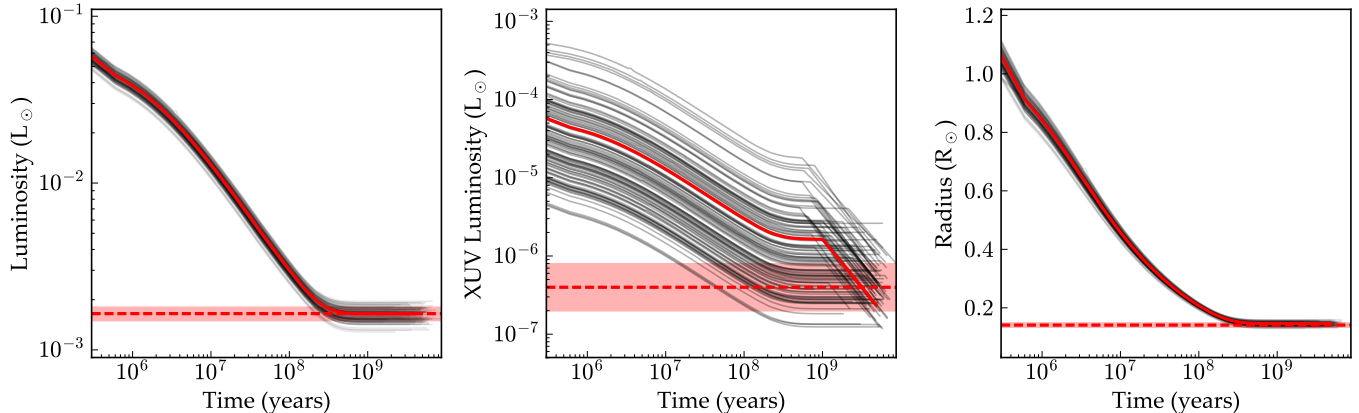


Figure 1. Luminosity, XUV luminosity, and radius evolution of Proxima Centauri. The dashed red lines indicate the measured values of each parameter (see text). 1σ uncertainties are shaded in light red. The mean (fiducial) evolution is indicated by the solid red tracks. The black lines correspond to 100 randomly drawn posterior samples from our MCMC chains (see §4.4.). By construction, all tracks match the observed values at the present day within 1σ .

the “constant-phase-lag” model (Goldreich 1966; Greenberg 2009; Heller et al. 2011). This model reduces the evolution to two parameters, the “tidal quality factor” Q and the Love number of degree 2, k_2 . While this model has known shortcomings (Touma & Wisdom 1994; Efroimsky & Makarov 2013), it provides a qualitatively accurate picture of tidal evolution, and produces similar results as the competing constant-time lag model (Heller et al. 2010; Barnes et al. 2013; Barnes 2017). Moreover, Kasting et al. (1993) used CPL to calculate the “tidal lock radius.” For this study, we use the model described in Heller et al. (2011), and validated it by reproducing the tidal evolution of the Earth-Moon orbit (MacDonald 1964; Barnes 2017) and the tidal heating of Io (Peale et al. 1979). We call this module `EQTIDE` as it is nearly identical to the code by the same name (Barnes 2017)¹⁰, and which served as a template for `VPLANET` development.

The values of Q and k_2 for Earth are well-constrained by lunar laser ranging (Dickey et al. 1994) to be 12 ± 2 and 0.299, respectively (Williams et al. 1978; Yoder 1995). However, their values for celestial bodies are poorly constrained because the timescales for the evolution are very long. Values of Q for stars are typically estimated to be of order 10^6 (e.g. Jackson et al. 2009); dry terrestrial planets have $Q \sim 100$ (Yoder 1995; Henning et al. 2009), and gas giants have $Q = 10^4 - 10^6$ (Aknes & Franklin 2001; Jackson et al. 2008b). In § 4 we will consider the possibility that Proxima b began with a hydrogen envelope and was perhaps more like Neptune than Earth. There is some debate regarding the location of tidal dissipation in gaseous exoplanets, whether it is in the envelope (high Q) or in the core (low Q) (e.g. Storch & Lai 2014). We will consider planets with very thin hydrogen envelopes, so we will make this latter assumption and use the Q value computed by `THERMINT` (see § 3.7) in simulations which track orbital, internal, atmospheric and stellar evolution for habitable evaporated core scenarios in § 4.6.

3.4. Orbital Evolution: `DISTORB`

The model for orbital evolution, `DISTORB` (for “disturbing function orbit evolution”), uses the 4th order secu-

lar disturbing function from Murray & Dermott (1999) (see their Appendix B), with equations of motion given by Lagrange’s planetary equations (again, see Murray & Dermott 1999) and presented in their entirety in Deitrick et al. (2017). This secular (i.e. long-term averaged) model does not account for the effects of mean-motion resonances; however, since we apply it to well-separated planets here, it is adequate for much of our parameter space. Since the model is 4th order in e and i , it can account for coupling of eccentricity and inclination, although it does begin to break down at higher eccentricity ($\gtrsim 0.3$) or mutual inclination ($\gtrsim 30^\circ$). We have compared our model to the `HNBody`¹¹ integrator (Rauch & Hamilton 2002) and find that for modest values of e and i the two methods are nearly indistinguishable. We apply this model to Proxima b and a possible longer period companion, hinted at in the discovery data.

3.5. Rotational Evolution from Orbits and the Stellar Torque: `DISTROT`

The planetary obliquity is a primary driver of climate, and hence we also track planet b’s spin-axis evolution carefully. Not only is it responsible for seasons, but a non-zero obliquity can result in tidal heating (Heller et al. 2011), which can change outgassing rates and atmospheric properties. Proxima b’s obliquity is affected by two key processes: tidal damping and perturbations from other planets. The `EQTIDE` module handles the former, `DISTROT` the latter.

Our obliquity evolution model, `DISTROT` (for “disturbing function rotation evolution”), uses the equations of motion originally developed in Kinoshita (1975, 1977) and utilized in numerous studies including Laskar (1986), Laskar et al. (1993a,b), and Armstrong et al. (2014). It treats the planet as an oblate spheroid (having an axisymmetric equatorial bulge), with a shape controlled by the rotation rate (see below). The planet is subject to a torque from the host star, which causes axial precession, and changes in its orbital plane due to perturbations from a companion planet, which directly change the obliquity angle. This model is thus dependent on `DISTORB` through the eccentricity, the inclination, the longitude of ascend-

¹⁰ `EQTIDE` is available at <https://github.com/RoryBarnes>

¹¹ Publicly available at <https://janus.astro.umd.edu/HNBody/>

ing node (Ω), and the derivatives dp/dt and dq/dt . This model is described in its entirety in Deitrick et al. (2017).

Since we couple obliquity evolution in `DISTROT` to tidal evolution in `EQTIDE`, it is necessary to account for changes in the planet’s shape (its dynamical ellipticity) as its rotation rate changes due to tides. Following the examples of Atobe & Ida (2007) and Brasser et al. (2014), we scale the planet’s oblateness coefficient, J_2 (from which the dynamical ellipticity, E_d , can be derived), with the radius R_p , rotation rate ω_{rot} , and mass M , as

$$J_2 \propto \frac{\omega_{rot}^2 R_p^3}{M}. \quad (1)$$

This is equivalent to assuming hydrostatic equilibrium, i.e., there is no frozen-in “fossil figure”. We use the Earth’s J_2 as a proportionality factor. As pointed out by Brasser et al. (2014), around a rotation period of 13 days, J_2 calculated in this way reaches the J_2 of Venus, which maintains this shape at a much slower rotation period, however, the slowest rotation rate for planet b is ~ 11 days, thus this inconsistency is not encountered in our simulations.

In the presence of strong tidal effects, as we would expect at Proxima b’s orbital distance, the obliquity damps extremely quickly (in a few hundred kyr). However, if another planetary mass companion is present, then gravitational perturbations can prevent the obliquity from damping completely. Furthermore, this equilibrium configuration, called a Cassini state, is confined to a configuration in which the total angular momentum vector of the planetary system, \hat{k} , the rotational angular momentum vector of the planet, \hat{s} , and the planet’s own orbital angular momentum vector, \hat{n} , all lie in the same plane (Colombo 1966).

To identify Cassini states, we use the formula

$$\sin \Psi = \frac{(\hat{k} \times \hat{n}) \times (\hat{s} \times \hat{n})}{|\hat{k} \times \hat{n}| |\hat{s} \times \hat{n}|}, \quad (2)$$

suggested by Hamilton & Ward (2004). In a Cassini state, the angle Ψ will oscillate (with small amplitude) about 0° or 180° , so $\sin(\Psi)$ will approach zero. We will refer to $\sin(\Psi)$ as the “Cassini parameter”. If a planet is in a Cassini state, its obliquity will not be damped to 0.

3.6. Radiogenic Heating: `RADHEAT`

The first of two geophysical modules tracks the abundances of radioactive elements in the planet’s core, mantle and crust. We consider 5 radioactive species: ^{26}Al , ^{40}K , ^{232}Th , ^{235}U , and ^{238}U . These elements have measured half-lives of 7.17×10^5 , 1.251×10^9 , 1.405×10^{10} , 7.038×10^8 , and 4.468×10^9 years, respectively. The energy associated with each decay is 6.415×10^{-13} , 2.134×10^{-13} , 6.834×10^{-12} , 6.555×10^{-12} and 8.283×10^{-12} J, respectively.

We will consider four different abundance ratios. First, we consider an Earth-like case with standard abundance concentrations (*e.g.* Korenaga 2003; Arevalo et al. 2009; Huang et al. 2013). Note that geoneutrino experiments are only able to measure the decay products of ^{232}Th and ^{238}U inside Earth (Raghavan et al. 1998; Araki et al. 2005; Dye 2010).

The second case uses chondritic abundances, in which we augment the mantle’s ^{40}K budget by a factor of 30 in number to match the potassium abundance seen in chondritic meteorites (Anders & Grevesse 1989; Arevalo et al. 2009). Such high potassium abundances could be present if the planet formed beyond the snowline where potassium, a volatile, is more likely to become embedded in solids, see § 2.1.

The third case is a planet containing an initial abundance of 1 part per trillion (ppt) of ^{26}Al . If the planet formed within 1 Myr and the planetary disk was enriched by a nearby supernova (or kilonova), then not all the ^{26}Al would have decayed. A planet that formed quickly, either by planetesimal accumulation or a direct collapse in the outer regions of Proxima’s protoplanetary disk, would likely have more than 1 ppt of ^{26}Al , but as we will see in § 4, this case provides so much heating that our model breaks down. The decay of ^{26}Al at $t = 0$ produces enough heat to melt 1 g of a CI meteorite, preventing their solidification for several half-lives (Hevey & Sanders 2006). Note that Earth required tens to hundreds of millions of years to form, so all the primordial ^{26}Al in the Solar System had already decayed.

The final case is an inert planet with no radioactive particles. This case is very unlikely in reality, but serves as a useful end-member case to bound the evolution of Proxima b.

3.7. Geophysical Evolution: `THERMINT`

We model the coupled core-mantle evolution of Proxima b with a 1-dimensional model that has been calibrated to modern-day Earth (Driscoll & Bercovici 2014; Driscoll & Barnes 2015); the reader is referred to those studies for a comprehensive description. Briefly, the model solves for the average core and mantle temperatures as determined by energy balance in the two layers and temperature-dependent parameterizations for heat loss. The code includes heat transport across the mantle-surface and core-mantle boundaries (CMB), mantle melt production and eruption rates, latent heat production by mantle and core solidification, and radiogenic and tidal heating, see § 3.3. Given the thermodynamic state of the core and the pressure of the stellar wind at the orbit of Proxima b, a magnetic moment scaling law is used to predict the core generated magnetic field and the resulting magnetopause radius (Driscoll & Bercovici 2014). However, we note that the host star’s strong magnetic field may compress the planet’s magnetosphere close to its surface (Vidotto et al. 2013; Cohen et al. 2014).

Our model has been validated by simulating the history of Earth since the moon-forming impact and reproduces 8 features of the modern Earth: upper mantle temperature, core/mantle boundary temperature, core/mantle boundary heat flux, average eruptive mass, upper mantle viscosity, inner core radius, surface heat flow, and magnetic moment. Fiducial values and uncertainties for these parameters were taken from Driscoll & Bercovici (2014), Driscoll & Barnes (2015), and Jaupart et al. (2015). This was accomplished by calibrating with observed values for each of these parameters and an error scale, such that a chi-squared deviation could be defined. The model was then sampled over the `THERMINT` and `RADHEAT` parameter spaces, with a given parameter’s range bounded by empirical and theoretical constraints. Sampling was per-

formed using a Markov-Chain Monte Carlo (MCMC) sampler (Foreman-Mackey et al. 2013), which is well-suited to deal with the complexity of the model and the large number of parameters.

This model produces the expected divergent evolution of Venus and Earth under the assumption that they formed with similar compositions and temperatures, but that Venus has had a stagnant lid and Earth a mobile lid (Driscoll & Bercovici 2014). While this model is generic in many ways, it does assume an Earth-like composition, structure, mass and radius. The minimum mass for Proxima b is close enough to Earth’s for this model to produce preliminary predictions for its thermal evolution. We note that THERMINT is limited to initial mantle temperatures above ~ 1500 K, below which point differentiation may not occur, and below 8000 K, where additional phase changes would require additional physics.

The THERMINT modules can be directly coupled to EQTIDE as demonstrated in Driscoll & Barnes (2015). All the tidal power is deposited in the mantle using a viscoelastic Maxwell dissipation model (Henning et al. 2009). Heating of the mantle changes viscosity, shear modulus, and in turn the dissipation efficiency (or tidal Q). The dissipation model predicts a maximum dissipation rate for mantle temperature near 1800 K, thus cooling planets that pass through this temperature can experience a spike in tidal power generation.

3.8. Galactic Effects: GALHABIT

Proxima Centauri appears to be tenuously bound to the binary α Cen A and B, with a semi-major axis of $\sim 8,700$ AU (Kervella et al. 2017), and is therefore susceptible to perturbations from the Milky Way. We model the changes to Proxima’s orbit produced by galactic tides and stellar encounters using the equations and prescriptions developed to study the Oort cloud (Heisler & Tremaine 1986; Heisler et al. 1987; Rickman et al. 2008), as Proxima has a similar orbit about α Cen A and B. These formulations have also been shown to be accurate in modeling groups of stars (Aguilar & White 1985). We utilize an updated galactic density of $\rho_0 = 0.102 \text{ M}_\odot \text{pc}^{-3}$ (Holmberg & Flynn 2000) and treat α Cen A and B as a single point mass with $M = 2.1 \text{ M}_\odot$ (*i.e.* the recently updated masses given by Pourbaix & Boffin (2016)). This approach is somewhat crude — the two stars produce a significant quadrupole moment associated with their orbit — as a back-of-the-envelope calculation indicates that the torque associated with this quadrupole potential would be equal to the galactic tidal torque at distance less than ~ 2000 AU. Hence, the effect of the binary host should be minor at Proxima’s current semi-major axis. However, the quadrupole’s importance is increased if Proxima has a significant eccentricity. Since modeling the triple system in a comprehensive way is significantly more complicated (see, *e.g.* Harrington 1968; Ford et al. 2000; Breiter & Vokrouhlický 2015), we restrict ourselves to the secular effects of galactic tides and passing stars and will revisit the triple star dynamics in future work.

At Proxima’s semi-major axis, galactic tides and stellar encounters can pump its eccentricity to values large enough to cause disruption from the system, and/or a periastron distance so close to the binary α Cen that we would expect consequences for any planetary system,

such as eccentricity excitation or destabilization (Kaib et al. 2013). In such situations, Proxima b may currently have significant tidal heating due to recent eccentricity excitation.

Following Heisler et al. (1987) and Rickman et al. (2008), we model stellar encounters with a stochastic Monte Carlo approach, estimating times of encounters from the stellar density and velocity dispersion, and then randomly drawing stellar magnitudes and velocities from the distributions published in García-Sánchez et al. (2001). The impact parameter and velocity are calculated from the relative velocities (stellar velocity relative to the apex velocity, *i.e.* the velocity of the star with respect to the Local Standard of Rest, see Rickman et al. (2008)), and then a Δv is applied to Proxima’s orbit according to the impulse approximation (Remy & Mignard 1985). The masses of passing stars are calculated using the empirical relations from Reid et al. (2002). We have tested this impulse approximation against an N-Body model (HNBody) with Bulirsch-Stoer integration in cases where errors are expected to be largest (smaller semi-major axes for Proxima), for a total of 337,235 comparison simulations. In all cases the errors (*i.e.* the difference between the resulting orbital elements in the N-Body and impulse approximation scenarios) were less than 1%, and the systematic offset in semi-major axis was 1.1×10^{-4} , which agrees well with the errors found in using the impulse approximation by Rickman et al. (2005).

As previously noted, the metallicities of α Cen A and B suggest that the system formed at a galactocentric distance of $\lesssim 4.5$ kpc (Loebman et al. 2016). To model the potential effects of radial migration on the triple star system, we scale the stellar density and gas density of the galaxy according to the radial scale lengths (R_* , R_{gas}) found by Kordopatis et al. (2015). The dark matter density at each distance is estimated from their spheroidal model—unlike the disk models used for stars and gas, this model is not axisymmetric. However, as the dark matter near the midplane of the disk makes up $\lesssim 1\%$ of the total density, it is a decent approximation to assume axisymmetry of the total mass density, as the Heisler & Tremaine (1986) tidal model assumes. We scale the velocity dispersions of the nearby stars as a decaying exponential with twice the stellar scale length, $2R_*$, multiplied by \sqrt{t} , where t is the time since galactic formation, as found to be broadly true in galactic simulations (Minchev et al. 2012; Roškar et al. 2012). In this fashion, the velocity dispersion grows slowly in time at all galactic radii, and it grows larger closer to the galactic center. The apex velocity will vary according to the detailed orbital motion of Proxima through the galaxy, including the radial migration. For the purposes of this study, we simply keep the apex velocity constant in time and space (though it is dependent on the spectral class of the perturbing star), assuming the current Solar value is typical.

With these scaling laws in place, we model radial migration as a single, abrupt jump in the galactocentric distance of the system. The reasoning behind this approximation is that N-Body simulations show migration typically occurs over the course of a single galactic orbit (Roskar 2010); hence, the migration time is short compared to the age of the stellar system. We then randomly

choose formation distances over the range (1.5, 4.5) kpc and migration times over the range (1, 5) Gyr since formation.

3.9. The Coupled Model: *vPLANET*

The previously described modules are combined into a single software program called *vPLANET*. This code, written in C, is designed to be modular so that for any given body, only specific modules are applied and specific parameters integrated in the forward time direction. Parameters are integrated using a 4th order Runge-Kutta scheme with a timestep equal to η times the shortest timescale for all active parameters, *i.e.* $x/(dx/dt)$, where x is a parameter. In general, we obtain convergence if $\eta \leq 0.01$. A more complete and quantitative description of *vPLANET* will be presented soon (Barnes et al., in prep.).

Each individual model is validated against observations in our Solar System or in stellar systems, as described above. When possible, conserved quantities are also tracked and required to remain within acceptable limits. With these requirements met, we model the evolution of Proxima Centauri b for predicted formation models to identify plausible evolutionary scenarios, focusing on cases that allow the planet to be habitable. As Proxima b is near the inner edge of the HZ, we are primarily concerned with transitions into or out of a runaway greenhouse. For water-rich planets, this occurs when the outgoing flux from a planet is $\sim 300 \text{ W/m}^2$ (Kasting et al. 1993; Abe 1993) and for dry planets it is at 415 W/m^2 (Abe et al. 2011). For water-rich planets, we use the relationship between HZ limits, luminosity and effective temperature as defined in Kopparapu et al. (2013).

4. RESULTS

4.1. Galactic Evolution

4.1.1. Proxima’s orbit about α Cen

If Proxima is bound to α Cen A and B, its orbit will be modified by the galactic tide and perturbations from passing stars. We run two experiments to explore the effects of radial migration: set **A** places the system in the solar neighborhood, randomly selecting orbital parameters broadly consistent with the observed positions, for 10,000 trials. In set **B**, we take the same initial conditions and randomly select formation distances over the range [1.5, 4.5] kpc (Loebman et al. 2016) and migration times over (1, 5) Gyr after formation, after which the system is moved to the solar neighborhood (8 kpc). In all cases, the initial orbital elements for Proxima are randomly selected from “Proxima-like” conditions (*i.e.*, semi-major axes between ~ 5000 and ~ 20000 AU, see Figs. 3 and 4) to simulate a myriad of possible histories for the current system. Simulations are halted whenever Proxima becomes gravitationally unbound ($e > 1$) or when it passes beyond 1 pc (at which point we consider it unbound). Our model assuredly breaks down at separations of 1 AU (and probably larger, see below) and hence we also terminate simulations if that occurs. In both sets, fewer than 1% of the simulations are halted due to any of the above conditions.

Figure 2 shows an example of the evolution of Proxima’s orbit in set **B**. Pericenter gets close to α Cen a number of times before radial migration occurs (dashed

line)—as discussed below, these close approaches are potentially disruptive to a planetary system. Angular momentum in \hat{Z} is exchanged between the eccentricity and inclination because of the galactic tides, while stellar encounters perturb all the orbital elements, adding or removing energy and angular momentum from the system.

We search both sets of simulations for the minimum pericenter distance, q_{min} , that Proxima experiences over the course of 7 Gyr (the oldest of α Cen’s age estimates). A previous study of planet stability in wide binaries (Kaib et al. 2013) found that an extended system (like the solar system) orbiting a solar mass star with a binary companion can be disrupted when galactic influences drive the binary’s pericenter to 50 – 250 AU. Extrapolating from that study, which considered a larger mass host star than Proxima and smaller companion stellar masses ($\lesssim 1M_{\odot}$) than α Cen, we anticipate disruptions of an extended planetary system (if Proxima has or ever had one) will occur when $q \lesssim 100 - 200$ AU. Bearing that in mind, we separate our simulations into 5 groups: those that had $q_{min} < 40$ AU (α Cen’s orbit extends to ~ 36 AU), those with $40 < q_{min} < 100$ AU, those with $100 < q_{min} < 200$ AU, those that never pass within 200 AU, and those that became gravitationally unbound. The numbers within each category are shown in Table 1 for both sets of simulations.

Figure 3 shows the distribution of set **A** simulations within each category as a function of the initial semi-major axis, eccentricity, and inclination. Also shown is the distribution of minimum pericenter (q_{min}) distances within this set. Note that the distributions for the intervals (40, 100) AU and (100, 200) AU shown here are “stacked” on top of the previous categories for ease of viewing. Figure 4 shows the same for set **B**. In the lower right panel, the small spike at 1 AU is a result of our halting the simulations that dip within 1 AU, which causes a pile up of simulations there. Presumably, the tail of the distribution would continue on toward smaller and smaller numbers if we did not halt the simulations at that point.

As we expect, configurations that start with high eccentricity or inclination close to 90° (perpendicular to the galactic midplane) are more likely to experience close encounters. This outcome is largely a consequence of the galactic tide acting on a system with low angular momentum in the $\pm\hat{Z}$ direction (perpendicular to the galactic disk). Random encounters with passing stars make the distribution messier—Proxima can be scattered into or out of the “close passage” regime, which randomizes the likelihood of close passages.

Close passages within 100 or 200 AU (orange and purple histograms) are potentially destructive to an extended planetary system orbiting Proxima (planets out to 20 to 30 AU), see next subsection. Close passages within 40 AU (red) are potentially destructive to the *stellar* system itself, and thus may not be representative of the real α Cen system. On the other hand, a close passage may have resulted in the scattering the α Cen A+B orbit into its current high eccentricity orbit. Regardless, our model does not account for the three-body physics of such an encounter, so robust conclusions should not be drawn from our results.

In set **B**, in which α Cen forms closer to the denser

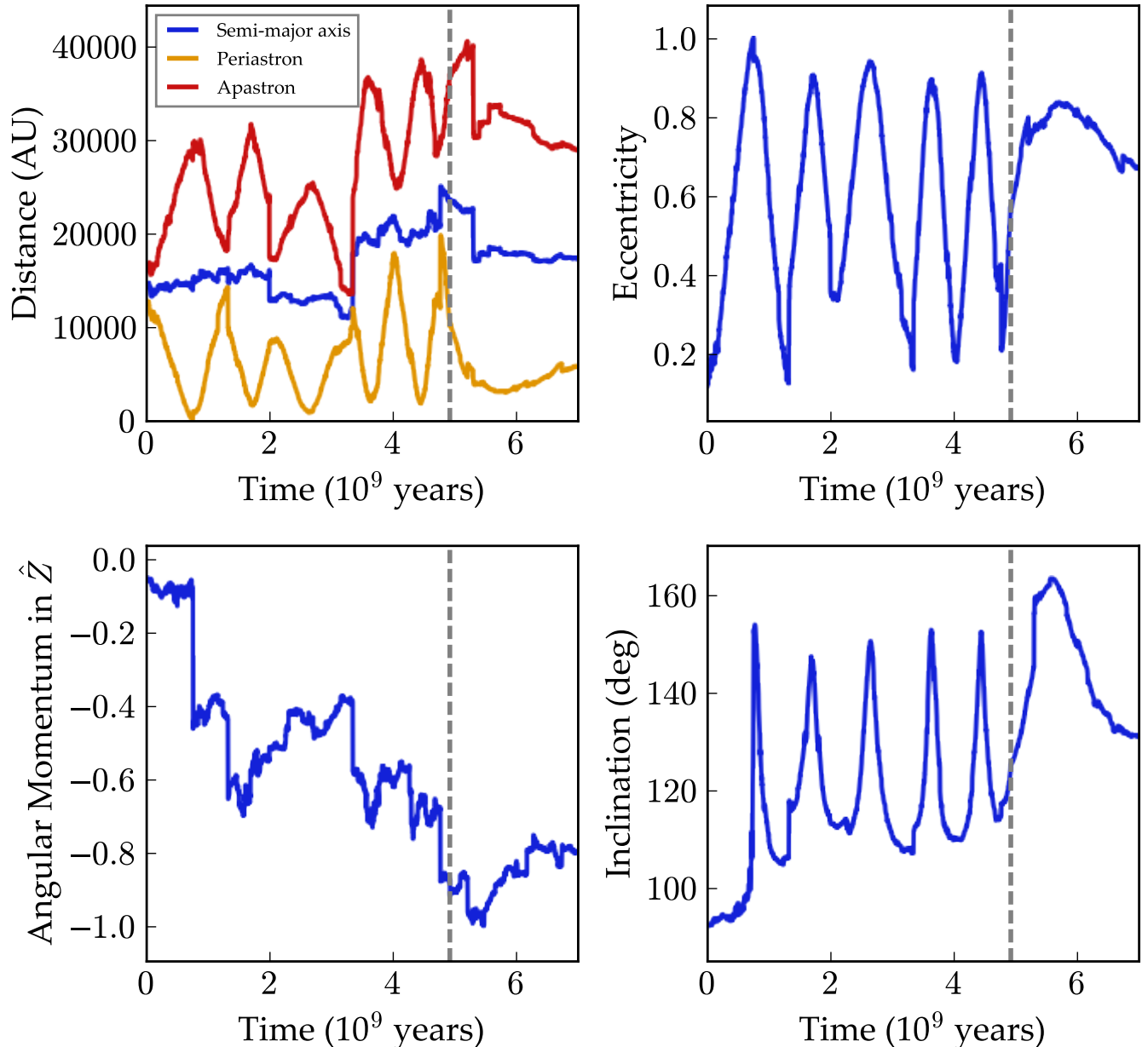


Figure 2. An example of the orbital evolution of Proxima in the galactic simulations. The upper left panel shows the semi-major axis, periastron distance, and apastron distance, the upper right shows the eccentricity, the lower left shows the angular momentum in the \hat{Z} -direction, and the lower right shows the inclination with respect to plane of the galactic disk. The system was given a formation distance of $R = 3.63$ kpc and the vertical dashed line shows the time of migration to 8 kpc. The angular momentum in \hat{Z} (the action J_z) and semi-major axis are unchanged by galactic tides—eccentricity and inclination exchange angular momentum in such a way that these quantities are conserved—thus their evolution is purely due to stellar encounters. In this particular case, the eccentricity of Proxima grows such that its periastron dips within 40 AU of α Cen A and B.

galactic center and undergoes radial migration, close passages are much more common than in set **A**. Closer to the galactic center, the system is subjected to stronger galactic tides and more frequent stellar encounters, which make close passages and complete disruption more likely. Figure 5 shows how the encounter rate scales with the galactocentric position.

4.1.2. Consequences for Proxima’s planetary system

To investigate the impact of close passages on a planetary system orbiting Proxima, we run short simulations in *HNBody*, wherein α Cen is placed in a high eccentric-

Table 1 – Results of Galactic Simulations

Minimum pericenter	Set A	Set B
(0, 40) AU	1301	2321
(40, 100) AU	709	826
(100, 200) AU	756	790
> 200 AU	7218	5981
Unbound	16	82

ity orbit that brings it close to Proxima (still treating α Cen as a single point mass). We ran three sets of simulations, each with a different type of planetary system: only Proxima b, Proxima b and the putative companion,

Proxima b with the Solar System’s gas giants (see Table 2), and Proxima b with super-Earths in the same orbits as the Solar System’s gas giants. In each set, we tested the effect of a close passage at 40 AU, 100 AU, and 200 AU.

In the first set, in which Proxima b is the only planet, nothing dramatic occurs (see Table 3). At low initial eccentricity ($e = 0.001$), the perturbation from α Cen’s passage at 40 AU results in a change of $< 10^{-6}$ in Proxima b’s eccentricity. Increasing Proxima b’s initial eccentricity to the maximum allowed by the observations ($e = 0.35$), we do see a larger deviation ($\Delta e = 10^{-4}$) but even in this case, the eccentricity quickly settles down to its original value (see Fig. 6, left hand panels). In the second set, with Proxima b and a super-Earth companion, the effects are also very minor. Even in the highest eccentricity case (both planets have $e = 0.35$ initially), the perturbation from α Cen is completely drowned out by the perturbations between the two planets.

With the third set, we are extending the study by Kaib et al. (2013) to a lower mass host star and a higher mass perturber. We confirm their findings that close passages are destructive to a system analogous to our outer solar system. Even at a close passage of 200 AU, the eccentricities of the Uranus and Neptune analogues are excited to the point that they cross orbits (Fig. 6, right hand panels). Though this planetary system is not completely destroyed over the course of this simulation (200,000 year), it is almost certainly rendered unstable on longer timespans. With close passages of 40 and 100 AU, one planet (or more) is ejected almost immediately after α Cen’s pericenter passage. If we perform the same experiment with Neptune removed (so that the planets extend to 20 AU), the system is destabilized at close passages of 40 or 100 AU, but not at 200 AU.

Giant planets may not, however, be common orbiting M dwarfs (Ida & Lin 2005; Bonfils et al. 2013). To be certain that the instability mentioned in the previous paragraph is not unique to planets as massive as our solar system giants, we rerun the third set of simulations, but giving the planets masses in the range 1 to $4 M_{\oplus}$. In this situation, the system is even *more* prone to instability than the higher mass cases, with close passages at 200 AU producing instabilities.

We conclude that close passages with α Cen might have truncated any planetary system or planet forming disk extending beyond ~ 10 to 20 AU from Proxima. In other words, the extent and structure of Proxima’s planetary system is limited by the presence of these companion stars. Late (*i.e.* in the relatively recent past) close passages could have destabilized a previously quiet planetary system, leading to major alterations in Proxima b’s orbit, potentially even a late arrival to its present day location. Future detections of additional planets may be able to constrain Proxima’s orbital history. If Proxima has relatively few planets, or their orbits are dynamically hot (*i.e.* high eccentricity or inclination), that may indicate that close encounters with α Cen have occurred. Conversely, planets beyond ~ 10 or 20 AU on circular, coplanar orbits may indicate a relatively peaceful history.

4.2. Orbital/Rotational/Tidal Evolution

We begin exploring the dynamical properties of the *planetary* orbits and spins by considering the tidal evo-

Table 2 – Hypothetical multiplanet systems of Proxima

Set	Planet mass (M_{\oplus})	a (AU)	e
PCb, e1	1.27	0.0482817	0.001
PCb, e2	1.27	0.0482817	0.2
PCb, e3	1.27	0.0482817	0.35
PCb/c, e1	1.27	0.0482817	0.001
	3.13	0.346	0.001
PCb/c, e2	1.27	0.0482817	0.2
	3.13	0.346	0.2
PCb/c, e3	1.27	0.0482817	0.35
	3.13	0.346	0.35
JSUN	317.79704651	5.20336	0.048393
	95.15193166	9.53707	0.054151
	14.53439881	19.19126	0.047168
	17.14527595	30.06896	0.008586
JSU	317.79704651	5.20336	0.048393
	95.15193166	9.53707	0.054151
	14.53439881	19.19126	0.047168
JSUNsm	1.27	5.20336	0.048393
	3.13	9.53707	0.054151
	1.016	19.19126	0.047168
	2.087	30.06896	0.008586
JSUsm	1.27	5.20336	0.048393
	3.13	9.53707	0.054151
	1.016	19.19126	0.047168

Table 3 – Outcomes of Galactic Perturbations on Proxima planetary systems

Set	Closest approach (AU)	Result
PCb, e1	200	Negligible
	100	Negligible
	40	Negligible
PCb, e2	200	Negligible
	100	Negligible
	40	Negligible
PCb, e3	200	Negligible
	100	Negligible
	40	Negligible
PCb/c, e1	200	Negligible
	100	Negligible
	40	Negligible
PCb/c, e2	200	Negligible
	100	Negligible
	40	Negligible
PCb/c, e3	200	Negligible
	100	Negligible
	40	Negligible
JSUN	200	Crossing orbits
	100	Disruption
	40	Disruption
JSU	200	Excited eccentricities
	100	Disruption
	40	Disruption
JSUNsm	200	Disruption
	100	Disruption
	40	Disruption
JSUsm	200	Disruption
	100	Disruption
	40	Disruption

lution of Proxima b if it is in isolation. In this case, we need only apply `EQTIDE` to both Proxima and Proxima b and track a, e, P_{rot} , and ψ . We find that if planet b

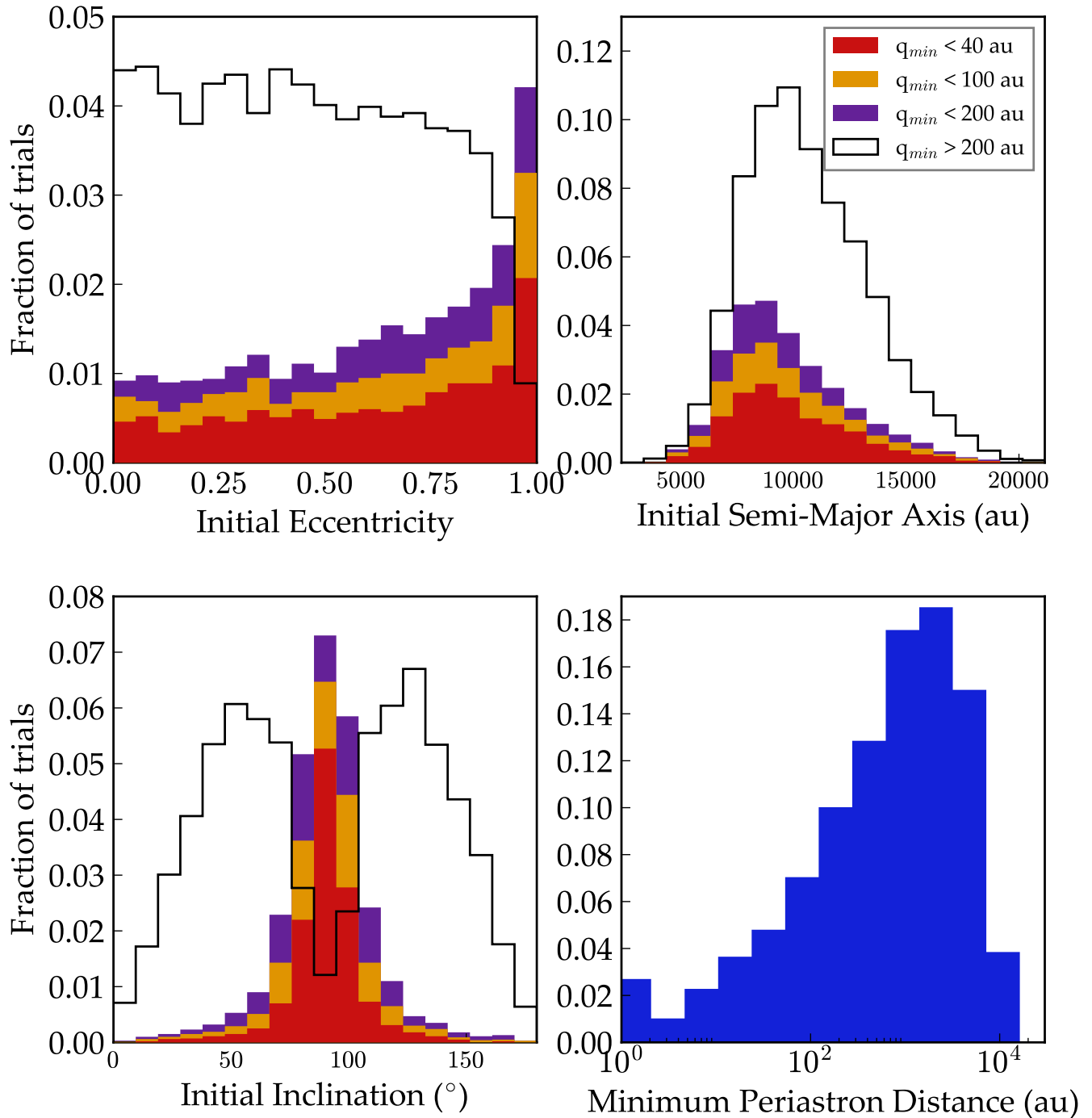


Figure 3. Distribution of Proxima Centauri's minimum pericenter, q , without radial migration. Simulations in which q passes below 40 AU are shown in red. Stacked on top of that, simulations with $40 < q < 100$ AU are in orange, and $100 < q < 200$ in purple, i.e. red is a subset of orange is a subset of purple. The black line indicates simulations that never had passages within 200 AU. *Top left:* Initial eccentricity. *Top right:* Initial semi-major axis. *Bottom left:* Initial inclination relative to the galactic disk. *Bottom right:* Minimum periastron distance in all cases over the entire simulation. Generally, eccentricity and inclination determine the likelihood of close passages between Proxima and α Cen, with high e and $i \sim 90^\circ$ (i.e. low \dot{Z} -angular momentum) cases being the most likely to have such events.

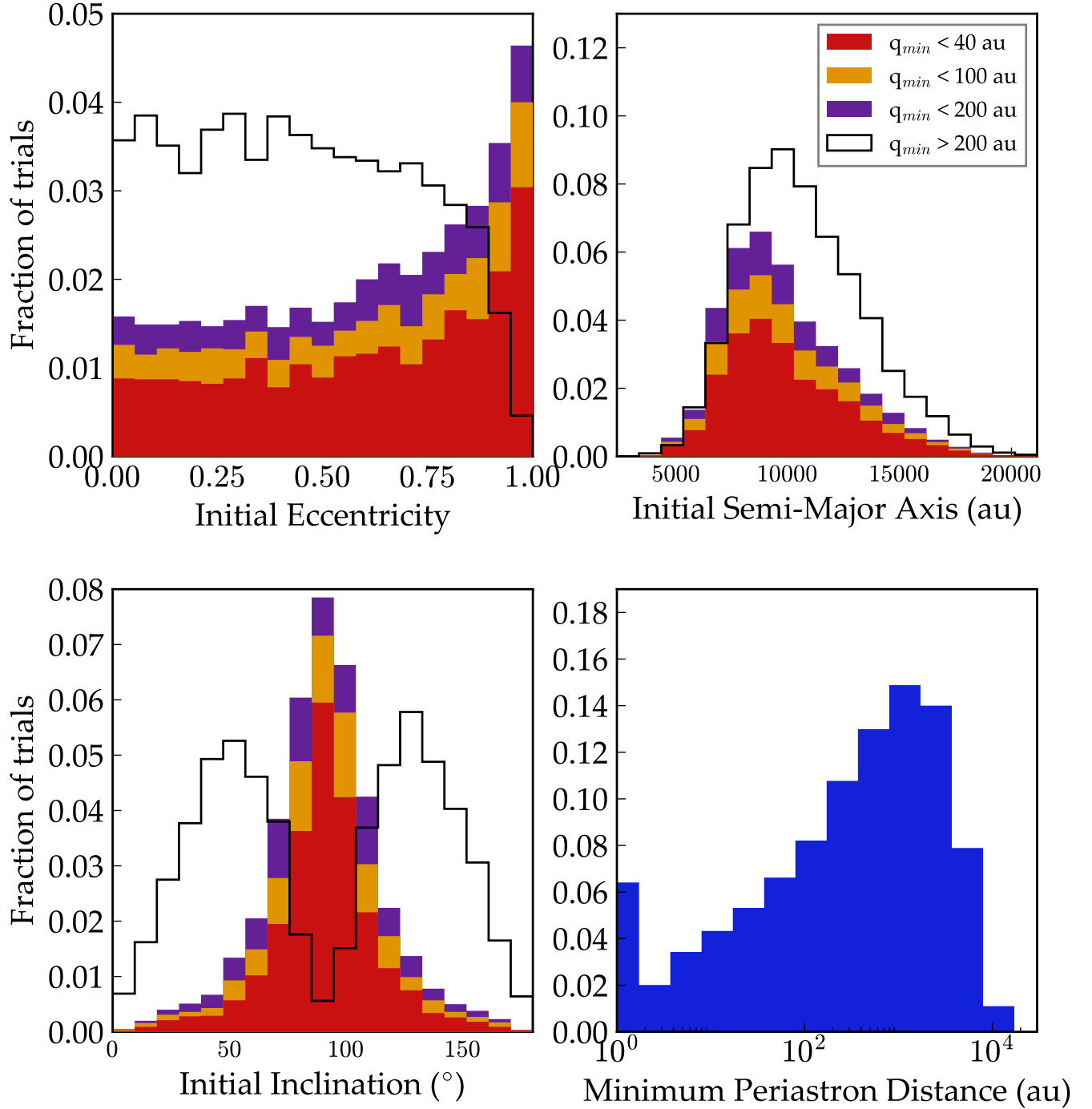


Figure 4. Same as Fig. 3 but with radial migration. Systems which formed interior to 4.5 kpc from the galactic center have close passages with α Cen more frequently than those which were placed in the solar neighborhood from the beginning.

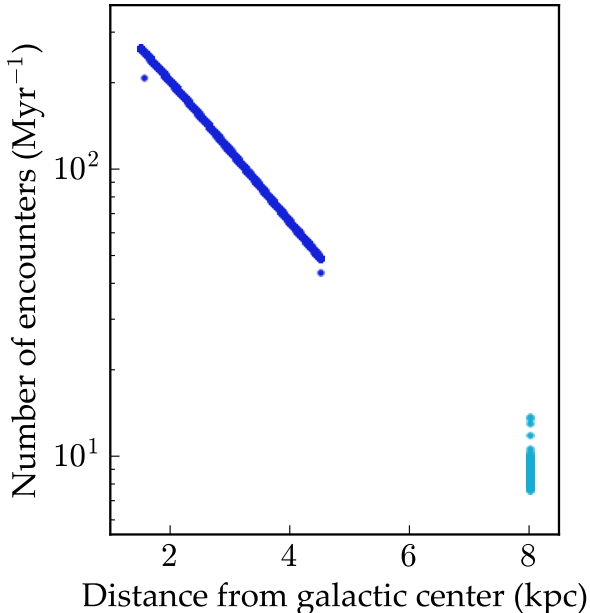


Figure 5. Stellar encounter rates as a function of galactocentric distance. Dark blue points correspond to pre-migration encounter rates, light blue to post-migration. There is some scatter in the solar-neighborhood points because of the time dependence of the stellar velocity dispersion. At the tail end of the simulations, we match the encounter frequency of 10.5 Myr^{-1} from previous studies (García-Sánchez et al. 2001; Rickman et al. 2008).

has $Q = 12$, then an initially Earth-like rotation state becomes tidally locked in $\sim 10^4$ years, so it seems likely that if b formed near its current location, then it reached a tidally locked state with negligible obliquity almost immediately. Note that, contrary to popular belief, the term “tidally locked” does not necessarily mean that the planet is synchronously rotating (see the end of this section).

Unlike the rotational angular momentum, the orbit can evolve on long timescales. In the top two panels of Fig. 7, we consider orbits that begin at $a = 0.05 \text{ AU}$ and with different eccentricities of 0.05 (dotted curves), 0.1 (solid curves) and 0.2 (dashed curves). In these cases a and e decrease and the amount of inward migration depends on the initial eccentricity, which takes 2–3 Gyr to damp to ~ 0.01 . For initial eccentricities larger than ~ 0.23 , the CPL model actually predicts eccentricity growth due to angular momentum exchange between the star and planet (Barnes 2017). This prediction is likely unphysical and due to the low order of the CPL model; therefore we do not include evolutionary tracks for higher eccentricities.

The equilibrium tide model posits that the lost rotational and orbital energy is transformed into frictional heating inside the planet. The bottom panel of Fig. 7 shows the average surface energy flux as a function of time. We address the geophysical implications of this tidal heating in § 4.5.2. Note that if planet b begins with a rotation period of 1 day and an obliquity of 23.5° , then the initial surface energy flux due to tidal heating is $\sim 1 \text{ kW/m}^2$.

Next, we consider the role of additional planets, specifically the putative planet with a 215 day orbit (Anglada-Escudé et al. 2016). For these runs we now add the

DISTORB and DISTROT modules and track the orbital elements of both planets, the spins of the star and planet b , and the dynamical ellipticity of planet b . A comprehensive exploration of parameter space is beyond the scope of this study, so we consider three end-member cases: a nearly coplanar, nearly circular system; a system with high eccentricities and inclinations; and a system with high e and low i . The initial orbital elements and rotational properties of the bodies are listed in Table 4.

In Fig. 8 we show the orbital evolution for the low e and i case over short (left) and long (right) timescales. As expected, the planets exchange angular momentum, but over the first million years there is no apparent drift due to tidal effects. On longer timescales, however, we see the eccentricity of b slowly decay due to tidal heating. Note the differences in timescale for the decay between Figs. 7 and 8. The perturbations from a hypothetical “planet c ” maintain significant eccentricities for long periods of time.

In Fig. 9, we plot the orbital evolution for the high e and i case. The eccentricity and inclination oscillations are longer, and the eccentricity cycles show several frequencies due to the activation of coupling between e and i . As in the low e and i case, the eccentricity damps more slowly than in the unperturbed case. Note as well that the inclination oscillation amplitude decays with time.

In Fig. 10, we plot the evolution of the rotational parameters for the two cases. In the top left panel, we show the evolution of the rotational period. The rotation becomes tidally locked very quickly (less than 1 Myr for all plausible values of Q for an ocean-bearing world). In the high e, i case, the planet briefly enters the 3:2 spin orbit frequency ratio (like the planet Mercury). The obliquity initially grows due to conservation of angular momentum (Correia et al. 2008), but then damps down. For the high e, i case, the obliquity reaches an equilibrium value near 0.1° , while the low e, i case drops all the way to 10^{-8} degrees. The bottom left panel shows the evolution of the dynamical ellipticity as predicted by the formulae from Atobe & Ida (2007). Realistically, the shape of the planet should lag this shape by a timescale dependent on the planet’s rigidity, but we ignore that delay here. The lower right panel shows the value of the Cassini parameter (see Equation 2) for the two cases, both of which become locked near zero, indicating the rotational and angular momentum have evolved into a Cassini state (in this case, Cassini state 2), in which the spin and orbit vectors of planet b are on opposite sides of the total angular momentum vector of the planetary system.

Figure 10 hints at the possibility of non-synchronous spin states for Proxima b , since the eccentricity is pumped to values large enough to force the rotation into a spin-orbit resonance. Ribas et al. (2016) found a significant probability that the planet is in a 3:2 spin orbit resonance. Our tidal model does not take into account potential triaxiality of the planet, and so we cannot reproduce their results (*i.e.* resonance trapping at $e \gtrsim 0.1$). An expanded version of the model (Rodríguez et al. 2012), shows that the 3:2 state occurs generally for $e \gtrsim 0.1$, consistent with the Ribas et al. (2016) result. In the case that Proxima has any additional planets, it is entirely possible for planet b to maintain an eccentricity above this value, even after 7 Gyrs. As an example, our third multiplanet case is like the configurations above,

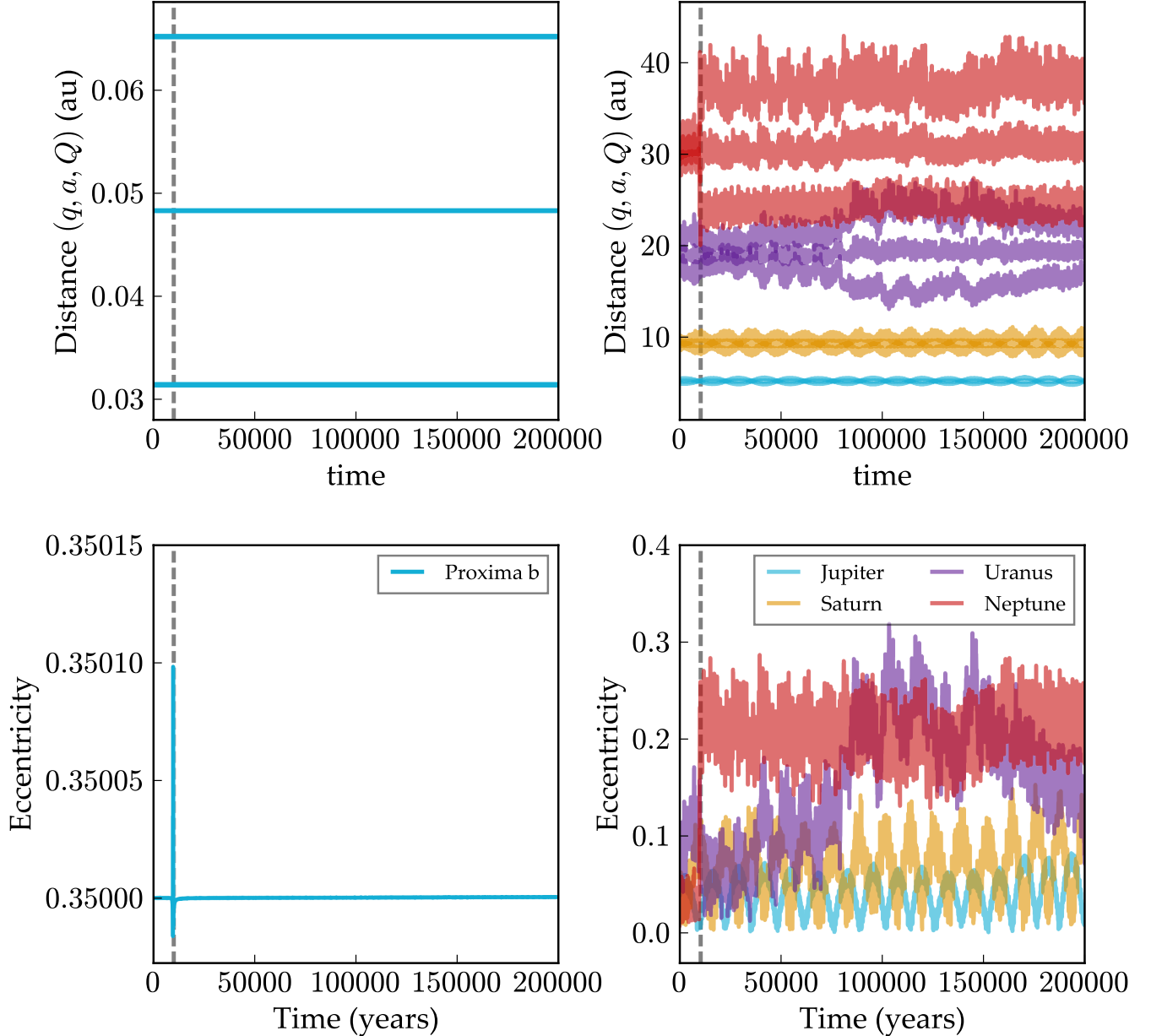


Figure 6. A glimpse of the effects that close passages with α Cen can have on Proxima’s planetary system. Two cases are shown here: *Left:* Proxima b solo, with an initial $e = 0.35$ and α Cen’s pericenter occurring at 40 AU; *Right:* An outer solar system analog orbiting Proxima, with α Cen’s pericenter at 200 AU. Dashed gray lines represent the time of α Cen’s pericenter passage. The top panels show the location of pericenter q , semi-major axis a , and apocenter Q for each planet, seen as three curves of the same color. In the Proxima b solo case, there is a spike of small amplitude in the eccentricity, but after close passage the eccentricity quickly settles to near its initial value. In the solar system analog case, the eccentricities of the outer two planets are excited to the point that their orbits cross—a highly unstable situation.

but coplanar and with a slightly higher eccentricity for planet b ($e = 0.3$ initially). The resulting eccentricity is shown in Figure 11. The eccentricity stays above 0.1 even after 7 Gyr of evolution. Though the evolution is not fully self-consistent (it will be affected by the planet’s true spin state), it demonstrates that perturbations can be strong enough to maintain a large eccentricity to force the planet into super-synchronous rotation.

4.3. Stellar Evolution

In Fig. 12 we plot the evolution of the conservative HZ limits of Kopparapu et al. (2013) (blue region) as a function of time for our fiducial case (§3.1); the HZ is

bounded by the runaway greenhouse limit on the side closest to the star and by the maximum greenhouse limit on the opposite side. The pre-MS luminosity evolution of Proxima forces the HZ to slowly move inward for ~ 1 Gyr, reaching the current orbit of Proxima b after ~ 169 Myr, see § 4.4.2.

The figure also shows the “dry” HZ limits of Abe et al. (2011), which apply to planets with very limited surface water ($\lesssim 1\%$ of the Earth’s water inventory); these planets are significantly more robust to an instellation-triggered runaway. Consequently, if Proxima b’s initial water content was very low, it would have spent signif-

Table 4 – Initial conditions for two-planet Proxima systems

	$m (M_{\oplus})$	a_s (au)	a_l (au)	e	i ($^{\circ}$)	ω ($^{\circ}$)	Ω ($^{\circ}$)	ψ ($^{\circ}$)	P_{rot} (days)
b	1.27	0.0482817	0.05	0.001	0.001	248.87	20.68	23.5	1
c	3.13	0.346	0.346	0.001	0.001	336.71	20		
b	1.27	0.0482817	0.05	0.2	20	248.87	20.68	23.5	1
c	3.13	0.346	0.346	0.2	0.001	336.71	20		

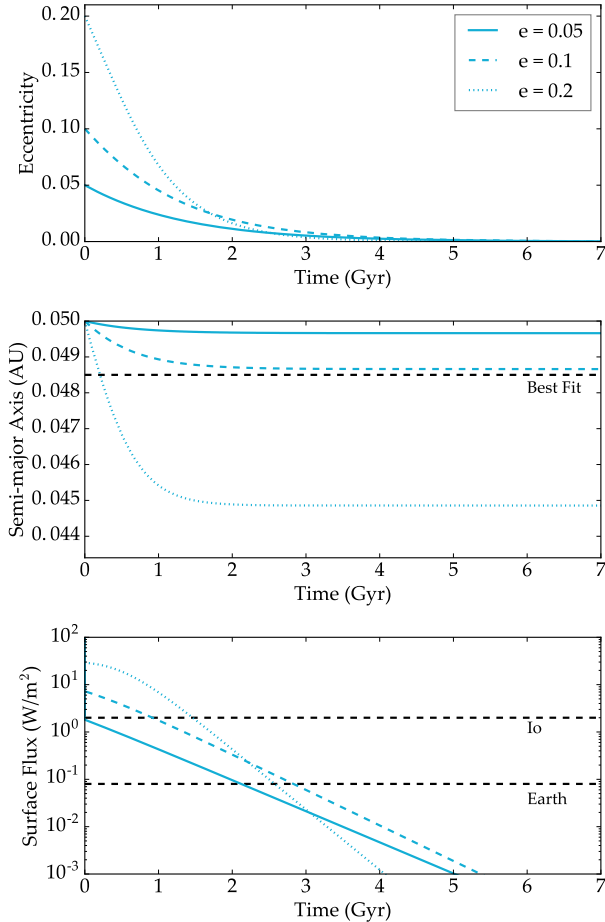


Figure 7. Evolution of planet b’s eccentricity (top), semi-major axis (middle), and tidal heating surface flux (bottom) assuming that initially $a = 0.05$ AU and $e = 0.05$ (dotted), 0.1 (solid) or 0.2 (dashed). For reference the best fit semi-major axis and surface energy fluxes of Io and the modern Earth are shown by dashed black lines.

icantly less time in a runaway greenhouse. However, a dry formation scenario for Proxima b does not help its present-day habitability. As we show in §4.4, Proxima b loses 1 ocean of water in $\lesssim 10$ Myr; if it formed with less water than that, it would be completely desiccated long before entering the Abe et al. (2011) HZ. One can envision cases in which the planet forms dry but with a protective hydrogen envelope, or forms after ~ 10 Myr, but such scenarios are unlikely *a priori* and hence we do not consider them here. In the atmospheric escape section below, we thus use the Kopparapu et al. (2013) HZ limits to determine whether or not Proxima b is in a runaway greenhouse at any given time.

4.4. Atmospheric Evolution

4.4.1. Fiducial cases

As we argued in §3.1, the large uncertainties in the evolutionary history of the star make precise estimates of Proxima b’s current atmospheric and water content impossible. In §4.4.2 below, we report the results of an ensemble of simulations that yield the posterior probability distribution for the planet’s present-day water content given uncertainties on each of the parameters of the model. However, it is still instructive to consider the evolution of the system under our fiducial stellar parameters (§3.1), which we briefly do here.

We consider two broad formation scenarios for Proxima b: one in which it formed with abundant water and a thin hydrogen envelope of up to 1% by mass (due to either *in situ* accretion or from planetary formation farther out followed by rapid disk-driven migration; see Luger et al. (2015)), and one in which it formed with abundant water but no hydrogen. In both cases, we assume a fiducial planet mass of $1.27M_{\oplus}$.

In Fig. 13 we show the evolution of the latter type of planet, which formed with no significant primordial envelope. We consider four different initial inventories of water: 1, 3, 5, and 10 terrestrial oceans ($1 \text{ TO} \equiv 1.39 \times 10^{24}$ g, the total mass of surface water on Earth; see Kasting (1988)), but even larger inventories of water are theoretically possible. As discussed in § 3.2, we also consider two end-member scenarios regarding the photolytically-produced O_2 : no surface sinks (solid lines) and efficient surface sinks (dashed lines). In all cases but one, the planet is completely desiccated within the first 170 Myr, building up between tens and hundreds of bars of O_2 in either its atmosphere or in the solid body. For an initial water content of 10 TO and no surface sinks, O_2 builds up to high enough levels to throttle the supply of H to the upper atmosphere and slow the total escape rate. In this scenario, ~ 1 TO of water remains, alongside a thick 500 bar O_2 atmosphere. If Proxima b formed with less than ten times Earth’s water content, and/or had a persistent convecting, reducing magma ocean, it is desiccated today according to our fiducial case.

Next, in Fig. 14, we show the results assuming Proxima b formed with a hydrogen envelope. We fix the initial water content at 3 TO and consider initial envelope mass fractions f_H ranging from 10^{-4} to 10^{-2} . In all cases, the envelope is lost completely within the first several hundred Myr. For $f_H \lesssim 10^{-3}$, the envelope is lost early enough such that all the water is still lost from the planet. For $f_H = 10^{-3}$, only about 0.1 TO remain once the planet enters the HZ; only for $f_H \sim 10^{-2}$ does the presence of the envelope guard against all water loss. In these calculations, we assumed inefficient surface sinks, so the escape of water at late times was bottlenecked by the presence of abundant O_2 . Planets that form with hydrogen envelopes may have quite reducing

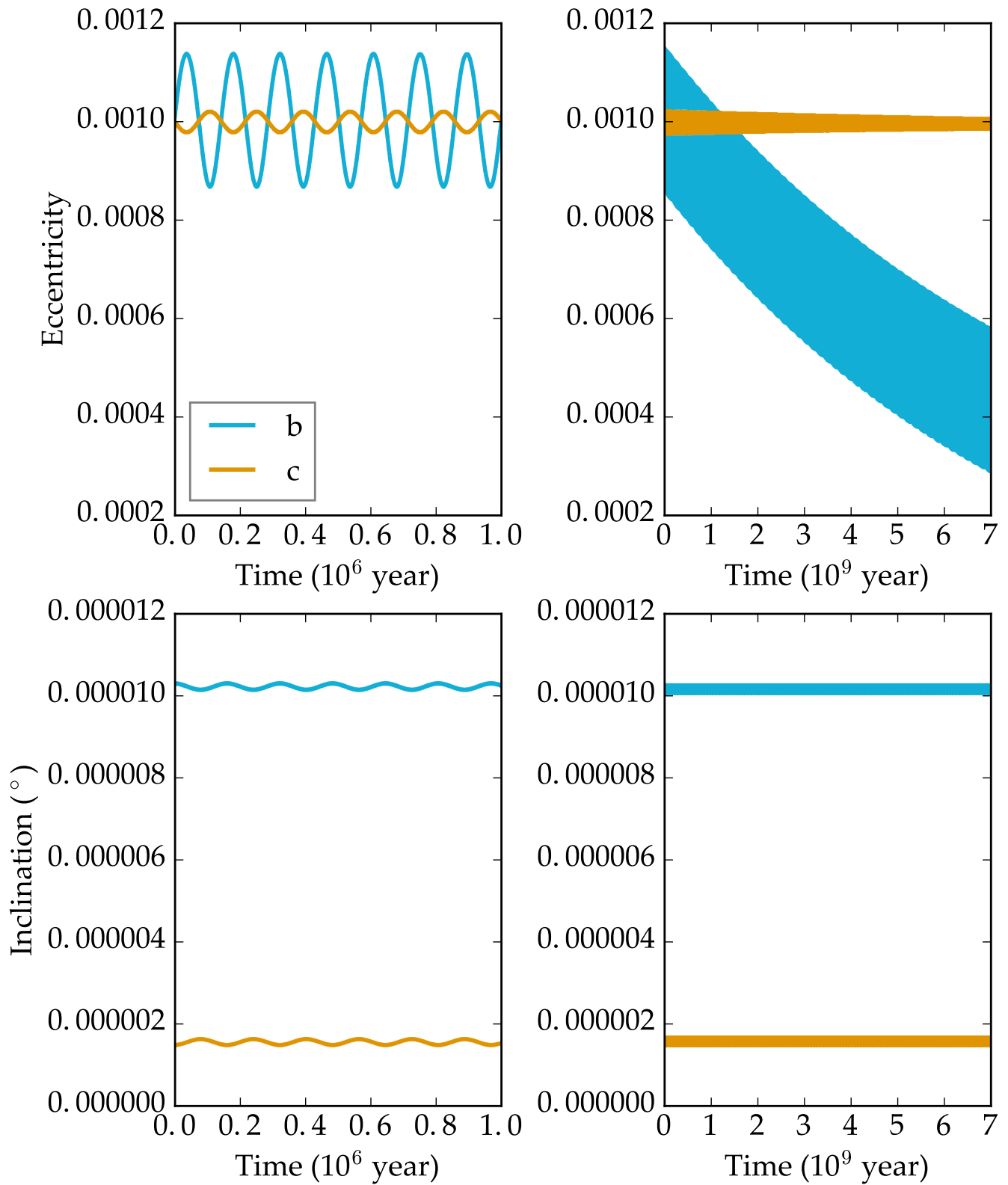


Figure 8. Evolution of orbital elements if a putative planet c exists with an orbital period of 215 days and both orbits are nearly circular and nearly coplanar. *Top Row:* Eccentricity. *Bottom Row:* Inclination.

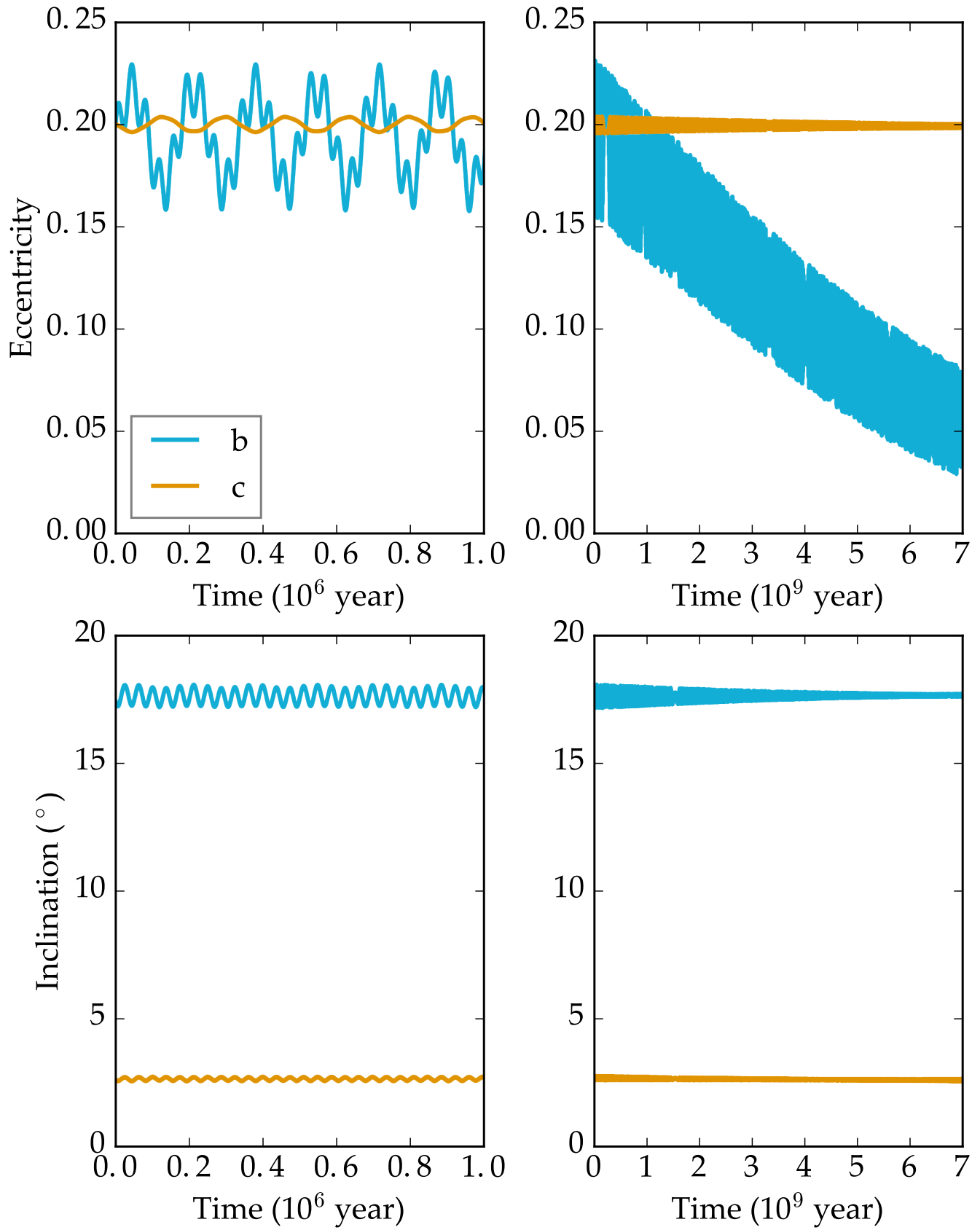


Figure 9. Same as Fig. 8, but for the high e, i case.

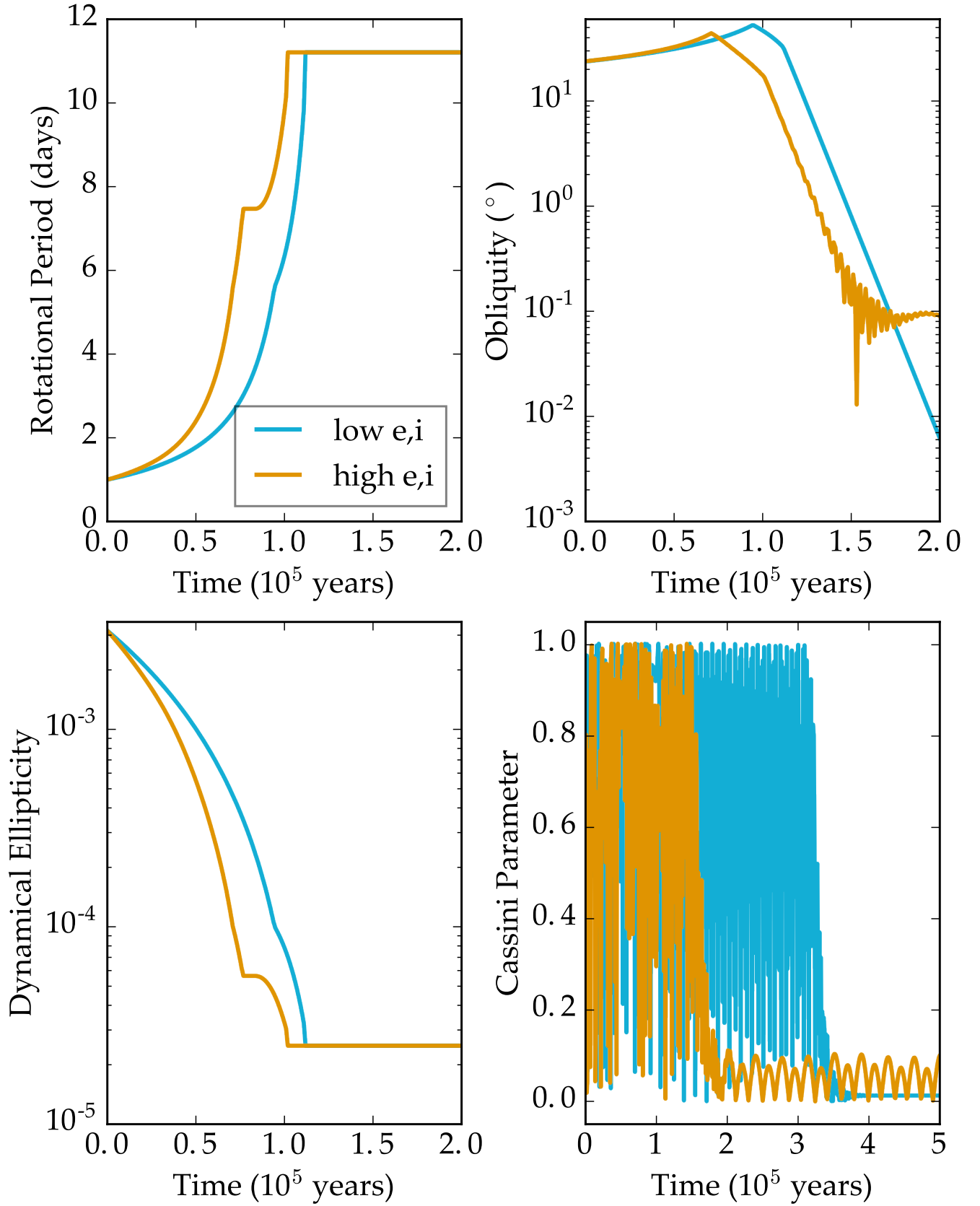


Figure 10. Evolution of rotational properties of planet b for the low e, i case (in blue), and high e, i case (in orange). *Top left:* Rotation Period. *Top right:* Obliquity. *Bottom left:* Dynamical Ellipticity. *Bottom right:* Cassini Parameter.

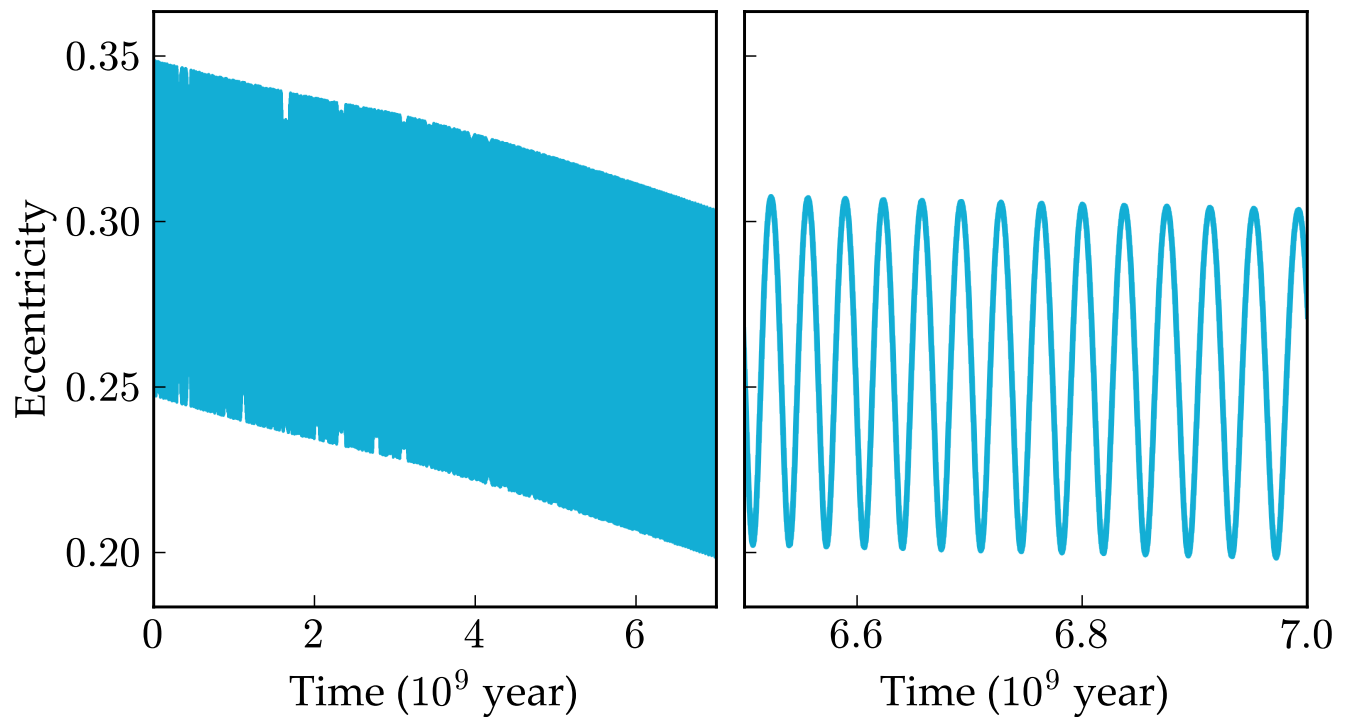


Figure 11. Evolution of the eccentricity of planet b with a companion planet, if the planets are coplanar and b's initial e is 0.3. The left panel shows the full 7 Gyr evolution, while the right is zoom to show the last 500 Myr. A slow, large amplitude cycle persists after billions of years and the eccentricity remains above 0.2, indicating that spin-orbit resonances, i.e. super-synchronous rotation, is possible.

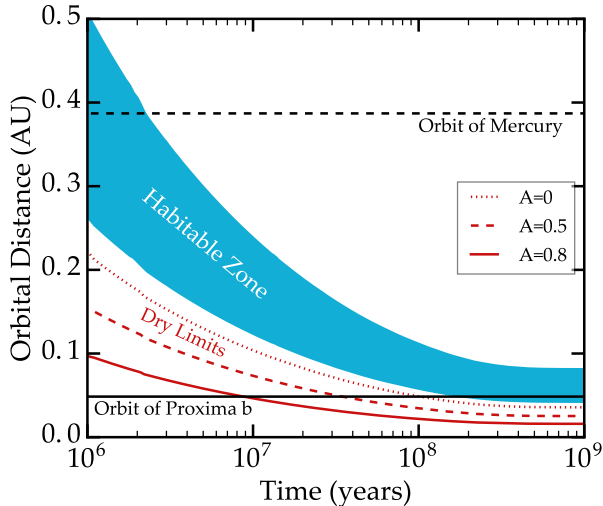


Figure 12. Evolution of the HZ of Proxima Centauri assuming the fiducial stellar parameters (§3.1), along with the orbits of Proxima Centauri b (solid line) and Mercury (dashed line). The blue region is the conservative HZ of Kopparapu et al. (2013), while the red lines are the HZ limits for dry planets of different albedos, A , from Abe et al. (2011).

surfaces, which could absorb most of the O_2 and lead to even higher total water loss. As before, a few tens to a few hundreds of bars of O_2 remain in the atmosphere or in the solid body at the end of the escape phase.

We note that we obtain slightly more hydrogen loss than Owen & Mohanty (2016), who find that planets more massive than $\sim 0.9 M_{\oplus}$ with $\sim 1\%$ hydrogen envelopes cannot fully lose their envelopes around M dwarfs, due primarily to the transition from hydrodynamic to ballistic escape at late times. However, their calculations were performed for a $0.4 M_{\odot}$ M dwarf, whose pre-main sequence phase lasts ~ 200 Myr, five times shorter than that for Proxima Centauri. Nevertheless, the discrepancy is small: we find that for envelope fractions greater than 1% or masses greater than our fiducial value of $1.27 M_{\oplus}$, the envelope does not completely escape, in which case Proxima b would likely be uninhabitable.

4.4.2. MCMC Simulations

In the previous section we showed that our model predicts that unless Proxima b formed with a substantial hydrogen envelope (mass fraction $f_H \gtrsim 0.001$) or more than 10 TO of water, it may be likely desiccated today under our fiducial stellar evolution tracks. However, the large uncertainties in the observed stellar properties and in our adopted model parameters translate to large uncertainties in these values. To robustly account for these uncertainties, in this section we perform a suite of Markov Chain Monte Carlo (MCMC) runs. MCMC allows one to sample from multi-dimensional probability distributions that are difficult or impossible to obtain directly, which is the case for the ensemble of parameters that control the evolution of the planet surface water and oxygen content in VPLANET. Here we develop a framework for inferring the probability distributions of these parameters conditioned on empirical data and our understanding of the physical processes at play.

The input parameters to our model make up the state

vector \mathbf{x} :

$$\mathbf{x} = \{f_{\text{sat}}, t_{\text{sat}}, \beta_{\text{xuv}}, M_{\star}, t_{\star}, a, m\}, \quad (3)$$

corresponding, respectively, to the XUV saturation fraction, the XUV saturation timescale, the XUV power law exponent, the stellar mass, the stellar age, the semi-major axis of the planet, and the mass of the planet. Given a value of \mathbf{x} , VPLANET computes the evolution of the system from time $t = 0$ to $t = t_{\star}$, yielding the output vector \mathbf{y} :

$$\mathbf{y}(\mathbf{x}) = \{L_{\star}, L_{\text{xuv}}, t_{\text{RG}}, m_{\text{H}}, m_{\text{H}_2\text{O}}, P_{\text{O}_2}\}, \quad (4)$$

corresponding, respectively, to the stellar luminosity, the stellar XUV luminosity, the duration of the runaway greenhouse phase, the mass of the planet’s hydrogen envelope, the mass of water remaining on its surface, and the amount of oxygen (expressed as a partial pressure) retained in either the atmosphere or the surface/mantle, all of which are evaluated at $t = t_{\star}$ (i.e., the present day). Additional parameters that control the evolution of the planet (initial water content, XUV absorption efficiency, etc.) are held fixed in individual runs; see below.

Our goal in this section is to derive posterior distributions for \mathbf{y} (and in particular for $m_{\text{H}_2\text{O}}$) given prior information on both \mathbf{x} and \mathbf{y} . Some parameters—such as the present-day stellar luminosity—are well-constrained, while others are less well-known and will thus be informed primarily by our choice of prior. This is the case for the XUV saturation fraction, saturation timescale, and power law exponent, which have been studied in detail for solar-like stars (Ribas et al. 2005) but are poorly constrained for M dwarfs (see, e.g., Luger & Barnes 2015). We therefore use flat-log priors for the saturation fraction and timescale, enforcing $-5 \leq \log(f_{\text{sat}}) \leq -2$ and $-0.3 \leq \log(t_{\text{sat}}/\text{Gyr}) \leq 1$. We use a Gaussian prior for the XUV power law exponent, with a mean of 1.23, the value derived by Ribas et al. (2005) for solar-like stars: $\beta_{\text{xuv}} \sim \mathcal{N}(-1.23, 0.1^2)$. We choose an ad hoc standard deviation $\sigma = 0.1$ and verify *a posteriori* that our results are not sensitive to this choice. As we show below, β_{xuv} does not strongly correlate with the total water lost or total amount of oxygen that builds up on the planet.

We also use a flat prior for the stellar mass ($0.1 \leq M_{\star}/M_{\oplus} \leq 0.15$). Although stronger constraints on the stellar mass exist (e.g., Delfosse et al. 2000; Ségransan et al. 2003), these are derived indirectly from mass-luminosity or mass-radius relations, which are notoriously uncertain for low mass stars (e.g., Boyajian et al. 2012). We thus enforce a prior on the present-day luminosity to constrain the value of M_{\star} via our stellar evolution model (see below). We enforce a Gaussian prior on the stellar age $t_{\star} \sim \mathcal{N}(4.8, 1.4^2)$ Gyr based on the constraints discussed in §2.3 and §2.4.

Our prior on the semi-major axis a is a combination of a Gaussian prior on the orbital period, $P \sim \mathcal{N}(11.186, 0.002^2)$ days (Anglada-Escudé et al. 2016), and the stellar mass prior. Finally, our prior on the planet mass m combines the empirical minimum mass distribution, $m \sin i \sim \mathcal{N}(1.27, 0.18^2) M_{\oplus}$ (Anglada-Escudé et al. 2016), and the *a priori* inclination distribution for randomly aligned orbits, $\sin i \sim \mathcal{U}(0, 1)$, where \mathcal{U} is a uniform distribution (e.g., Luger et al. 2017).

We further condition our model on measured values

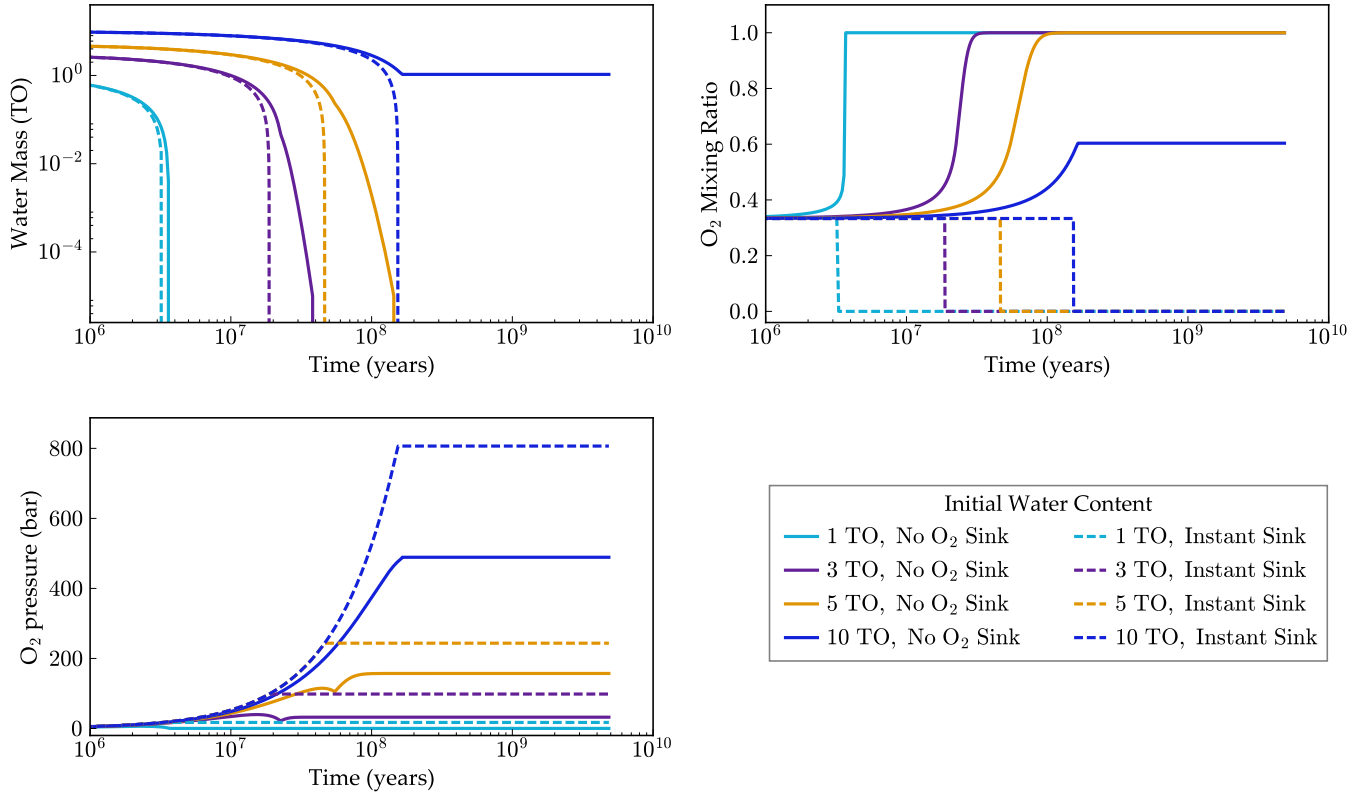


Figure 13. Evolution of the water content and atmospheric O₂ pressure on Proxima b for the fiducial stellar parameters and different initial conditions. The initial water content is varied between 1 and 10 TO (various colors) for two different end-member scenarios: no O₂ surface sinks (solid lines) and instantaneous oxygen absorption at the surface (dashed lines). The planet mass is held constant at $1.27 M_{\oplus}$ and the initial hydrogen envelope fraction is set to zero for all runs. In all but one of the runs, Proxima b is completely desiccated. For an initial water content of 10 TO and no surface sinks, the buildup of ~ 500 bars of atmospheric O₂ slows the loss rate of H, preventing the last ~ 1 TO of water from being lost. In the scenario that efficient oxygen sinks are present, the atmospheric O₂ mixing ratio never grows sufficiently to limit the escape of H, and desiccation occurs in all cases. Note that in this scenario, the curves in the “O₂ pressure” panel correspond to the equivalent O₂ pressure absorbed at the surface.

of the stellar luminosity L_* and stellar XUV luminosity L_{xuv} . We take $L_* \sim \mathcal{N}(1.65, 0.15^2) \times 10^{-3} L_\odot$ (Demory et al. 2009) and $\log L_{\text{xuv}} \sim \mathcal{N}(-6.36, 0.3^2)$. We base the latter on Ribas et al. (2016), who compiled a comprehensive list of measurements of the emission of Proxima Centauri in the wavelength range 0.6–118 nm. Summing the fluxes over this range and neglecting the contribution of flares, we obtain an XUV flux at Proxima b of $F_{\text{xuv}} \approx 252 \text{ erg cm}^{-2} \text{ s}^{-1}$, corresponding to $\log(L_{\text{xuv}}/L_\odot) = -6.36$ for $a = 0.0485 \text{ AU}$. Given the lack of uncertainties for many of the values compiled in Ribas et al. (2016) and the fact that some of those estimates are model extrapolations, it is difficult to establish a reliable error estimate for this value. We make the *ad hoc*, but conservative, choice $\sigma = 0.3 \text{ dex}$, noting that the three measurements that inform the X-ray luminosity of the star in Ribas et al. (2016) (which dominates its XUV emission) have a spread corresponding to $\sigma = 0.2 \text{ dex}$. However, more rigorous constraints on the XUV emission of Proxima with reliable uncertainties are direly needed to obtain more reliable estimates of water loss from Proxima b.

Given these constraints, we wish to find the posterior distribution of each of the parameters in Equations (3) and (4). We thus define our likelihood function \mathcal{L} for a given state vector \mathbf{x} as

$$\ln \mathcal{L}(\mathbf{x}) = -\frac{1}{2} \left[\frac{(L_*(\mathbf{x}) - L_*)^2}{\sigma_{L_*}^2} + \frac{(L_{\text{xuv}}(\mathbf{x}) - L_{\text{xuv}})^2}{\sigma_{L_{\text{xuv}}}^2} \right] + \ln \text{Prior}(\mathbf{x}) + C, \quad (5)$$

where $L_*(\mathbf{x})$ and $L_{\text{xuv}}(\mathbf{x})$ are, respectively, the model predictions for the present-day stellar luminosity and stellar XUV luminosity given the state vector \mathbf{x} , L_* and L_{xuv} are their respective observed values, and $\sigma_{L_*}^2$ and $\sigma_{L_{\text{xuv}}}^2$ are the uncertainties on those observations. The $\ln \text{Prior}(\mathbf{x})$ term is the prior probability and C is an arbitrary normalization constant. Expressed in this form, the observed values of L_* and L_{xuv} are our “data,” while the constraints on the other parameters are “priors,” though the distinction is purely semantic.

Given this likelihood function, we use the Python code package `emcee` (Foreman-Mackey et al. 2013) to obtain the posterior probability distributions for each of the parameters of interest. We initialize each of the parameters in \mathbf{x} by drawing from their respective prior distributions and run 40 parallel chains of 5,000 steps each, discarding the first 500 steps as burn-in. The marginalized posterior distributions for the stellar mass, saturation fraction, saturation timescale, age, semi-major axis, planet mass, present-day stellar luminosity, present-day stellar XUV luminosity, and duration of the runaway greenhouse are shown in Figure 15 as the black histograms. The red curves indicate our priors/data, and the blue curves are Gaussian fits to the posteriors. The fit to the runaway greenhouse duration posterior yields $t_{\text{RG}} = 169 \pm 13 \text{ Myr}$.

By construction, the planet mass, stellar age, present-day stellar luminosity, and present-day stellar XUV luminosity posteriors reflect their prior distributions. As mentioned above, the stellar mass posterior is entirely informed by the luminosity posterior via the Spada et al. (2013) stellar evolution tracks. The stellar mass in turn constrains the semi-major axis (via the prior on the pe-

riod and Kepler’s laws). The XUV saturation fraction is fairly well constrained by the present-day XUV luminosity; a log-normal fit to its posterior yields $\log f_{\text{sat}} = -3.1 \pm 0.5$, which is fully consistent with the observation that M dwarfs saturate at or below $\log f_{\text{sat}} \approx -3$ (Jackson et al. 2012; Shkolnik & Barman 2014). The longer tail at high f_{sat} results from the fact that this parameter is strongly correlated with the saturation timescale, t_{sat} (see Figure 20 below). If saturation is short-lived, the initial saturation fraction must be higher to match the present-day XUV luminosity. Interestingly, our runs do not provide any constraints on t_{sat} , whose value is equally likely (in log space) across the range [0.5, 10] Gyr. Finally, the posterior for the XUV power law exponent β_{xuv} (not shown in the Figure) is the same as the adopted prior, as the present data are insufficient to constrain it.

The two quantities that are most relevant to habitability — the final water content $m_{\text{H}_2\text{O}}$ and final O_2 atmospheric pressure P_{O_2} of Proxima b — depend on four additional parameters we must specify: the initial water content $m_{\text{H}_2\text{O}}^0$, the initial hydrogen mass m_{H}^0 (if the planet formed with a primordial envelope), the XUV escape efficiency ϵ_{xuv} , and the O_2 uptake efficiency ζ_{O_2} of the planet surface. In principle, planet formation models could provide priors on $m_{\text{H}_2\text{O}}^0$ and m_{H}^0 , but such models depend on additional parameters that are unknown or poorly constrained. The same is true for the XUV escape efficiency, which can be modeled as in Ribas et al. (2016), and the rate of absorption of O_2 at the surface, which can be computed as in Schaefer et al. (2016). However, given the large number of unknown parameters needed to constrain these four parameters, for simplicity we perform independent MCMC runs for fixed combinations of these parameters. This approach circumvents potential biases arising from incorrect priors on these parameters while still highlighting how our results scale with different assumptions about their values. Note that the net water loss posteriors are qualitatively similar for $\epsilon_{\text{xuv}} = 0.15$ and $\epsilon_{\text{xuv}} = 0.05$, justifying our use of energy-limited escape.

In the runs discussed below, our default values are $m_{\text{H}_2\text{O}}^0 = 5 \text{ TO}$, $m_{\text{H}}^0 = 0 \text{ M}_\oplus$, $\epsilon_{\text{xuv}} = 0.15$, and $\zeta_{\text{O}_2} = 0$, and we vary each of these parameters in turn. Figure 16 shows the marginalized posterior distributions for the present-day water content (left column) and present-day O_2 atmospheric pressure (middle column), as well as a joint posterior for the two parameters (right column) for three different values of ϵ_{xuv} : **(a)** 0.15, **(b)** 0.05, and **(c)** 0.01. In the first two cases, the planet loses all or nearly all of the 5 TO it formed with, building up several hundred bars of O_2 (with distributions peaking at about 700 bars and with a spread of several hundred bars). For $\epsilon_{\text{xuv}} = 0.15$, about 10% of runs result in no substantial oxygen remaining in the atmosphere; in these runs, the escape was so efficient as to remove all of the O_2 along with the escaping H. In the final case, the amount of water lost is significantly smaller: about 2 TO on average, with a peak in the distribution corresponding to a loss of about 0.8 TO. The amount of O_2 remaining is similarly smaller, but still exceeding 100 bars and with a similar spread as before. Finally, the joint posterior plots emphasize how correlated the present-day water and oxygen content of Proxima b are. Since the rate at which oxygen

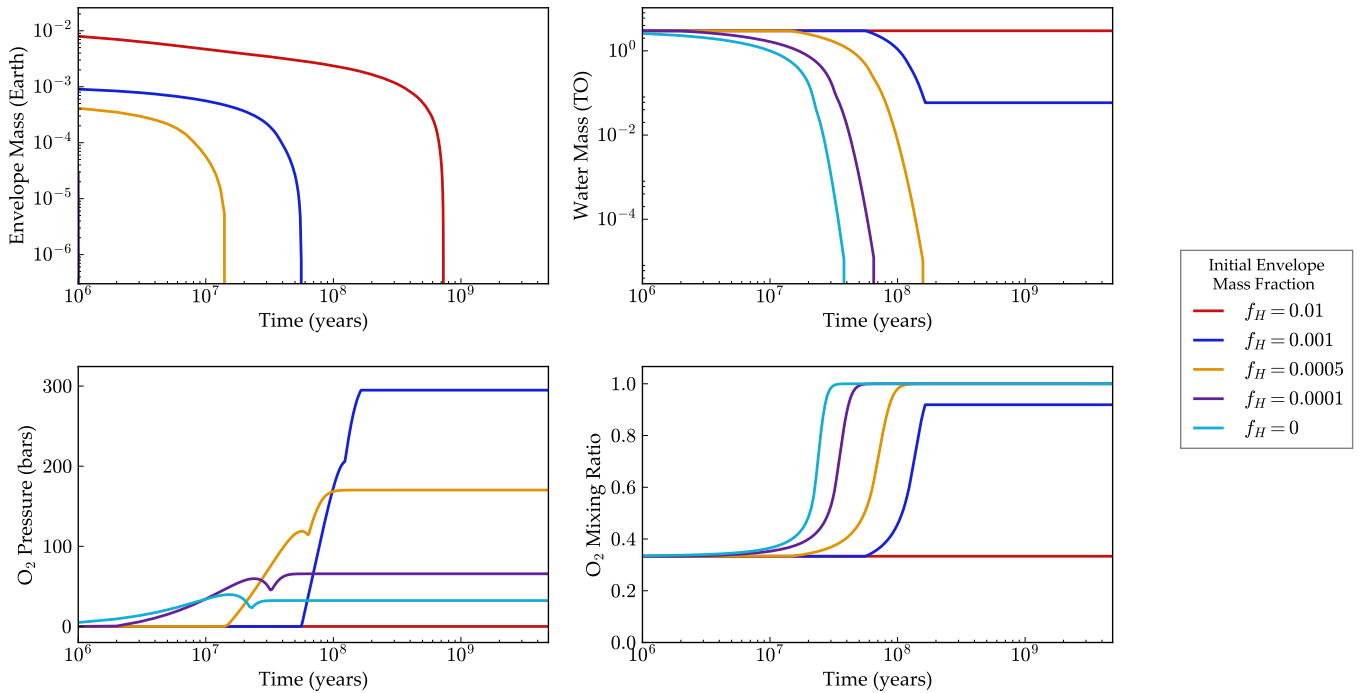


Figure 14. Evolution of the water and O_2 contents assuming Proxima b formed with a hydrogen envelope and 3 TO. Line colors correspond to different initial envelope mass fractions f_H , ranging from 0.0001 to 0.01. In all cases, the envelope escapes completely prior to 1 Gyr. For $f_H \lesssim 0.001$, the H envelope escapes quickly enough to allow complete desiccation of the planet prior to its arrival in the HZ at ~ 170 Myr. For $f_H \approx 0.01$, the envelope escapes a few hundred Myr *after* the planet enters the HZ, preventing any water from being lost and O_2 from accumulating in the atmosphere. This is the most favorable scenario for a potentially habitable Proxima b.

builds up in the atmosphere is initially constant (Luger & Barnes 2015), and since the amount of water lost scales with the duration of the escape period, there is a tight linear correlation between the two quantities (lower right hand corner of the joint posterior plots). However, as the atmospheric mixing ratio of oxygen increases, the rate at which hydrogen escapes—and thus the rate at which oxygen is produced—begins to decrease, leading to a break in the linear relationship once ~ 600 – 700 bars of oxygen build up and leading to the peak in the O_2 posteriors at around that value.

Figure 17 is similar to Figure 16, but shows runs assuming Proxima Cen b formed with 10 TO of water. As before, the rows correspond to different escape efficiencies (0.15, 0.05, 0.01, from top to bottom). The amount of water lost increases in all cases, and for $\epsilon_{\text{xuv}} = 0.15$ the planet is desiccated or almost desiccated in about 20% of runs. The amount of O_2 that builds up is similar to that in the previous figure, but O_2 pressures exceeding 1000 bars are now possible in 20–30% of cases for XUV efficiencies of 0.15 or 0.05.

It is interesting to note that in Figures 16 and 17 the posterior distributions for $\epsilon_{\text{xuv}} = 0.15$ and $\epsilon_{\text{xuv}} = 0.05$ are qualitatively similar. The median amount of water remaining in Figure 16 is ~ 0.1 and 0.3 TO for $\epsilon_{\text{xuv}} = 0.15$ and 0.05 , respectively, while the median oxygen pressure is ~ 600 bar in both cases. In Figure 17, the median water remaining is ~ 3 and 5 TO for $\epsilon_{\text{xuv}} = 0.15$ and 0.05 and the median oxygen pressure is again the same in both cases at ~ 700 bar. This is because the total amount of water lost does *not* scale linearly with ϵ_{xuv} , as the hydrodynamic drag on oxygen atoms acts as a negative feedback that stabilizes the net water loss rate. At high efficiency, the drag on the oxygen atoms is stronger and more of the energy goes into driving oxygen escape, which is *less* efficient at depleting the water (since oxygen atoms are heavier). At low efficiency, most of the energy goes into driving hydrogen escape, which is *more* efficient at depleting the water. As a result, our water loss amounts change little when ϵ_{xuv} is varied by a factor as large as ~ 3 .

In Figure 18 we explore the effect of varying the initial hydrogen content of the planet. From top to bottom, the rows correspond to initial hydrogen masses equal to 0.01, 0.001, and $10^{-4} M_{\oplus}$. In the first two cases, the effect of the envelope is clear, as most planets lose no water and build up no oxygen. These are mostly cases in which a portion of the hydrogen envelope remains at the present day. However, if the initial hydrogen mass is on the order of $10^{-4} M_{\oplus}$ (corresponding to roughly 100 times Earth’s total atmospheric mass), the shielding effect of the envelope is almost negligible; compare panel (c) to the top panel in Figure 16 (the default run). In this case, most of the water is lost to space in the majority of the runs.

In Figure 19 we show the posteriors assuming the O_2 uptake efficiency of the surface $\zeta_{O_2} = 1$, corresponding to instant O_2 removal by the surface. Compare to the top panel of Figure 16. In this case, the O_2 posterior corresponds to the total amount of oxygen absorbed by the surface, expressed in bars. While the total amount of oxygen retained by the planet is similar, the fraction of runs in which the planet loses all of its water increases from $\sim 0.2\%$ to $\sim 0.8\%$. This increase occurs because

the buildup of atmospheric O_2 throttles the escape of hydrogen by decreasing its mixing ratio in the upper atmosphere; when O_2 is quickly absorbed at the surface, hydrogen can escape more easily.

Finally, it is interesting to explore the various correlations between the parameters of the model. It is clear from the previous figures that the amount of oxygen that builds up strongly correlates with the amount of water lost from the planet, but additional correlations also exist. In Figure 20 we plot the joint posteriors for the XUV saturation fraction, XUV saturation timescale, XUV power law exponent, present-day XUV luminosity, present-day water content, and present-day O_2 content for a run with $m_{\text{H}_2\text{O}}^0 = 5$ TO, $m_{\text{H}}^0 = 0$, $\epsilon_{\text{xuv}} = 0.01$, and $\zeta_{O_2} = 0$. The marginalized posteriors are shown at the top. The strongest correlations are between the final water and O_2 contents and the XUV saturation fraction (first column, bottom two panels). The higher the XUV saturation fraction, the more water is lost and the more O_2 builds up. While this result may be unsurprising, neither the saturation timescale (second column) nor the power law exponent (third column) correlate as strongly with the water and O_2 content. For saturation timescales longer than about 2 Gyr, the exact duration of the saturation phase does not affect the evolution of the planet, since nearly all of the water loss occurs in the first few 100 Myr. For the same reason, the value of the power law exponent does not significantly correlate with the water or oxygen. On the other hand, the present-day XUV luminosity does correlate with water loss, as it implies a higher XUV luminosity at early times. An accurate determination of f_{sat} and more precise measurements of L_{xuv} are therefore critical to determining the evolution of the water content of Proxima b.

4.4.3. Summary of Atmospheric Evolution Simulations

The posterior distributions of Proxima b’s present-day water and oxygen content support our findings in §4.4.1 based on the fiducial model parameters. Given our assumptions and evolutionary model, the planet spent $t_{\text{RG}} = 169 \pm 13$ Myr in a runaway greenhouse. During this time, we find that it may have lost on the order of 5 TO of water and built up more than 500 bars of O_2 on average for a wide range of model assumptions. However, the posterior distributions for the water content (Figures 16–19, left columns) are distinctly non-Gaussian, with substantial peaks at or near a present-day water content of 0 for initial water contents up to 10 TO.

There are three broad scenarios in which Proxima b does not lose most of its initial water content. The first scenario is for initial water inventories of 10 TO (or higher). In these cases Proxima b may lose up to half its water and build up on the order of 500 bars of O_2 , but may be habitable today.

The second scenario is for an XUV escape efficiency $\epsilon_{\text{xuv}} \sim 0.01$, in which case only about 1 TO is lost on average. Such a low escape efficiency may have been possible during the first ~ 10 Myr, when the XUV flux at Proxima b likely exceeded 10^5 erg/cm²/s and recombination radiation contributed significantly to cooling the flow (Murray-Clay et al. 2009). In this case, hydrodynamic models predict efficiencies as low as 0.02–0.03 (Bolmont et al. 2017). For reference, for Proxima b’s present-day XUV flux, the model of Bolmont et al. (2017)

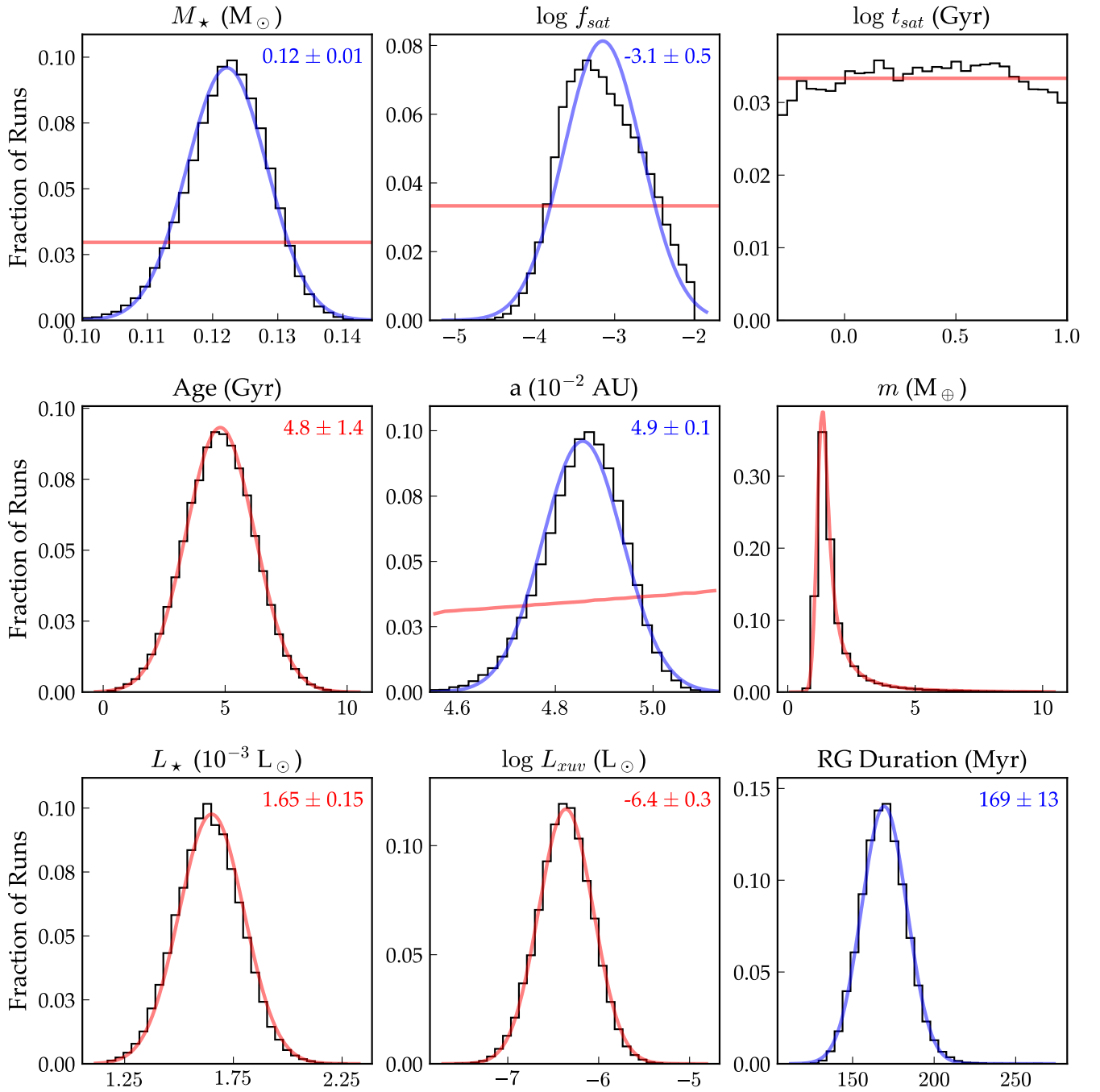


Figure 15. Posterior distributions for the various stellar parameters used in the model. The first eight parameters are model inputs, with their corresponding priors shown in red. The combination of these priors and the physical models in VPLANET constrain the stellar and planetary parameters shown in this section. Blue curves show Gaussian fits to the posterior distributions, with the mean and standard deviation indicated at the top right. The last panel shows the duration of the runaway greenhouse phase for Proxima Centauri b, one of the model outputs, which we find to be 169 ± 13 Myr.

predicts $\epsilon_{\text{xuv}} \approx 0.1$.

The final scenario in which Proxima b does not lose most of its water is if it formed with a substantial hydrogen envelope. For an initial envelope mass fraction $\gtrsim 10^{-4}$ (corresponding to a mass greater than 100 times Earth’s total atmospheric mass), the envelope takes several hundred Myr to fully escape, shielding the surface water during the star’s most active phase. This corresponds to the “habitable evaporated core” scenario of Luger et al. (2015). However, this scenario requires a certain amount of fine tuning, see § 4.6. If Proxima b formed with more than 0.01 of its mass in hydrogen and/or if it is significantly more massive than $1.27 M_{\oplus}$, the envelope may not have completely escaped and the planet may not be habitable today.

For reference, Figures 21 and 22 show a synthesis of runs of our model assuming the fiducial stellar parameters and varying several of the planet properties. The two figures help identify cases in which Proxima Cen b may presently be habitable.

4.5. Internal Evolution

4.5.1. Role of Radiogenic Abundances

Modeling the internal evolution of Proxima b is challenging due to the large number of unknowns about its composition, structure, thermal state, atmosphere, and the evolution of its radiation environment. In this section we first consider how radiogenic abundances could affect its evolution, followed by considerations of tidal heating.

As described in § 3.6 we consider four possible abundance patterns for Proxima b: Earth-like, chondritic, 1 ppt ^{26}Al , and inert (no radioactivity). In all cases we begin with a core temperature of 6000 K and a mantle temperature of 3000 K.

In Fig. 23 we show the evolution of the radiogenic power, mantle temperature, inner core radius, magnetic moment, magnetopause radius and surface energy flux for the four cases. The dashed black lines represent the modern Earth’s value. In the top left panel we show the evolution of the total radiogenic power produced in the core, mantle and surface. Initially, the power from ^{26}Al is over 2×10^{18} W, but with a half-life of 700,000 years, its contribution to the energy budget drops to 0 within 10^7 years. The Earth-like case is hidden behind the ^{26}Al curve except at $t = 0$.

The mantle temperature is shown in the top right panel. As expected the model predicts a rapid cooling in response to the decay of ^{26}Al , so that after 100 Myr the mantle temperatures are similar and the planet settles into an Earth-like evolution. Thus, if heating from ^{26}Al is just a passing energy source, it may not affect the evolution. At this time, we merely point out that the influence of ^{26}Al could be significant for planets with formation times of order 1 Myr, which is similar to ^{26}Al ’s half-life. The inert case temperature drops quickly with no radiogenic power in the interior, while the chondritic case shows increased temperature for the entirety of the simulation for the mantle heat flow to accommodate the high heat source.

The cases with earliest inner core solidification (Figure 23, middle left panel) are the inert and chondritic ones, which have the most and least total radiogenic power, respectively. In the inert case the interior loses secular

heat faster with no radiogenic heat source. Counterintuitively the chondritic case also cools faster than the nominal model, likely because the core cooling rate is roughly a constant fraction of the total surface heat flow, which is much higher in this case. We note that changing the core composition could have a major impact on the inner core solidification rate and should be the subject of future work.

The middle right panel of Figure 23 shows the evolution of the planet’s magnetic moment for the four different cases. Each case shows similar behavior — a gradually decaying field as the core cools, with a cusp when the inner core first nucleates. The ^{26}Al case shows the largest field due to an early super-heating of the core, despite being otherwise very similar to the Earth case.

Finally, the bottom right panel shows the surface energy flux for each case. Not surprisingly the chondritic case maintains the highest heat fluxes, near 1 W/m^2 , which is similar to Io’s value of 2.5 W/m^2 (Veeder et al. 1994).

4.5.2. Evolution with Tidal Heating

Next, we examine the role of tidal heating on the evolution of the planet’s interior and orbit. For simplicity we consider the “Earth” radiogenic case with three initial eccentricities: 0.05, 0.1 and 0.2. In Fig. 24 we show the evolution of 9 quantities as a function of time.

The tidal power in these cases can be in excess of 100 TW, or twice the total power of the modern Earth. Similar to Driscoll & Barnes (2015), we find that the planet’s tidal properties evolve in response to the thermal state of the interior, avoiding unrealistically large tidal powers predicted by simpler equilibrium tide models; see above. Tidal heating increases mantle temperature, lowering mantle viscosity, which raises the tidal Q after an initial peak during mantle solidification. A “tidal steady state”, as defined in Driscoll & Barnes (2015), is possible where the surface heat flow balances tidal dissipation in the mantle so that the planet cools very slowly. This quasi-steady state relies on the negative feedback between mantle temperature and tidal dissipation and the positive feedback between temperature and heat flow, so that a decrease in temperature causes increased tidal heating, pushing the temperature back up.

The mantle cooling rate is more sensitive to tidal dissipation than the core because dissipation in the model occurs only in the mantle. The core cooling rate does change somewhat with tidal dissipation, but its effect on the magnetic moment is muted because the magnetic moment depends on core convective heat flux to the $1/3$ power. Note, however, that the inner core grows earlier and more rapidly than in the Earth case of Fig. 23 because a hotter mantle is less viscous, thinning the thermal boundary layer above the core-mantle boundary layer, allowing the core to cool slightly faster (Driscoll & Barnes 2015). Although none of our cases achieves a fully solid core, which would quench the dynamo, they are approaching that limit, and given the uncertainty in both the composition and structure of Proxima b, it is possible that the core has already solidified, preventing a core dynamo, and exposing the atmosphere to stellar flares.

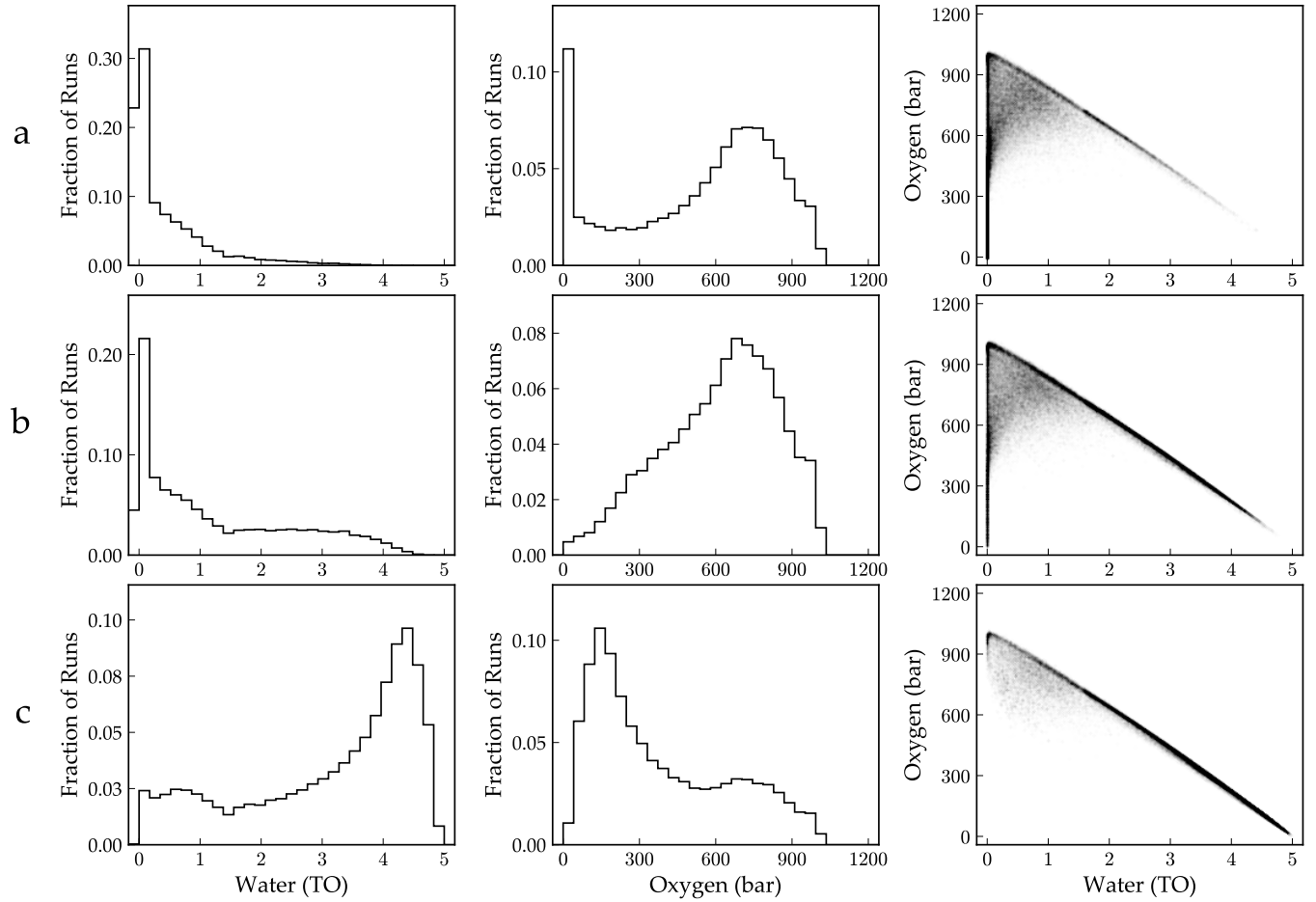


Figure 16. Marginalized posteriors for the present-day water content (left) and atmospheric oxygen pressure (center) on Proxima Centauri b. The joint posteriors for these two parameters are shown at the right. **(a)** Posteriors for the default run ($m_{\text{H}_2\text{O}}^0 = 5 \text{ TO}$, $m_{\text{H}}^0 = 0$, $\epsilon_{\text{xuv}} = 0.15$, $\zeta_{\text{O}_2} = 0$). **(b)** Same as (a), but for $\epsilon_{\text{xuv}} = 0.05$. **(c)** Same as (a), but for $\epsilon_{\text{xuv}} = 0.01$. For $\epsilon_{\text{xuv}} \gtrsim 0.05$, the planet is desiccated or almost desiccated and builds up between 500 and 900 bars of O_2 in most runs. For $\epsilon_{\text{xuv}} \sim 0.01$, the planet loses less water and builds up less O_2 , though the loss of more than 1 TO is still likely.

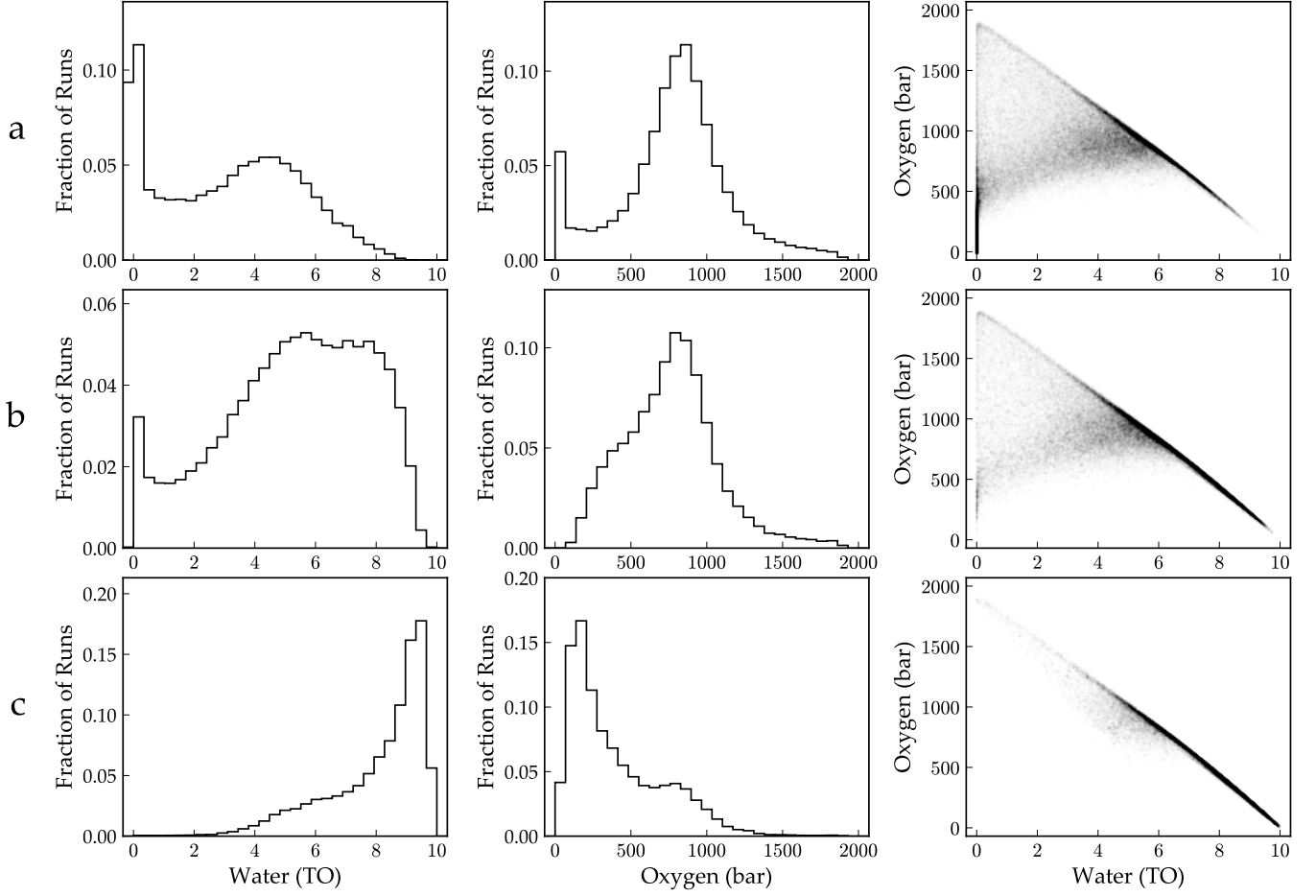


Figure 17. Similar to Figure 16, but for an initial water content $m_{\text{H}_2\text{O}}^0 = 10$ TO. As before, the rows correspond to XUV escape efficiencies of 0.15, 0.05, and 0.01 from top to bottom, respectively. For high XUV efficiency, Proxima Cen b loses more than 5 TO in most runs (and is desiccated in $\sim 20\%$ of runs). At lower efficiency, the planet loses less water. The amount of O_2 that builds up is similar to before, but a buildup of more than 1000 bars is now possible.

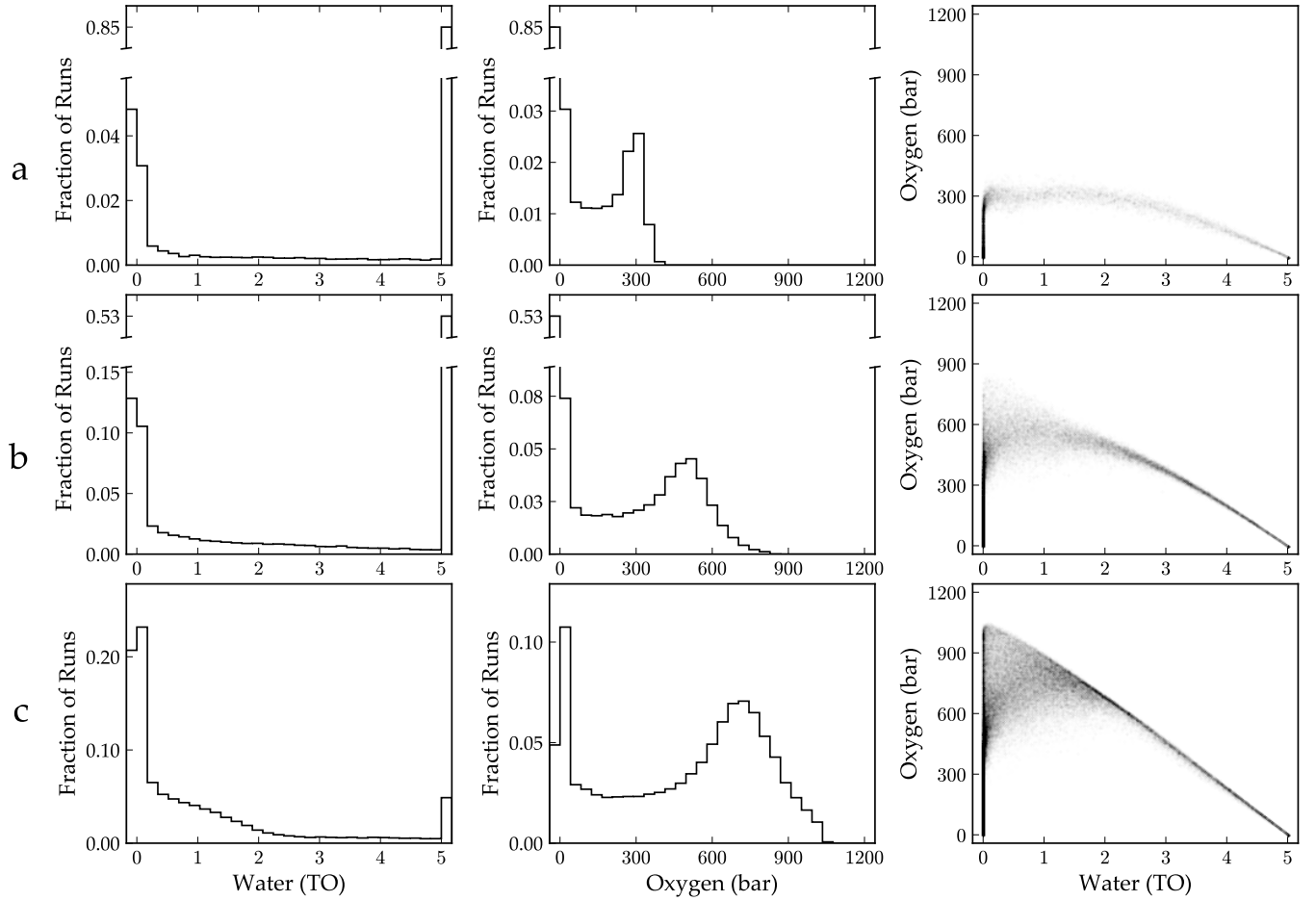


Figure 18. Similar to Figure 16, but this time varying the initial mass of the primordial hydrogen envelope of Proxima Cen b. Other parameters are set to their default values. The initial mass of hydrogen is $m_{\text{H}}^0 =$ (a) $0.01 M_{\oplus}$, (b) $0.001 M_{\oplus}$, and (c) $10^{-4} M_{\oplus}$. Note the broken axes in the first two rows. In the first two cases, no water is lost in more than half of the runs; in such cases, a thin hydrogen envelope remains today. In the final case, most planets lost all their hydrogen and all their water. In order to prevent the runaway loss of its water, Proxima Cen b must have formed with more than 0.01% of its mass in the form of a hydrogen envelope.

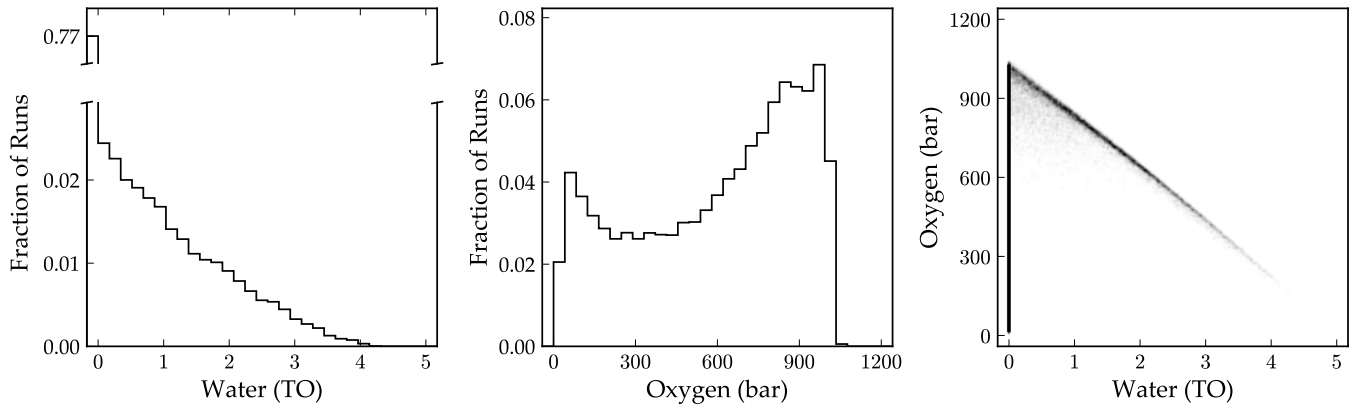


Figure 19. The same as panel (a) in Figure 16, but for efficient surface sinks ($\zeta_{\text{O}_2} = 1$). The O_2 posterior now corresponds to the amount of oxygen (in bars) absorbed at the planet surface. The absence of atmospheric O_2 facilitates the loss of hydrogen, which must no longer diffuse through the O_2 to escape. In this case, nearly 80% of runs result in complete desiccation (note the broken axis in the first panel). In all cases, Proxima b loses at least 1 TO.

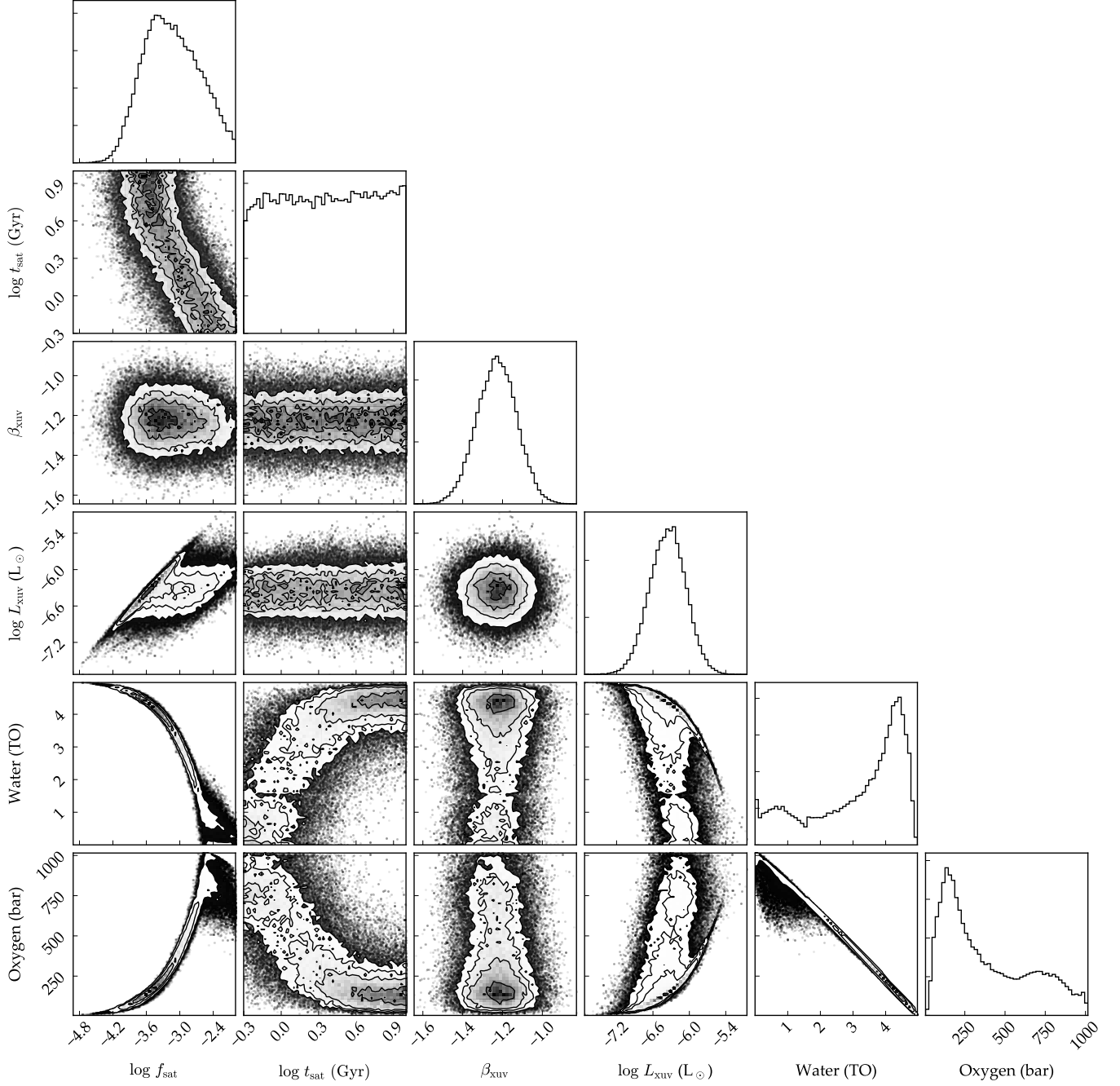


Figure 20. Joint posteriors of selected parameters for a run with $\epsilon_{\text{xuv}} = 0.01$ [same as Figure 16(c)]. In addition to the correlation between the amount of water lost and the amount of O_2 that builds up, several strong correlations stand out. The strongest ones are between the XUV saturation fraction f_{sat} and the water content (negative) and O_2 pressure (positive). Since most of the water loss occurs in the first few 100 Myr, the value of f_{sat} is the single most important parameter controlling the present-day water and O_2 content of Proxima Cen b. The saturation timescale also correlates with the water and oxygen, but not as strongly; for $t_{\text{sat}} \gtrsim 2$ Gyr, its exact value does not significantly affect the evolution of the planet. Shorter saturation timescales correlate with higher saturation fractions and therefore indirectly affect the evolution. Interestingly, the correlation between the XUV power law slope β_{xuv} and the water or O_2 content is negligible, since once saturation ends the water loss rate plummets — the final water content depends almost entirely on the properties of the star early on.

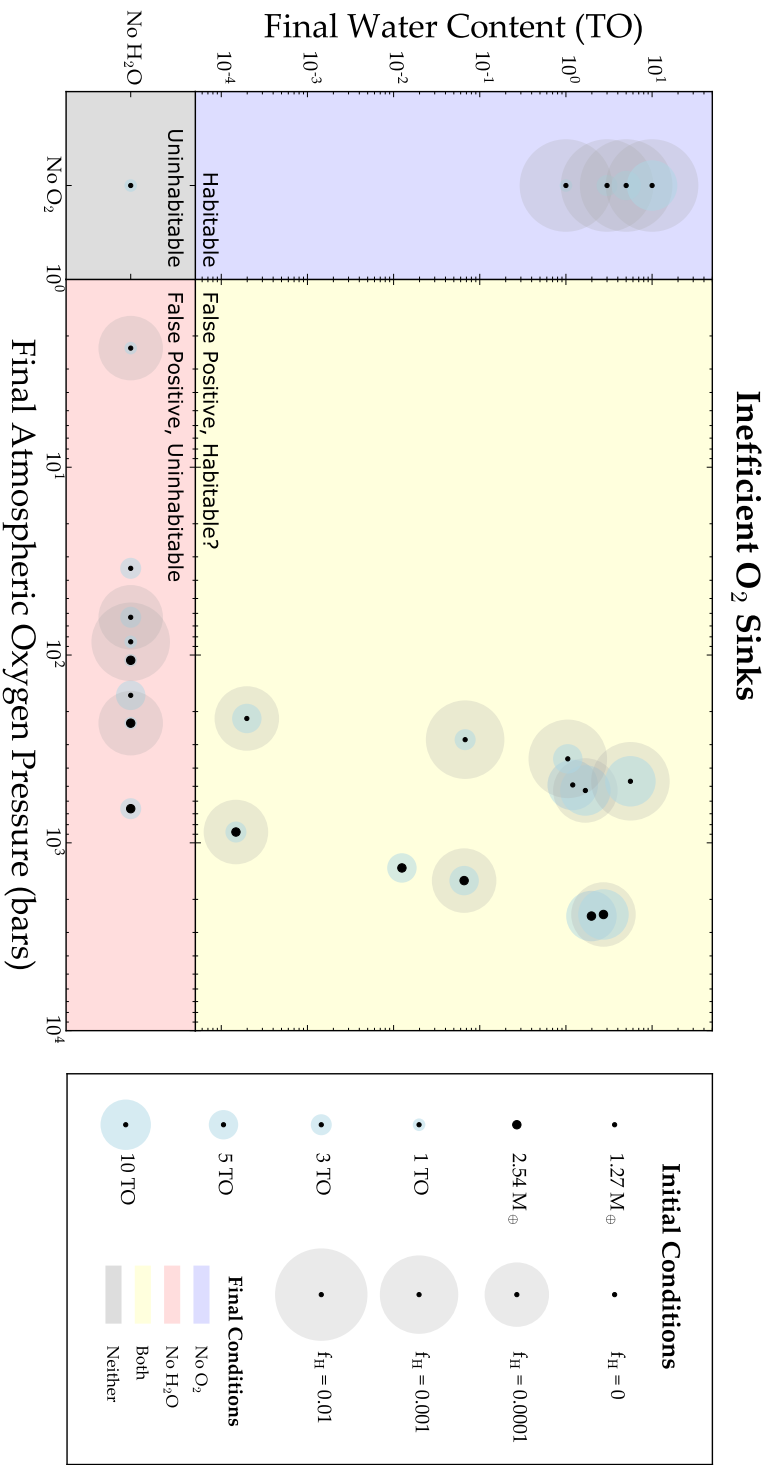


Figure 21. Multiple evolutionary pathways for the water on Proxima b. These plots show the final water and final atmospheric O₂ content of the planet for a suite of different initial conditions, assuming inefficient surface sinks for O₂. Different marker styles indicate different values of the planet mass, the initial water content, and the initial hydrogen envelope mass fraction f_H (the final value of f_H is zero for all planets shown here). Each panel is divided into quadrants, corresponding to planets that at the end of the simulation have water but no O₂ (top left, blue), water and O₂ (top right, yellow), neither water nor O₂ (bottom left, gray), and O₂ but no water (bottom right, red). Habitable planets are those in the region shaded blue. Planets in the grey region are desiccated and therefore uninhabitable. Planets in the red region are likewise uninhabitable, but may have atmospheric O₂, which could be incorrectly attributed to biology. Finally, planets in the yellow region are habitable, since they have abundant surface water, but may also have substantial atmospheric O₂, which could be an impediment to the origin of life. These planets are also particularly problematic in the context of atmospheric characterization, as the presence of water and O₂ could fool observers into believing they are inhabited.

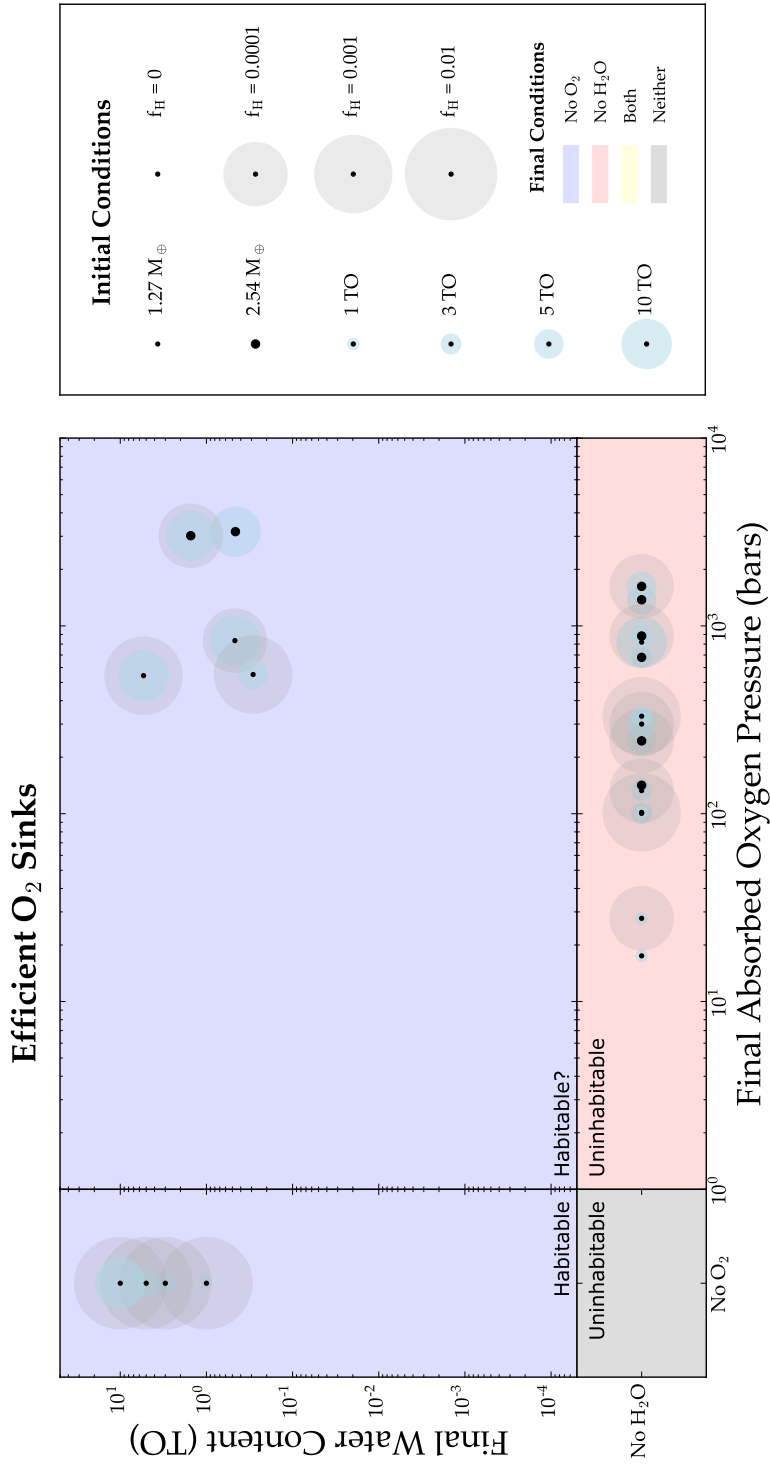


Figure 22. Same as Fig. 22, but assuming Proxima b has efficient O₂ sinks, preventing the buildup of significant oxygen in the atmosphere. The *x* axis now shows the total amount of oxygen absorbed at the surface.

4.6. Habitable Evaporated Core Scenarios

Since a possible path towards habitability for Proxima b is the “habitable evaporated core” scenario of Luger et al. (2015), we seek to model how the presence of a hydrogen envelope and surface oceans undergoing atmospheric escape impact the tidal and orbital evolution of Proxima b. To do so, we couple the atmospheric escape physics of `ATMESC`, tidal evolution using `EQTIDE`, the Earth-calibrated geophysical interior models of `RADHEAT` and `THERMINT` and the stellar evolution of `STELLAR`.

We model the combined tidal contributions of the envelope, oceans, and solid interior via the following equation

$$-Im(k_2) = -Im(k_2)_{interior} + \frac{k_{2_{ocean}}}{Q_{ocean}} + \frac{k_{2_{envelope}}}{Q_{envelope}}, \quad (6)$$

where $Im(k_2)$ is the imaginary part of the Love number, k_2 is the Love number of order 2, and Q is the tidal quality factor (see Barnes et al. 2013; Driscoll & Barnes 2015). In Eq. (6) we remove terms if there is no component to contribute to Proxima b’s net tidal interaction, *i.e.* no ocean or no envelope.

In the general case when a hydrogen envelope is present, we only consider the coupled tidal effects of the interior and the envelope as any water is likely to be supercritical due to the high pressure exerted by the envelope. In our model, we account for this case by neglecting the ocean term from Eq. (6) when the mass of the hydrogen envelope is non-zero. When an envelope is not present, we consider the tidal contribution of surface oceans only if the planet is not in the runaway greenhouse limit since otherwise all water would be present in the atmosphere as steam. To determine if the planet is in the runaway greenhouse limit, we check to see if the flux the planet receives is greater than or equal to the mass-dependent runaway greenhouse limit of Kopparapu et al. (2014) appropriate for Proxima Centauri. In our model when the planet is in the runaway greenhouse limit, we neglect the ocean term from Eq. (6) and the planet’s $Im(k_2)$ is set by the solid interior term in Eq. (6).

We simulate four cases that bracket the potential past tidal evolution of Proxima b. The first case, “CPL,” is a simple application of the constant phase lag tidal model that probes how Proxima b’s orbit would evolve due to tides if it was an Earth-like planet with persistent surface oceans. This case assumes constant tidal $Q = 12$, consistent with observations of Earth today (Dickey et al. 1994; Williams et al. 1978; Yoder 1995). This low tidal Q is due to efficient energy dissipation by oceans and leads to rapid tidal evolution, while still acknowledging that the tidal Q of the surface oceans may depend on the total ocean mass and the presence and topology of shallow seas, which should be explored in future studies. The “No Ocean” case assumes a dry, rocky planet in which the tidal interaction is dominated by the planet’s interior as determined by `RADHEAT` and `THERMINT`. The “Ocean” case couples the rocky planet from the “No Ocean” case with an ocean containing an initial water inventory of 10 TO with $Q_{ocean} = 12$ (Dickey et al. 1994; Williams et al. 1978; Yoder 1995). We chose an initial water inventory of 10 TO to ensure that water loss due to atmospheric escape would not desiccate the planet such that the liquid surface oceans would exist after the runaway greenhouse phase allowing both the oceans and interior

to impact the planet’s tidal evolution. Finally, the “Envelope” case examines the tidal history of the “habitable evaporated core” scenario first explored by Luger et al. (2015), and described in detail for Proxima b above. For this simulation, we couple the interior evolution from the “No Ocean” case, liquid surface oceans, and a hydrogen envelope that has an initial mass fraction of 0.001 of the planet’s total mass with $Q_{envelope} = 10^4$. This choice of the tidal Q for the gaseous envelope is consistent with measurements of Neptune’s tidal Q (Zhang & Hamilton 2008). The “Envelope” case starts with 3.5 TO of liquid surface oceans to demonstrate the envelope’s ability to shield surface water from atmospheric escape (see § 4.4). We set $k_{2_{ocean}} = 0.3$ and $k_{2_{envelope}} = 0.01$ to let the thermal interior and oceans determine k_2 as these components likely dominate the tidal dissipation in the planet. All four simulations include the full stellar evolution of the star as determined by the `STELLAR` module. Simulations which include liquid surface oceans and/or a gaseous envelope use the atmospheric escape module `ATMESC`. Atmospheric escape calculations assume $\epsilon_{XUV} = 0.15$ as per the fiducial case of § 4.4. The results of the simulations are shown in Figure 25.

The “No Ocean” case, with tidal dissipation occurring primarily in the mantle, reaches a tidal Q of ~ 500 and undergoes minimal tidally-driven orbital evolution until after ~ 1 Gyr. Initially, the bulk of the surface flux stems from rotational tidal energy dissipation which lessens as the planet approaches a tidally locked state at around 15 Myr. Early on in the “Ocean” case, the planet is in a runaway greenhouse phase in which all the water is locked up in the atmosphere and subject to escape of hydrogen and oxygen via photolysis, decreasing the water mass. Its tidal evolution mirrors the “No Ocean” case as the tidal dissipation takes place in the mantle. After the stellar luminosity decreases to its main sequence value, the planet enters the HZ at ~ 150 Myr and the remaining water condenses to the surface. The presence of surface oceans after the runaway greenhouse phase for the “Ocean” and “Envelope” cases dramatically decreases the tidal Q , leading to rapid orbital circularization and a substantial surface flux increase via tidal energy dissipation.

Early on, the “Envelope” case has a slightly different surface flux and tidal Q than the “Ocean” and “No Ocean” cases as the envelope contributes minimally to the initial tidal evolution and as the planet’s radius evolves as the envelope experiences atmospheric escape. In the “Envelope” case, stellar XUV flux completely strips the hydrogen envelope after about 5×10^7 years, causing the mantle to again dictate the tidal interaction. The hydrogen envelope shields the planet’s water before it is completely stripped away, allowing enough to survive subsequent photolysis. About 1 TO of the initial 3.5 TO remain once the planet enters the HZ, assuming the planet has inefficient oxygen sinks (see § 4.4). With the envelope gone, surface water dominates the tidal interaction and the planet’s evolution mirrors the “Ocean” case.

The coupling of tidal evolution, interior geophysics, surface oceans, atmospheric escape, and stellar evolution permit a complicated evolutionary history for Proxima b which depend immensely on its properties at formation. Future planet formation studies that examine ini-

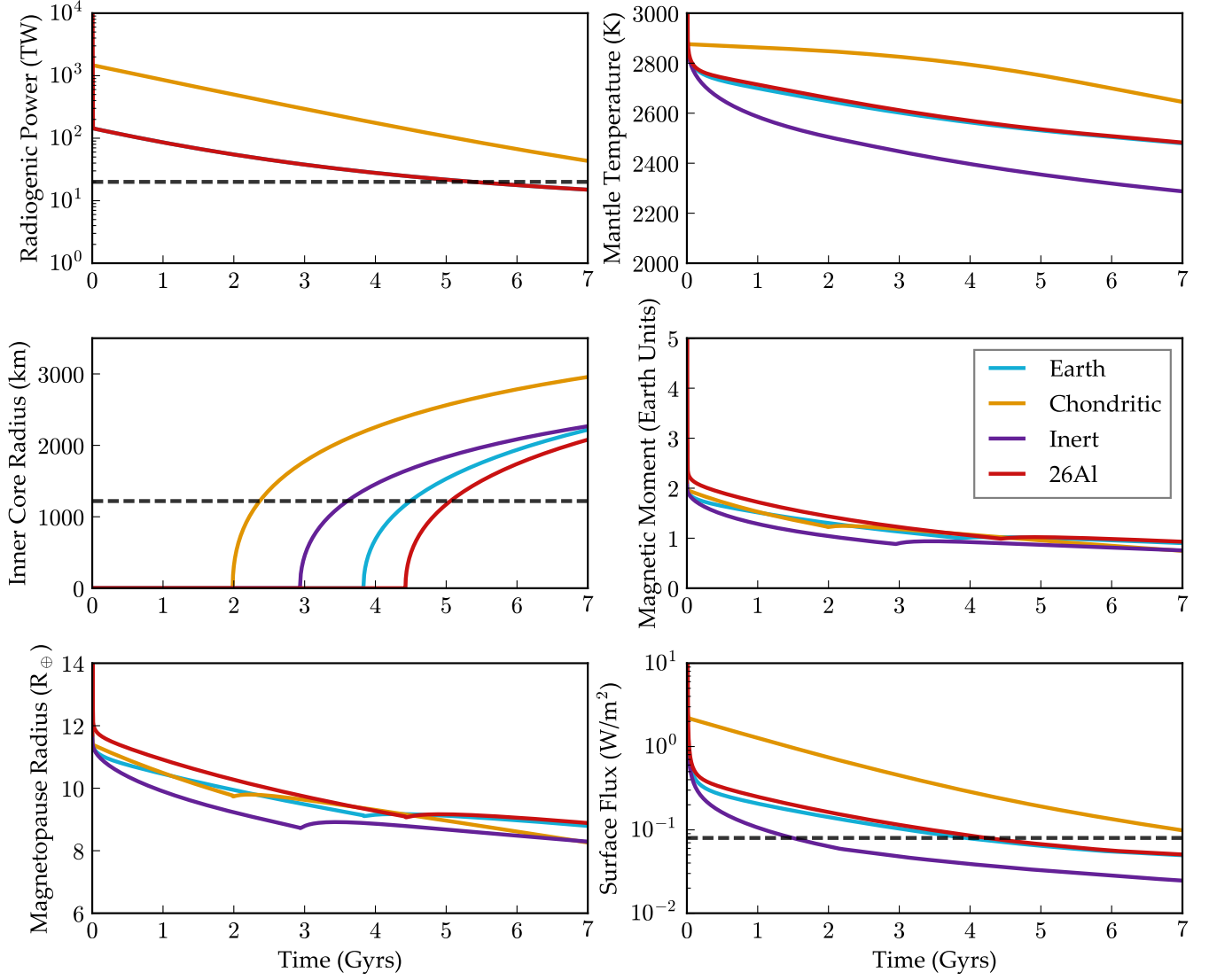


Figure 23. Evolution of internal properties of planet b for different assumptions of radiogenic inventory: Earth-like in blue, chondritic in orange, 1 part per trillion ^{26}Al in red, and inert in purple. Values for the modern Earth are shown with the dashed black line. *Top left:* Radiogenic power. The Earth curve is behind the ^{26}Al curve except for time = 0. *Top right:* Mantle Temperature. *Middle left:* Size of the solid inner core. *Middle right:* Magnetic moment. *Bottom left:* Magnetopause radius assuming the solar wind pressure at Proxima b is 0.2 times that at Earth. *Bottom right:* Surface energy flux.

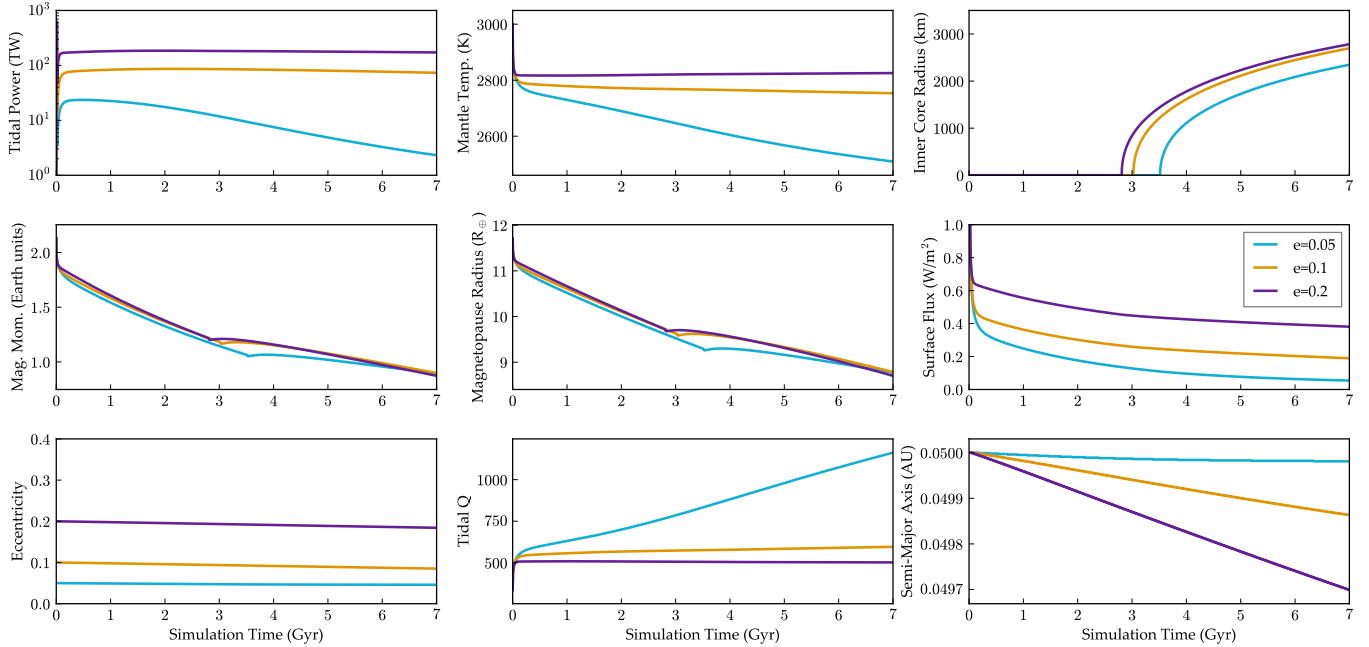


Figure 24. Evolution of internal properties of planet b for three different initial eccentricities, as shown in the legend, and assuming the Earth-like levels of radiogenic isotopes. *Top left:* Power generated by tidal heating. *Top middle:* Mantle temperature. *Top right:* Radius of the inner core. *Middle left:* Magnetic moment. *Middle:* Magnetopause radius. *Middle right:* Surface energy flux. *Bottom left:* Orbital eccentricity. *Bottom middle:* Tidal Q . *Bottom right:* Semi-major axis.

tial volatiles, analogous to Raymond et al. (2004, 2007), are critical to constrain potential evolutionary histories for this system.

5. DISCUSSION

In the previous section we outlined numerous influences on the history of Proxima b. We considered processes spanning the planet’s core to the Milky Way galaxy and find that effects at all these scales could be important in the history of our closest exoplanet. In this section, we summarize the results in terms of the potential atmospheres that Proxima b might have, which are considered in detail in Meadows et al. (2018). Then we examine the likelihood that it is currently habitable.

5.1. Atmospheric States

5.1.1. Earth-Like

We find that some scenarios produce a planet today that has surface water and rotates super-synchronously, i.e. is “Earth-like.” In particular, the “habitable evaporated core” scenario (Luger et al. 2015) is promising as it can mitigate both the high-luminosity pre-MS phase and any devastating tidal heating that may occur during orbital circularization from a primordial non-circular orbit after orbital destabilization (Barnes et al. 2013; Driscoll & Barnes 2015). Even if the planet became desiccated during the pre-MS phase, impact from water-rich bodies could simultaneously blow off the CO_2 and/or O_2 atmosphere while delivering water. This scenario would require a specific set of events to occur, but we note that close passages between Proxima and α Cen A and B could destabilize any putative “exo-Oort Clouds” that could have existed around the stars. The observed dust belt (Anglada et al. 2017) may be a remnant of such an encounter. Current numerical models do not permit a

robust calculation of the probability of such an event, but we cannot exclude it at this time.

Tidal damping of the spin is rapid, but there are at least four possibilities as to how the planet may currently rotate super-synchronously, all of which rely on Proxima b orbiting with non-zero eccentricity today. For $e > 0$, torques on the planet tend to increase the rotation period into either a “pseudo-equilibrium” value (Goldreich 1966; Zanazzi & Lai 2017), or into a spin-orbit resonance (Rodríguez et al. 2012; Ribas et al. 2016). The first possibility is that, if the system is on the younger side of the age distribution, and the initial eccentricity was very large, then the eccentricity might not have damped away, see Fig. 7. Second, the results of Section 4.1 demonstrate that a close encounter between Proxima and α Cen A and B can destabilize an extended planetary system (Fig. 6) and scatter Proxima b into a close, high eccentricity orbit. Since Proxima’s orbit evolves stochastically, and we cannot constrain the timing of the galactic migration, this instability could have occurred in the recent past, leaving Proxima b on an eccentric orbit today. Third, the planetary system could have experienced a late stage instability, independent of α Cen A and B. The so-called Nice instability in our Solar System occurred ~ 700 Myr after it formed (Gomes et al. 2005), and evidence is mounting that compact planetary systems are marginally stable and instabilities can occur Gyr after formation (Volk & Gladman 2015). Fourth, perturbations from other planets may delay circularization sufficiently that the orbit of Proxima b is currently large enough for capture into a spin-orbit resonance. We conclude that it is plausible that the rotation period of Proxima b is non-synchronous.

The obliquity of Proxima b is likely small, even in a Cassini state due to the influence of companion plan-

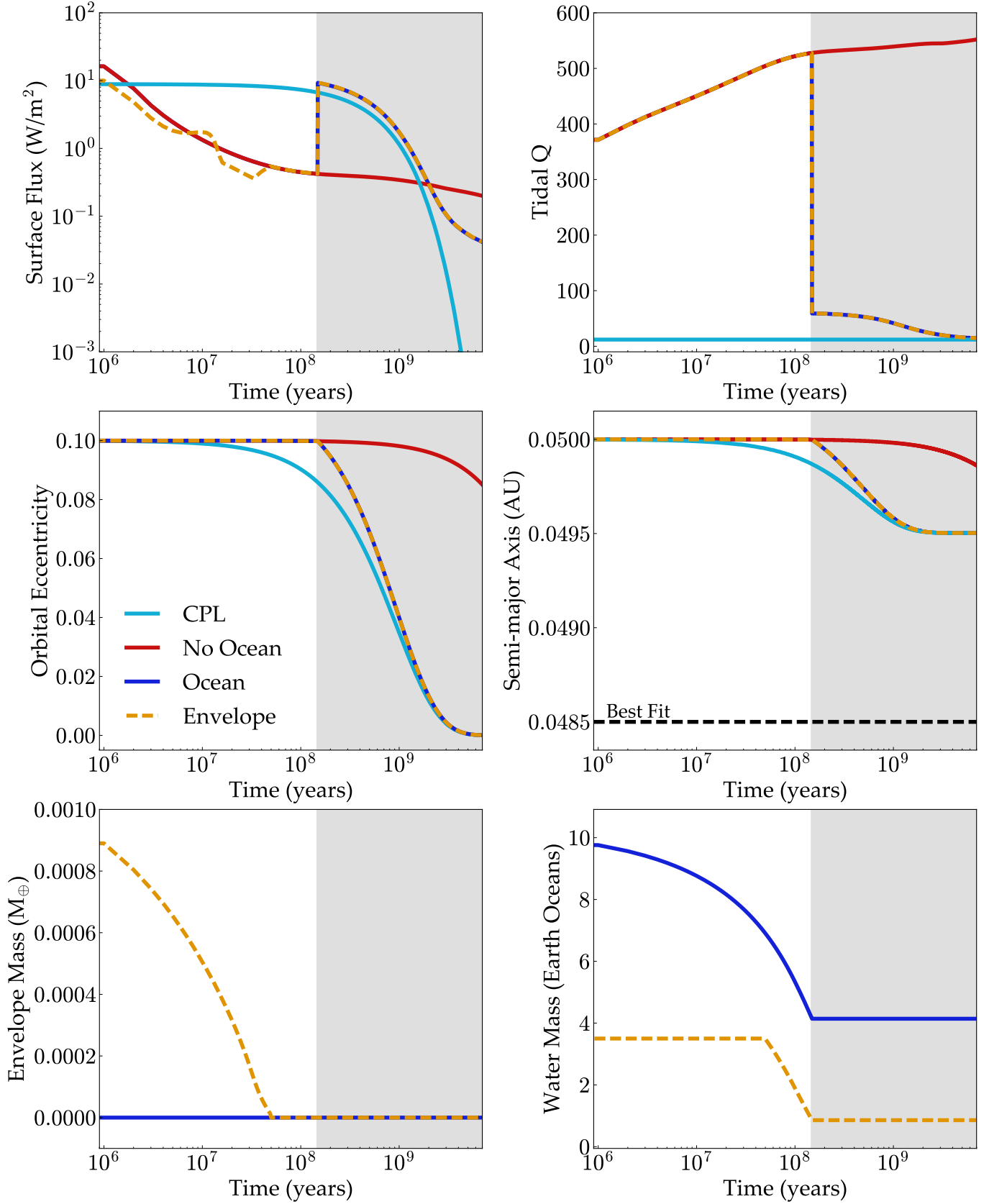


Figure 25. Evolution of the orbital, tidal and atmospheric properties of Proxima b for the “CPL” case in light blue, “No Ocean” case in red, “Ocean” case in dark blue, and the “Envelope” case in orange with the dashed line for clarity. The grey shaded region indicates when the planet is in the HZ. *Top left:* Surface Flux. *Top right:* Tidal Q. *Middle left:* Orbital Eccentricity. *Middle right:* Semi-major Axis. *Bottom left:* Envelope Mass. *Bottom right:* Surface Water Mass.

ets, due to tidal damping. Thus, we do not expect the obliquity to significantly impact the climate in the form of seasons or heat transport. The approximately zero obliquity of Proxima b is one feature that will produce a different climate than Earth’s.

5.1.2. *Habitable and Synchronously Rotating*

If the eccentricity is modest today, then Proxima b could be rotating synchronously. Although this rotation state has previously been considered dangerous for habitability (Mumford 1909; Dole 1964; Kasting et al. 1993), these planets may still be habitable (Joshi et al. 1997; Pierrehumbert 2011; Yang et al. 2013; Shields et al. 2016). If the planet is on a circular orbit and $\sin(\psi) = 0$, then the substellar point is constant in latitude and longitude and every location on the planet is either in permanent starlight or darkness. In this case, the daylight side may experience near-constant cloud-cover as the high temperature at the sub-stellar point constantly evaporates water (Yang et al. 2013). However, that result is for longer rotation periods that lead to weak a Coriolis force. Proxima b, with an orbital period of 11.2 days, may have a strong enough Coriolis force to shear the substellar clouds and weaken the cloud-albedo feedback. On the other hand, if the planet is covered in a global ocean and the greenhouse forcing is weak, then the planet may be in an “eyeball state” in which the planet is covered in ice except for a circular patch of open ocean at the substellar point (Pierrehumbert 2011).

If $e > 0$, then Proxima b will librate once per orbit as the ratio between the (constant) rotational frequency and the (oscillating) orbital frequency changes from pericenter to apocenter and back (Makarov et al. 2016). In this case, regions near the terminator can experience a day/night cycle, in which the star rises and sets from the same point in the horizon once per orbit. We are unaware of any research that explores the climate of a librating exoplanet, but our results suggest this state is the most likely for Proxima b and therefore such a simulation could be very enlightening. We hypothesize that for low eccentricity (low amplitude libration) the cloud feedback of Yang et al. (2013) would still operate, but that for larger e , the apparent movement of the substellar point could significantly impact the feedback, possibly destroying it. For reference, for $e = 0.05$, the librational amplitude is $\sim 5^\circ$.

5.1.3. *Super-Io*

Although Proxima b may have liquid water and be Earth-like, the planetary interior may be significantly hotter than Earth due to tidal heating or increased radiogenic abundances. Non-circular orbits, non-zero obliquities, and non-synchronous rotation all contribute to tidal heating, and hence even if the planet has water and super-synchronous rotation, it is probably not an “Earth twin” as far as the internal properties are concerned. Barnes et al. (2009) dubbed hot and very volcanically active terrestrial planets “super-Ios,” see also Jackson et al. (2008a). If the planet formed in colder region, it may be enhanced in ^{40}K relative to Earth and its interior may be very hot regardless of tidal heating. Although not modeled here, outgassing rates on Proxima b are probably higher than Earth’s due to tidal heating

and/or larger radiogenic heating, and potentially altering photochemistry and atmospheric structure. With no constraints on the composition of the solid planet, the thermal evolution and outgassing are poorly constrained, but the planet’s interior may be so hot that the surface is similar to Io’s. If the planet’s composition is similar to Io and volcanoes are constantly erupting, sulfur species may be present and remotely detectable in the atmospheres (Jackson et al. 2008a; Misra et al. 2015).

5.1.4. *Habitable and Dry*

As shown in Fig. 12, a dry planet would enter a potentially habitable state earlier than an Earth-like planet, and hence it may be that Proxima b is a habitable world, but with little liquid water (Abe et al. 2011). This could occur if the planet formed *in situ* and the gas disk was able to shield the planet from water loss. The “habitable evaporated core” scenario is also a possibility if the core was dry and a thin layer of hydrogen could be blown away. On the other hand, a planet without much water does not need to spend much time in a runaway greenhouse to become desiccated. Based on the modeling in § 4, we conclude that this possibility is very unlikely, but we cannot exclude it.

5.1.5. *Venus-Like*

Regardless of whether Proxima b spent significant time in a runaway greenhouse prior to the arrival of the HZ, it could be in a runaway greenhouse state like Venus. If it formed *in situ*, then this possibility is more likely because its first ~ 170 Myr were spent interior to the HZ and hence it may have developed a dense CO_2 atmosphere as has occurred on Venus. In the companion paper (Meadows et al. 2018), we show that this case is indeed uninhabitable as the surface temperature reaches 640 K and the planet is too hot for liquid water. Our companion paper, (Meadows et al. 2018), shows that the higher surface temperature results from greenhouse warming by CO_2 alone.

Even if the planet avoided desiccation during the pre-MS stage, it is reasonable to assume that a Venus-like atmosphere is still possible. CO_2 is a very abundant molecule in planetary atmospheres, and given its strong ability to heat the surface, high molecular weight, and strong chemical bonds, it may be able to accumulate in the atmospheres of planets in the HZ to large enough levels to trigger the runaway greenhouse.

A final possibility, mentioned above, is that past tidal heating drove the planet into a runaway greenhouse (Barnes et al. 2013). If the planet was ever in a high eccentricity state ($e > 0.35$) then the surface energy flux from the interior could have reached the critical limit of $\sim 300 \text{ W/m}^2$ (Kasting et al. 1993; Abe 1993; Goldblatt 2015). Such high surface fluxes may be short-lived if the heating can only come from the ocean (Driscoll & Barnes 2015).

5.1.6. *Mini-Neptune*

Proxima b may have formed with sufficient hydrogen that some has been retained despite all the high energy processes that can remove it. This possibility is especially likely if it formed beyond the snow line and migrated in. Similarly to Owen & Mohanty (2016), we find

that if Proxima b formed with $\gtrsim 1\%$ of its mass in the form of a hydrogen envelope (and/or is significantly more massive than $1.27M_{\oplus}$), it could still possess some hydrogen, in which case the surface may be too hot and/or the surface pressure is too high for habitability. If Proxima b has a mass much larger than the minimum, its surface gravity could retain H in spite of high XUV fluxes (Luger et al. 2015; Owen & Mohanty 2016; Lehmer & Catling 2017). Future measurements of Proxima b’s radius can inform its present-day composition and thus settle this issue. However, we also note that our model does not include several important processes, such as flaring and coronal mass ejections, that remove additional mass than our model. A proper assessment of the longevity of a hydrogen envelope requires a better understanding of Proxima’s activity since its birth, as well as sophisticated space weather models (Garraffo et al. 2016; Airapetian et al. 2017).

5.1.7. Abiotic Oxygen Atmosphere

If Proxima b formed with one or more TO of water, photolysis followed by hydrogen escape during the stellar pre-MS phase could have led to the buildup of substantial O_2 in the atmosphere. Although oxygen is highly reactive, thousands of bars of oxygen can be liberated through this mechanism (Luger & Barnes 2015) and hence all sinks for it may become saturated (Schaefer et al. 2016). In principle, thousands of bars of oxygen could remain in the atmosphere, but this figure is most likely lower, as much of the oxygen will be consumed in the process of oxidizing the surface. In this scenario, the planet may have an atmosphere dominated by oxygen molecules.

In many of the scenarios in which Proxima b develops an O_2 -rich atmosphere, it also retains at least some of its initial water. After the end of the Pre-MS phase, the H_2O and CO_2 greenhouse warming could be sufficient to prevent water from accumulating on the surface, and hence it could have significant abundance in the stratosphere. The residence time of water is therefore of crucial importance, and it may be short due to flaring, coronal mass ejections, and other forms of stellar activity, especially while the system is young. Thus, even though the planet may have had H_2O after the HZ arrived, water may have remained in the stratosphere and been photolyzed by high energy radiation and the H atoms lost to space, ultimately producing a dry planet. We do not model this possibility here, but such a scenario was found to be plausible in Ribas et al. (2016).

5.1.8. Water and Oxygen, but Uninhabitable?

The joint oxygen/water posterior in Figure 20 reveals an interesting possibility in which large amounts of oxygen are built up by the pre-MS runaway, but not all the water is lost. In this case Proxima b may be uninhabitable, given that little free energy may be available at the surface for early organisms to exploit. Life on Earth is thought to have emerged in an extremely reducing environment (Oparin 1924; Haldane 1929), with access to large energy gradients to fuel early metabolisms; such a reducing environment may not have ever been present on Proxima b. While the simultaneous detection of water and oxygen has traditionally been envisaged as an ideal combination for life detection (Des Marais et al. 2002;

Meadows 2017), in the case of Proxima b, it is insufficient to prove that life is present. More information will be necessary to confirm the presence of life on Proxima b (Meadows et al. 2018).

If the greenhouse gases are at low enough levels in the atmosphere, then it may be possible for liquid water to accumulate on the planetary surface and this planet would meet our definition of “habitable.” However, as argued above, such a planet would likely be incapable of abiogenesis. Thus, the detection of large amounts of atmospheric oxygen, e.g. through O_4 bands, as well as the presence of surface liquid by other means, e.g. glint (Robinson et al. 2010), would still not be sufficient evidence that the planet is habitable (Schwieterman et al. 2016; Meadows 2017; Meadows et al. 2018).

5.1.9. No Atmosphere and No Water

Since Proxima b is subjected to repeated flaring events and other activity (Walker 1981; Davenport et al. 2016), the atmosphere may be constantly or permanently destroyed. Such a process is difficult to envision, as it would require all the volatiles in the mantle to have been degassed and blown away. However, if the planet was tidally and/or radiogenically heated for a long time, mantle convection may have been vigorous enough to completely devolatilize the planet through outgassing. This possibility is most likely if the planet is of order 7 Gyr old and if the core has solidified, quenching the magnetic dynamo (Driscoll & Barnes 2015). Another possibility is that a recent stellar eruption has temporarily stripped away the atmosphere, which will later reform by outgassing.

5.1.10. Sub-surface Liquid Water Layer

A final possibility is that Proxima b, receiving only 65% of Earth’s insolation, may have an ice-covered surface, but with a liquid water mantle, similar to Europa. For such a planet, the water is heated by the energy from accretion, radiogenic sources and/or tidal heating. Water ice is much more absorptive at the longer wavelengths of light that Proxima emits and so it may be difficult to ice over the planet (Pierrehumbert 2011; Joshi & Haberle 2012; Shields et al. 2013; Checlair et al. 2017), especially since it probably spent hundreds of Myr in a runaway greenhouse. But if a reflective haze and/or cloud layer could form, it could reflect away the light before it reaches the surface (e.g. Arney 2016). This possibility is most likely if the planet is rotating super-synchronously, otherwise the “eyeball state” could develop (Pierrehumbert 2011).

Unlike the icy worlds in our Solar System, Proxima b has sufficient gravity that atmospheric molecules can remain bound to the planet, unless stellar activity removes them. If the subsurface layer is inhabited, then biomolecular gases may float to the ice layer and slowly find their way to the atmosphere. If they remain in the atmosphere for long periods of time, they could constitute a biosignature. If the planet has no atmosphere, then reflectance spectroscopy could reveal organic compounds on the surface, similar to those seen on Europa (e.g. Noll et al. 1995).

5.2. *Is Proxima b Habitable?*

Planetary habitability is a complicated feature to model quantitatively and Proxima b is no exception. We do know that the planet has sufficient energy to support life, almost assuredly has significant abundances of bioessential elements since they are some of the most common in the galaxy, and is old enough for life to have gained a foothold. The biggest questions are if it is terrestrial, if it possesses vast reservoirs of liquid water, and if it quickly formed a highly oxidized atmosphere. Without tighter constraints on the initial volatile inventory, it is impossible to determine the probability that it does support liquid water, so we cannot answer the eponymous question. As always, more data are needed.

However, our analysis does provide some important information on where to focus future efforts. As liquid water is vital, it is paramount to determine the pathways that allow the planet to have accreted and retained the water. Even if the planet forms with water, our investigations have shown that it will not necessarily be retained. If it formed *in situ* or arrived in the HZ at the time of the dispersal of the gas disk, then Proxima b had to endure ~ 170 Myr in a runaway greenhouse state; see § 4.4.

Even if the planet arrived in its orbit late, perhaps following an orbital instability, the water may have to survive a “tidal greenhouse” in which tidal heating drives water loss, see § 4.5 and Barnes et al. (2013). Such high tidal heating rates may require very large eccentricity and/or abnormally low Q values, but the former is certainly possible during planet-planet scattering events (Chatterjee et al. 2008), or perhaps by Kozai-like oscillation driven by perturbations from the α Cen A and B pair if the orbit of Proxima Centauri was much smaller in the past (Desidera & Barbieri 2007). If an additional planet in the system is massive, on an eccentric orbit, and/or on a highly inclined orbit, then it, too, may induce perturbations that maintain eccentricities (Takeda & Rasio 2005), possibly in the range of a tidal greenhouse. A planet in a Cassini state may receive additional tidal heating due to non-zero obliquity (Heller et al. 2011), further increasing the risk of a tidal greenhouse. As shown in § 4.5, the eccentricity of b will damp, but the timescale can be very long. Large eccentricities are not well-modeled by equilibrium tide theory, even with a proper accounting of geophysical features as in the THERMINT module, so it is difficult at present to assess the role of tidal heating in water retention.

Another possible route to water loss is through temporary or permanent atmosphere erosion by flares and coronal mass ejections. These events could blast away the atmosphere completely, in which case liquid water on the surface is not stable. Should the atmosphere reform, the water may return to the liquid state, but it is certainly plausible that some events are powerful enough to remove the water in one event, or, more likely, repeated bombardments would slowly remove the atmosphere (Cohen et al. 2015). Our analysis doesn’t provide a direct measurement of this phenomenon, but we note that if the dynamo is quenched, perhaps because the core has completely nucleated, charged particles can reach the surface. Even if the planet does have a magnetic field, Vidotto et al. (2013) find that planets around typical M dwarfs may have their magnetopause distances driven to

the planet surface by the star’s magnetic field. However, it is not clear that a magnetic field is always beneficial for life, as it also increases the cross-sectional area of the planet for charged particles and funnels the energy into the magnetic poles, possibly increasing mass loss.

These processes are all clear dangers for the habitability of Proxima b. Yet, we are also able to identify pathways that produce decidedly Earth-like versions of planet b. As shown in Fig. 25, if the planet formed with 0.1% of its mass in a hydrogen envelope, 3.5 Earth oceans of water, then the combined effects of the stellar evolution, envelope evolution and atmospheric escape, tidal evolution, orbital evolution, and geophysical evolution predict a planet with 1 Earth ocean of surface water, no hydrogen envelope, no abiotic oxygen build-up, and a semi-major axis within the observed uncertainties. If this scenario is true, then our model predicts Proxima b could be a true Earth analog today.

Proxima b may or may not be habitable. While we are only able to identify a narrow range of pathways that permit habitability, we must bear in mind that our model, while including phenomena over sizescales of meters to kpc, is simple and does not include many potential feedbacks. The geochemistry of exoplanets is a gaping hole in scientific knowledge, and one can easily imagine how other systems may maintain liquid water with geochemical cycles not present in our Solar System.

6. CONCLUSIONS

We have performed a detailed analysis of the evolution of the Alpha Centauri triple star system with a specific focus on Proxima Centauri b’s habitability. We find that many disparate factors are important, including the stellar system’s orbit in the galaxy (§ 4.1), the orbital and rotational evolution of the planets (§ 4.2), the stellar evolution (§ 4.3), the atmospheric evolution (§ 4.4), and the geophysical evolution (§ 4.5). We find that many evolutionary pathways are permitted by the data and hence the planet may currently exist in one of many possible states.

We conclude that Proxima b may be habitable, and identify the retention of water as the biggest obstacle for Proxima b to support life. Water loss may occur through multiple channels operating in tandem or in isolation, including desiccation during the Pre-MS, excessive tidal heating, or atmospheric destruction by flares and coronal mass ejections. We find the most likely pathway for habitability is if planet b formed with a thin hydrogen envelope of order 10^{-4} to $10^{-2} M_{\oplus}$ which was eroded by the early XUV evolution of the host star; see § 4.3 and Luger et al. (2015). In that case, Proxima b is a “habitable evaporated core” and has followed a very different trajectory than Earth did on their paths to liquid surface water. Our conclusions regarding water loss, tidal effects, and potential habitability are broadly consistent with the independent and simultaneous analysis in (Ribas et al. 2016).

Regardless of Proxima’s habitability, it offers scientists an unprecedented window into the nature of terrestrial planets. At only 1.3 pc distance, we will be able to study this planet in detail with future missions, should they be designed appropriately; see Meadows et al. (2018). If Proxima b is uninhabitable, we may be able to determine how that happened and how Earth avoided the same fate.

At a minimum, the discovery of Proxima Centauri b, as well as more recent discoveries such as the TRAPPIST-1 planets and LHS 1140 b (Gillon et al. 2017; Dittman et al. 2017), have ushered in a new era of comparative planetology and analyses such as this one can provide a foundation for interpreting observational data, such as in (Meadows et al. 2018).

The research described here shows that numerous possibilities exist for Proxima b's current state. These hypotheses can be tested with future telescopes and spacecraft, such as the TMT and LUVOIR. In the second paper in this series (Meadows et al. 2018), the general features of the atmospheres we predict are transformed into self-consistent atmospheric models and the observable features are computed. The generation of evolutionary pathways provides a foundation to interpret future observations, and the results of the second paper find that it is indeed possible to distinguish most of the planetary states we predict.

We thank G. Anglada-Escudé for sharing the results, and for leading the Pale Red Dot campaign. This work was supported by the NASA Astrobiology Institute's Virtual Planetary Laboratory under Cooperative Agreement number NNA13AA93A. David Fleming is supported by an NSF IGERT DGE-1258485 fellowship. This work was performed in part under contract with the California Institute of Technology (Caltech)/Jet Propulsion Laboratory (JPL) funded by NASA through the Sagan Fellowship Program executed by the NASA Exoplanet Science Institute. N.A. Kaib acknowledges support from HST-AR-13898. The results reported herein benefited from the authors affiliation with the NASA's Nexus for Exoplanet System Science (NExSS) research coordination network sponsored by NASA's Science Mission Directorate.

REFERENCES

- Abe, Y. 1993, *Lithos*, 30, 223
- Abe, Y., Abe-Ouchi, A., Sleep, N. H., & Zahnle, K. J. 2011, *Astrobiology*, 11, 443
- Aguilar, L. A. & White, S. D. M. 1985, *ApJ*, 295, 374
- Airapetian, V. S., Glocer, A., Khazanov, G. V., Loyd, R. O. P., France, K., Sojka, J., Danchi, W. C., & Liemohn, M. W. 2017, *ApJ*, 836, L3
- Aksnes, K. & Franklin, F. A. 2001, *AJ*, 122, 2734
- Alibert, Y. & Benz, W. 2017, *A&A*, 598, L5
- Allen, C. & Herrera, M. A. 1998, *Rev. Mexicana Astron. Astrofis.*, 34, 37
- Allende Prieto, C., Barklem, P. S., Lambert, D. L., & Cunha, K. 2004, *A&A*, 420, 183
- Anders, E. & Grevesse, N. 1989, *Geochim. Cosmochim. Acta*, 53, 197
- Anglada, G., Amado, P. J., Ortiz, J. L., Gómez, J. F., Macías, E., Alberdi, A., Osorio, M., Gómez, J. L., de Gregorio-Monsalvo, I., Pérez-Torres, M. A., Anglada-Escudé, G., Berdiñas, Z. M., Jenkins, J. S., Jimenez-Serra, I., Lara, L. M., López-González, M. J., López-Puertas, M., Morales, N., Ribas, I., Richards, A. M. S., Rodríguez-López, C., & Rodríguez, E. 2017, *ApJ*, 850, L6
- Anglada-Escudé, G., Amado, P. J., Barnes, J., Berdiñas, Z. M., Butler, R. P., Coleman, G. A. L., de La Cueva, I., Dreizler, S., Endl, M., Giesers, B., Jeffers, S. V., Jenkins, J. S., Jones, H. R. A., Kiraga, M., Kürster, M., López-González, M. J., Marvin, C. J., Morales, N., Morin, J., Nelson, R. P., Ortiz, J. L., Ofir, A., Paardekooper, S.-J., Reiners, A., Rodríguez, E., Rodríguez-López, C., Sarmiento, L. F., Strachan, J. P., Tsapras, Y., Tuomi, M., & Zechmeister, M. 2016, *Nature*, 536, 437
- Anosova, J., Orlov, V. V., & Pavlova, N. A. 1994, *A&A*, 292, 115
- Araki, T., Enomoto, S., Furuno, K., Gando, Y., Ichimura, K., Ikeda, H., Inoue, K., Kishimoto, Y., Koga, M., Koseki, Y., Maeda, T., Mitsui, T., Motoki, M., Nakajima, K., Ogawa, H., Ogawa, M., Owada, K., Ricol, J.-S., Shimizu, I., Shirai, J., Suekane, F., Suzuki, A., Tada, K., Takeuchi, S., Tamae, K., Tsuda, Y., Watanabe, H., Busenitz, J., Classen, T., Djurcic, Z., Keefer, G., Leonard, D., Piepke, A., Yakushev, E., Berger, B. E., Chan, Y. D., Decowski, M. P., Dwyer, D. A., Freedman, S. J., Fujikawa, B. K., Goldman, J., Gray, F., Heeger, K. M., Hsu, L., Lesko, K. T., Luk, K.-B., Murayama, H., O'Donnell, T., Poon, A. W. P., Steiner, H. M., Winslow, L. A., Mauger, C., McKeown, R. D., Vogel, P., Lane, C. E., Miletic, T., Guillian, G., Learned, J. G., Maricic, J., Matsuno, S., Pakvasa, S., Horton-Smith, G. A., Dazeley, S., Hatakeyama, S., Rojas, A., Svoboda, R., Dieterle, B. D., Detwiler, J., Gratta, G., Ishii, K., Tolich, N., Uchida, Y., Batygov, M., Bugg, W., Efrementko, Y., Kamyshev, Y., Kozlov, A., Nakamura, Y., Karwowski, H. J., Markoff, D. M., Nakamura, K., Rohm, R. M., Tornow, W., Wendell, R., Chen, M.-J., Wang, Y.-F., & Piquemal, F. 2005, *Nature*, 436, 499
- Arevalo, R., McDonough, W. F., & Luong, M. 2009, *Earth and Planetary Science Letters*, 278, 361
- Armstrong, J. C., Barnes, R., Domagal-Goldman, S., Breiner, J., Quinn, T. R., & Meadows, V. S. 2014, *Astrobiology*, 14, 277
- Arney, G. 2016, *AsBio*, accepted
- Atobe, K. & Ida, S. 2007, *Icarus*, 188, 1
- Atri, D. 2017, *MNRAS*, 465, L34
- Baraffe, I., Chabrier, G., Allard, F., & Hauschildt, P. H. 1998, *A&A*, 337, 403
- Baraffe, I., Homeier, D., Allard, F., & Chabrier, G. 2015, *A&A*, 577, A42
- Barnes, J. R., Jenkins, J. S., Jones, H. R. A., Jeffers, S. V., Rojo, P., Arriagada, P., Jordán, A., Minniti, D., Tuomi, M., Pinfield, D., & Anglada-Escudé, G. 2014, *MNRAS*, 439, 3094
- Barnes, R. 2017, *Celestial Mechanics and Dynamical Astronomy*, 129, 509
- Barnes, R., Greenberg, R., Quinn, T. R., McArthur, B. E., & Benedict, G. F. 2011, *ApJ*, 726, 71
- Barnes, R., Jackson, B., Raymond, S. N., West, A. A., & Greenberg, R. 2009, *ApJ*, 695, 1006
- Barnes, R., Mullins, K., Goldblatt, C., Meadows, V. S., Kasting, J. F., & Heller, R. 2013, *Astrobiology*, 13, 225
- Barnes, R., Raymond, S. N., Jackson, B., & Greenberg, R. 2008, *Astrobiology*, 8, 557
- Bazot, M., Christensen-Dalsgaard, J., Gizon, L., & Benomar, O. 2016, *MNRAS*, 460, 1254
- Benedict, G. F., McArthur, B., Nelan, E., Story, D., Whipple, A. L., Shelus, P. J., Jefferys, W. H., Hemenway, P. D., Franz, O. G., Wasserman, L. H., Duncombe, R. L., van Altena, W., & Fredrick, L. W. 1998, *AJ*, 116, 429
- Benedict, G. F., Nelan, E., McArthur, B., Story, D., van Altena, W., Ting-Gao, Y., Jefferys, W. H., Hemenway, P. D., Shelus, P. J., Whipple, A. L., Franz, O. G., Fredrick, L. W., & Duncombe, R. L. 1993, *PASP*, 105, 487
- Bixel, A. & Apai, D. 2017, *ApJ*, 836, L31
- Bolmont, E., Selsis, F., Owen, J. E., Ribas, I., Raymond, S. N., Leconte, J., & Gillon, M. 2017, *MNRAS*, 464, 3728
- Bonfils, X., Delfosse, X., Udry, S., Forveille, T., Mayor, M., Perrier, C., Bouchy, F., Gillon, M., Lovis, C., Pepe, F., Queloz, D., Santos, N. C., Ségransan, D., & Bertaux, J.-L. 2013, *A&A*, 549, A109
- Bouchy, F. & Carrier, F. 2001, *A&A*, 374, L5
- . 2002, *A&A*, 390, 205

- Boyajian, T. S., von Braun, K., van Belle, G., McAlister, H. A., ten Brummelaar, T. A., Kane, S. R., Muirhead, P. S., Jones, J., White, R., Schaefer, G., Ciardi, D., Henry, T., López-Morales, M., Ridgway, S., Gies, D., Jao, W.-C., Rojas-Ayala, B., Parks, J. R., Sturmann, L., Sturmann, J., Turner, N. H., Farrington, C., Goldfinger, P. J., & Berger, D. H. 2012, *ApJ*, 757, 112
- Brasser, R., Ida, S., & Kokubo, E. 2014, *MNRAS*, 440, 3685
- Breiter, S. & Vokrouhlický, D. 2015, *MNRAS*, 449, 1691
- Carrier, F. & Bourban, G. 2003, *A&A*, 406, L23
- Carter-Bond, J. C., O'Brien, D. P., & Raymond, S. N. 2012, *ApJ*, 760, 44
- Chaplin, W. J., Basu, S., Huber, D., Serenelli, A., Casagrande, L., Silva Aguirre, V., Ball, W. H., Creevey, O. L., Gizon, L., Handberg, R., Karoff, C., Lutz, R., Marques, J. P., Miglio, A., Stello, D., Suran, M. D., Pricopi, D., Metcalfe, T. S., Monteiro, M. J. P. F. G., Molenda-Žakowicz, J., Appourchaux, T., Christensen-Dalsgaard, J., Elsworth, Y., García, R. A., Houdek, G., Kjeldsen, H., Bonanno, A., Campante, T. L., Corsaro, E., Gaulme, P., Hekker, S., Mathur, S., Mosser, B., Régulo, C., & Salabert, D. 2014, *ApJS*, 210, 1
- Chatterjee, S., Ford, E. B., Matsumura, S., & Rasio, F. A. 2008, *ApJ*, 686, 580
- Checlair, J., Menou, K., & Abbot, D. S. 2017, *ApJ*, 845, 132
- Ciesla, F. J., Mulders, G. D., Pascucci, I., & Apai, D. 2015, *ApJ*, 804, 9
- Cincunegui, C., Díaz, R. F., & Mauas, P. J. D. 2007, *A&A*, 461, 1107
- Cohen, O., Drake, J. J., Glocer, A., Garraffo, C., Poppenhaeger, K., Bell, J. M., Ridley, A. J., & Gombosi, T. I. 2014, *ApJ*, 790, 57
- Cohen, O., Ma, Y., Drake, J. J., Glocer, A., Garraffo, C., Bell, J. M., & Gombosi, T. I. 2015, *ApJ*, 806, 41
- Coleman, G. A. L., Nelson, R. P., Paardekooper, S. J., Dreizler, S., Giesers, B., & Anglada-Escudé, G. 2017, *MNRAS*
- Colombo, G. 1966, *AJ*, 71, 891
- Correia, A. C. M., Levrard, B., & Laskar, J. 2008, *A&A*, 488, L63
- Damasso, M. & Del Sordo, F. 2017, *A&A*, 599, A126
- Darwin, G. H. 1880, Royal Society of London Philosophical Transactions Series I, 171, 713
- Davenport, J. R. A., Kipping, D. M., Sasselov, D., Matthews, J. M., & Cameron, C. 2016, *ApJ*, 829, L31
- Deitrick, R., Barnes, R., Quinn, T. R., Armstrong, J., Charnay, B., & Wilhelm, C. 2017, *ArXiv e-prints*
- Delfosse, X., Forveille, T., Ségransan, D., Beuzit, J.-L., Udry, S., Perrier, C., & Mayor, M. 2000, *A&A*, 364, 217
- Demory, B.-O., Ségransan, D., Forveille, T., Queloz, D., Beuzit, J.-L., Delfosse, X., di Folco, E., Kervella, P., Le Bouquin, J.-B., Perrier, C., Benisty, M., Duvert, G., Hofmann, K.-H., Lopez, B., & Petrov, R. 2009, *A&A*, 505, 205
- Des Marais, D. J., Harwit, M. O., Jucks, K. W., Kasting, J. F., Lin, D. N. C., Lunine, J. I., Schneider, J., Seager, S., Traub, W. A., & Wolf, N. J. 2002, *Astrobiology*, 2, 153
- Desidera, S. & Barbieri, M. 2007, *A&A*, 462, 345
- Dickey, J. O., Bender, P. L., Faller, J. E., Newhall, X. X., Ricklefs, R. L., Ries, J. G., Shelus, P. J., Veillet, C., Whipple, A. L., Wiant, J. R., Williams, J. G., & Yoder, C. F. 1994, *Science*, 265, 482
- Dittman, J., Irwin, J., Charbonneau, D., & Bonfils, X. 2017, *Nature*, 333
- Dole, S. H. 1964, Habitable planets for man
- Dotter, A., Chaboyer, B., Jevremović, D., Kostov, V., Baron, E., & Ferguson, J. W. 2008, *ApJS*, 178, 89
- Downes, J. J., Román-Zúñiga, C., Ballesteros-Paredes, J., Mateu, C., Briceno, C., Hernández, J., Petr-Gotzens, M. G., Calvet, N., Hartmann, L., & Maucó, K. 2015, *MNRAS*, 450, 3490
- Dressing, C. D. & Charbonneau, D. 2013, *ApJ*, 767, 95
- Driscoll, P. & Bercovici, D. 2014, *Physics of the Earth and Planetary Interiors*, 236, 36
- Driscoll, P. E. & Barnes, R. 2015, *Astrobiology*, 15, 739
- Dye, S. T. 2010, *Earth and Planetary Science Letters*, 297, 1
- Efroimsky, M. & Makarov, V. V. 2013, *ApJ*, 764, 26
- Endl, M. & Kürster, M. 2008, *A&A*, 488, 1149
- Erkaev, N. V., Kulikov, Y. N., Lammer, H., Selsis, F., Langmayr, D., Jaritz, G. F., & Biernat, H. K. 2007, *A&A*, 472, 329
- Ferraz-Mello, S., Rodríguez, A., & Hussmann, H. 2008, *Celestial Mechanics and Dynamical Astronomy*, 101, 171
- Ford, E. B., Kozinsky, B., & Rasio, F. A. 2000, *ApJ*, 535, 385
- Foreman-Mackey, D., Hogg, D. W., Lang, D., & Goodman, J. 2013, *PASP*, 125, 306
- García-Sánchez, J., Weissman, P. R., Preston, R. A., Jones, D. L., Lestrade, J.-F., Latham, D. W., Stefanik, R. P., & Paredes, J. M. 2001, *A&A*, 379, 634
- Garraffo, C., Drake, J. J., & Cohen, O. 2016, *ApJ*, 833, L4
- Gillon, M., Triaud, A. H. M. J., Demory, B.-O., Jehin, E., Agol, E., Deck, K. M., Lederer, S. M., de Wit, J., Burdanov, A., Ingalls, J. G., Bolmont, E., Leconte, J., Raymond, S. N., Selsis, F., Turbet, M., Barkaoui, K., Burgasser, A., Burleigh, M. R., Carey, S. J., Chaushev, A., Copperwheat, C. M., Delrez, L., Fernandes, C. S., Holdsworth, D. L., Kotze, E. J., Van Grootel, V., Almléay, Y., Benkhaldoun, Z., Magain, P., & Queloz, D. 2017, *Nature*, 542, 456
- Goldblatt, C. 2015, *Astrobiology*, 15, 362
- Goldreich, P. 1966, *AJ*, 71, 1
- Gomes, R., Levison, H. F., Tsiganis, K., & Morbidelli, A. 2005, *Nature*, 435, 466
- Greenberg, R. 2009, *Astrophys. J.*, 698, L42
- Haldane, J. B. S. 1929, *The Rationalist Annal.*, 3
- Hamilton, D. P. & Ward, W. R. 2004, *AJ*, 128, 2510
- Harrington, R. S. 1968, *AJ*, 73, 190
- Hayden, M. R., Bovy, J., Holtzman, J. A., Nidever, D. L., Bird, J. C., Weinberg, D. H., Andrews, B. H., Majewski, S. R., Allende Prieto, C., Anders, F., Beers, T. C., Bizyaev, D., Chiappini, C., Cunha, K., Frinchaboy, P., García-Hernández, D. A., García Pérez, A. E., Girardi, L., Harding, P., Hearty, F. R., Johnson, J. A., Mészáros, S., Minchev, I., O'Connell, R., Pan, K., Robin, A. C., Schiavon, R. P., Schneider, D. P., Schultheis, M., Shetrone, M., Skrutskie, M., Steinmetz, M., Smith, V., Wilson, J. C., Zamora, O., & Zasowski, G. 2015, *ApJ*, 808, 132
- Heisler, J. & Tremaine, S. 1986, *Icarus*, 65, 13
- Heisler, J., Tremaine, S., & Alcock, C. 1987, *Icarus*, 70, 269
- Heller, R., Jackson, B., Barnes, R., Greenberg, R., & Homeier, D. 2010, *A&A*, 514, A22
- Heller, R., Leconte, J., & Barnes, R. 2011, *Astro. & Astrophys.*, 528, A27+
- Henning, W. G., O'Connell, R. J., & Sasselov, D. D. 2009, *Astrophys. J.*, 707, 1000
- Hernández, J., Hartmann, L., Megeath, T., Gutermuth, R., Muzerolle, J., Calvet, N., Vivas, A. K., Briceno, C., Allen, L., Stauffer, J., Young, E., & Fazio, G. 2007, *ApJ*, 662, 1067
- Hevey, P. J. & Sanders, I. S. 2006, *Meteoritics & Planetary Science*, 41, 95
- Hinkel, N. R. & Kane, S. R. 2013, *MNRAS*, 432, 36
- Holmberg, J. & Flynn, C. 2000, *MNRAS*, 313, 209
- Huang, Y., Chubakov, V., Mantovani, F., Rudnick, R. L., & McDonough, W. F. 2013, *Geochemistry, Geophysics, Geosystems*, 14, 2003
- Hunten, D. M. 1973, *Journal of Atmospheric Sciences*, 30, 1481
- Hunten, D. M., Pepin, R. O., & Walker, J. C. G. 1987, *Icarus*, 69, 532
- Ida, S. & Lin, D. N. C. 2005, *ApJ*, 626, 1045
- Innes, R. T. A. 1915, *Circular of the Union Observatory Johannesburg*, 30, 235
- Jackson, A. P., Davis, T. A., & Wheatley, P. J. 2012, *MNRAS*, 422, 2024
- Jackson, B., Barnes, R., & Greenberg, R. 2008a, *MNRAS*, 391, 237
- . 2009, *Astrophys. J.*, 698, 1357
- Jackson, B., Greenberg, R., & Barnes, R. 2008b, *Astrophys. J.*, 678, 1396
- Jaupart, C., Labrosse, S., Lucazaeu, F., & Mareschal, J. C. Temperatures, Heat and Energy in the Mantle of the Earth, 2nd edn., 253–305
- Johnson, J. A. & Apps, K. 2009, *ApJ*, 699, 933
- Joshi, M. M. & Haberle, R. M. 2012, *Astrobiology*, 12, 3
- Joshi, M. M., Haberle, R. M., & Reynolds, R. T. 1997, *Icarus*, 129, 450
- Kaib, N. A., Raymond, S. N., & Duncan, M. 2013, *Nature*, 493, 381
- Kasting, J. F. 1988, *Icarus*, 74, 472
- Kasting, J. F., Whitmire, D. P., & Reynolds, R. T. 1993, *Icarus*, 101, 108
- Kervella, P., Thévenin, F., & Lovis, C. 2017, *A&A*, 598, L7

- Kinoshita, H. 1975, *SAO Special Report*, 364
 —. 1977, *Celestial Mechanics*, 15, 277
- Kipping, D. M., Cameron, C., Hartman, J. D., Davenport, J. R. A., Matthews, J. M., Sasselov, D., Rowe, J., Siverd, R. J., Chen, J., Sandford, E., Bakos, G. Á., Jordán, A., Bayliss, D., Henning, T., Mancini, L., Penev, K., Csubry, Z., Bhatti, W., Da Silva Bento, J., Guenther, D. B., Kuschnig, R., Moffat, A. F. J., Rucinski, S. M., & Weiss, W. W. 2017, *AJ*, 153, 93
- Kopparapu, R. K., Ramirez, R., Kasting, J. F., Eymet, V., Robinson, T. D., Mahadevan, S., Terrien, R. C., Domagal-Goldman, S., Meadows, V., & Deshpande, R. 2013, *ApJ*, 765, 131
- Kopparapu, R. K., Ramirez, R. M., SchottelKotte, J., Kasting, J. F., Domagal-Goldman, S., & Eymet, V. 2014, *ApJ*, 787, L29
- Kopparapu, R. k., Wolf, E. T., Haqq-Misra, J., Yang, J., Kasting, J. F., Meadows, V., Terrien, R., & Mahadevan, S. 2016, *ApJ*, 819, 84
- Kordopatis, G., Binney, J., Gilmore, G., Wyse, R. F. G., Belokurov, V., McMillan, P. J., Hatfield, P., Grebel, E. K., Steinmetz, M., Navarro, J. F., Seabroke, G., Minchev, I., Chiappini, C., Bienaymé, O., Bland-Hawthorn, J., Freeman, K. C., Gibson, B. K., Helmi, A., Munari, U., Parker, Q., Reid, W. A., Siebert, A., Siviero, A., & Zwitter, T. 2015, *MNRAS*, 447, 3526
- Korenaga, J. 2003, *Geophys. Res. Lett.*, 30, 20
- Kreidberg, L. & Loeb, A. 2016, *ApJ*, 832, L12
- Laird, J. B. 1985, *ApJ*, 289, 556
- Lammer, H., Erkaev, N. V., Odert, P., Kislyakova, K. G., Leitzinger, M., & Khodachenko, M. L. 2013, *MNRAS*, 430, 1247
- Laskar, J. 1986, *A&A*, 157, 59
- Laskar, J., Joutel, F., & Boudin, F. 1993a, *A&A*, 270, 522
- Laskar, J., Joutel, F., & Robutel, P. 1993b, *Nature*, 361, 615
- Lehmer, O. R. & Catling, D. C. 2017, *ApJ*, 845, 130
- Li, Y., Stefansson, G., Robertson, P., Monson, A., Caas, C., & Mahadevan, S. 2017, *Research Notes of the AAS*, 1, 49
- Lissauer, J. J. 2007, *ApJ*, 660, L149
- Liu, H.-G., Jiang, P., Huang, X., Yu, Z.-Y., Yang, M., Jia, M., Awiphan, S., Pan, X., Liu, B., Zhang, H., Wang, J., Li, Z., Du, F., Li, X., Lu, H., Zhang, Z., Tian, Q.-G., Li, B., Ji, T., Zhang, S., Shi, X., Wang, J., Zhou, J.-L., & Zhou, H. 2018, *The Astronomical Journal*, 155, 12
- Loebman, S. R., Debattista, V. P., Nidever, D. L., Hayden, M. R., Holtzman, J. A., Clarke, A. J., Roškar, R., & Valluri, M. 2016, *ApJ*, 818, L6
- Lopez, E. D. & Fortney, J. J. 2014, *ApJ*, 792, 1
- Lopez, E. D., Fortney, J. J., & Miller, N. 2012, *ApJ*, 761, 59
- Lovelock, J. E. 1965, *Nature*, 207, 568
- Lovis, C., Snellen, I., Mouillet, D., Pepe, F., Wildi, F., Astudillo-Defru, N., Beuzit, J.-L., Bonfils, X., Cheetham, A., Conod, U., Delfosse, X., Ehrenreich, D., Figueira, P., Forveille, T., Martins, J. H. C., Quanz, S. P., Santos, N. C., Schmid, H.-M., Ségransan, D., & Udry, S. 2017, *A&A*, 599, A16
- Luger, R. & Barnes, R. 2015, *Astrobiology*, 15, 119
- Luger, R., Barnes, R., Lopez, E., Fortney, J., Jackson, B., & Meadows, V. 2015, *Astrobiology*, 15, 57
- Luger, R., Lustig-Yaeger, J., Fleming, D. P., Tilley, M. A., Agol, E., Meadows, V. S., Deitrick, R., & Barnes, R. 2017, *ApJ*, 837, 63
- Luhman, K. L. 2012, *ARA&A*, 50, 65
- Lundkvist, M., Kjeldsen, H., & Silva Aguirre, V. 2014, *A&A*, 566, A82
- Lurie, J. C., Henry, T. J., Jao, W.-C., Quinn, S. N., Winters, J. G., Ianna, P. A., Koerner, D. W., Riedel, A. R., & Subasavage, J. P. 2014, *AJ*, 148, 91
- MacDonald, G. J. F. 1964, *Reviews of Geophysics and Space Physics*, 2, 467
- Makarov, V. V., Frouard, J., & Dorland, B. 2016, *MNRAS*, 456, 665
- Malmberg, D., de Angeli, F., Davies, M. B., Church, R. P., Mackey, D., & Wilkinson, M. I. 2007, *MNRAS*, 378, 1207
- Matthews, R. & Gilmore, G. 1993, *MNRAS*, 261, L5
- Matvienko, A. S. & Orlov, V. V. 2014, *Astrophysical Bulletin*, 69, 205
- Meadows, V. S. 2017, *Astrobiology*, 17, 1022
- Meadows, V. S., Arney, G. N., Schwieterman, E. W., Lustig-Yaeger, J., Lincowski, A. P., Robinson, T., Domagal-Goldman, S. D., Deitrick, R., Barnes, R. K., Fleming, D. P., Luger, R., Driscoll, P., Quinn, T., & Crisp, D. 2018, *Astrobiology*, 18, 133
- Mesa, D., Zurlo, A., Milli, J., Gratton, R., Desidera, S., Langlois, M., Vigan, A., Bonavita, M., Antichi, J., Avenhaus, H., Baruffolo, A., Biller, B., Boccaletti, A., Bruno, P., Cascone, E., Chauvin, G., Claudi, R. U., De Caprio, V., Fantinel, D., Farisato, G., Girard, J., Giro, E., Hagelberg, J., Incorvaia, S., Janson, M., Kral, Q., Lagadec, E., Lagrange, A.-M., Lessio, L., Meyer, M., Peretti, S., Perrot, C., Salasnich, B., Schlieder, J., Schmid, H.-M., Scuderi, S., Sissa, E., Thalmann, C., & Turatto, M. 2017, *MNRAS*, 466, L118
- Minchev, I., Famaey, B., Quillen, A. C., Dehnen, W., Martig, M., & Siebert, A. 2012, *A&A*, 548, A127
- Misra, A., Krissansen-Totton, J., Koehler, M. C., & Sholes, S. 2015, *Astrobiology*, 15, 462
- Mulders, G. D., Ciesla, F. J., Min, M., & Pascucci, I. 2015, *ApJ*, 807, 9
- Mumford, N. W. 1909, *Popular Astronomy*, 17, 497
- Murray, C. D. & Dermott, S. F. 1999, *Solar system dynamics*
- Murray-Clay, R. A., Chiang, E. I., & Murray, N. 2009, *ApJ*, 693, 23
- Neuforge-Verheecke, C. & Magain, P. 1997, *A&A*, 328, 261
- Noll, K. S., Weaver, H. A., & Gonnella, A. M. 1995, *J. Geophys. Res.*, 100, 19057
- Oparin, A. 1924, *The Origin of Life (Moscow)*, tr. in J. D. Bernal, *The Origin of Life*, Cleveland: World, 1967
- Owen, J. E. & Mohanty, S. 2016, *MNRAS*, 459, 4088
- Owen, J. E. & Wu, Y. 2013, *ArXiv e-prints*
- . 2017, *ApJ*, 847, 29
- Peale, S. J., Cassen, P., & Reynolds, R. T. 1979, *Science*, 203, 892
- Pierrehumbert, R. & Gaidos, E. 2011, *ApJ*, 734, L13
- Pierrehumbert, R. T. 2011, *ApJ*, 726, L8
- Pourbaix, D. & Boffin, H. M. J. 2016, *A&A*, 586, A90
- Pourbaix, D., Nidever, D., McCarthy, C., Butler, R. P., Tinney, C. G., Marcy, G. W., Jones, H. R. A., Penny, A. J., Carter, B. D., Bouchy, F., Pepe, F., Hearnshaw, J. B., Skuljan, J., Ramm, D., & Kent, D. 2002, *A&A*, 386, 280
- Poveda, A., Allen, C., Herrera, M. A., Cordero, G., & Lavalley, C. 1996, *A&A*, 308, 55
- Raghavan, R. S., Schoenert, S., Enomoto, S., Shirai, J., Suekane, F., & Suzuki, A. 1998, *Physical Review Letters*, 80, 635
- Rauch, K. P. & Hamilton, D. P. 2002, in *Bulletin of the American Astronomical Society*, Vol. 34, AAS/Division of Dynamical Astronomy Meeting #33, 938
- Raymond, S. N., Barnes, R., & Mandell, A. M. 2008, *MNRAS*, 384, 663
- Raymond, S. N., Quinn, T., & Lunine, J. I. 2004, *Icarus*, 168, 1
- Raymond, S. N., Scalo, J., & Meadows, V. S. 2007, *ApJ*, 669, 606
- Reid, I. N., Gizis, J. E., & Hawley, S. L. 2002, *AJ*, 124, 2721
- Reiners, A. & Basri, G. 2008, *A&A*, 489, L45
- Remy, F. & Mignard, F. 1985, *Icarus*, 63, 1
- Ribas, I., Bolmont, E., Selsis, F., Reiners, A., Leconte, J., Raymond, S. N., Engle, S. G., Guinan, E. F., Morin, J., Turbet, M., Forget, F., & Anglada-Escudé, G. 2016, *A&A*, 596, A111
- Ribas, I., Guinan, E. F., Güdel, M., & Audard, M. 2005, *Astrophys. J.*, 622, 680
- Rickman, H., Fouchard, M., Froeschlé, C., & Valsecchi, G. B. 2008, *Celestial Mechanics and Dynamical Astronomy*, 102, 111
- Rickman, H., Fouchard, M., Valsecchi, G. B., & Froeschlé, C. 2005, *Earth Moon and Planets*, 97, 411
- Robinson, T. D., Meadows, V. S., & Crisp, D. 2010, *ApJ*, 721, L67
- Rodríguez, A., Callegari, N., Michtchenko, T. A., & Hussmann, H. 2012, *MNRAS*, 427, 2239
- Rogers, L. A. 2015, *ApJ*, 801, 41
- Roskar, R. 2010, PhD thesis, University of Washington
- Roškar, R., Debattista, V. P., Quinn, T. R., & Wadsley, J. 2012, *MNRAS*, 426, 2089
- Sahu, K. C., Bond, H. E., Anderson, J., & Dominik, M. 2014, *ApJ*, 782, 89
- Schaefer, L., Wordsworth, R. D., Berta-Thompson, Z., & Sasselov, D. 2016, *ApJ*, 829, 63
- Schwieterman, E. W., Meadows, V. S., Domagal-Goldman, S. D., Deming, D., Arney, G. N., Luger, R., Harman, C. E., Misra, A., & Barnes, R. 2016, *ApJ*, 819, L13

- Ségransan, D., Kervella, P., Forveille, T., & Queloz, D. 2003, *A&A*, 397, L5
- Sellwood, J. A. & Binney, J. J. 2002, *MNRAS*, 336, 785
- Selsis, F., Kasting, J. F., Levrard, B., Paillet, J., Ribas, I., & Delfosse, X. 2007, *Astro. & Astrophys.*, 476, 1373
- Shapley, H. 1951, *Proceedings of the National Academy of Science*, 37, 15
- Shields, A. L., Barnes, R., Agol, E., Charnay, B., Bitz, C., & Meadows, V. S. 2016, *Astrobiology*, 16, 443
- Shields, A. L., Meadows, V. S., Bitz, C. M., Pierrehumbert, R. T., Joshi, M. M., & Robinson, T. D. 2013, *Astrobiology*, 13, 715
- Shkolnik, E. L. & Barman, T. S. 2014, *AJ*, 148, 64
- Sotin, C., Grasset, O., & Mocquet, A. 2007, *Icarus*, 191, 337
- Spada, F., Demarque, P., Kim, Y.-C., & Sills, A. 2013, *ApJ*, 776, 87
- Storch, N. I. & Lai, D. 2014, *MNRAS*, 438, 1526
- Strangeway, R. J., Russell, C. T., & Luhmann, J. G. 2010, in *European Planetary Science Congress 2010*, 334
- Takeda, G. & Rasio, F. A. 2005, *ApJ*, 627, 1001
- Thévenin, F., Provost, J., Morel, P., Berthomieu, G., Bouchy, F., & Carrier, F. 2002, *A&A*, 392, L9
- Thoul, A., Scudlaire, R., Noels, A., Vatoz, B., Briquet, M., Dupret, M.-A., & Montalbán, J. 2003, *A&A*, 402, 293
- Tian, F. 2015, *Earth and Planetary Science Letters*, 432, 126
- Touma, J. & Wisdom, J. 1994, *AJ*, 108, 1943
- Turbet, M., Leconte, J., Selsis, F., Bolmont, E., Forget, F., Ribas, I., Raymond, S. N., & Anglada-Escudé, G. 2016, *A&A*, 596, A112
- Veeder, G. J., Matson, D. L., Johnson, T. V., Blaney, D. L., & Goguen, J. D. 1994, *J. Geophys. Res.*, 99, 17095
- Vidotto, A. A., Jardine, M., Morin, J., Donati, J.-F., Lang, P., & Russell, A. J. B. 2013, *A&A*, 557, A67
- Volk, K. & Gladman, B. 2015, *ApJ*, 806, L26
- Voûte, J. 1917, *MNRAS*, 77, 650
- Walker, A. R. 1981, *MNRAS*, 195, 1029
- Wargelin, B. J., Saar, S. H., Pojmański, G., Drake, J. J., & Kashyap, V. L. 2017, *MNRAS*, 464, 3281
- Watson, A. J., Donahue, T. M., & Walker, J. C. G. 1981, *Icarus*, 48, 150
- Weiss, L. M. & Marcy, G. W. 2014, *ApJ*, 783, L6
- Wertheimer, J. G. & Laughlin, G. 2006, *AJ*, 132, 1995
- West, A. A., Hawley, S. L., Bochanski, J. J., Covey, K. R., Reid, I. N., Dhital, S., Hilton, E. J., & Masuda, M. 2008, *AJ*, 135, 785
- Williams, J. G., Sinclair, W. S., & Yoder, C. F. 1978, *Geophys. Res. Lett.*, 5, 943
- Williams, J. P. & Cieza, L. A. 2011, *ARA&A*, 49, 67
- Willson, R. C., Gulkis, S., Janssen, M., Hudson, H. S., & Chapman, G. A. 1981, *Science*, 211, 700
- Wood, B. E., Linsky, J. L., Müller, H.-R., & Zank, G. P. 2001, *ApJ*, 547, L49
- Wordsworth, R. D., Forget, F., Selsis, F., Millour, E., Charnay, B., & Madeleine, J.-B. 2011, *ApJ*, 733, L48
- Yadav, R. K., Christensen, U. R., Wolk, S. J., & Poppenhaeger, K. 2016, *ApJ*, 833, L28
- Yang, J., Cowan, N. B., & Abbot, D. S. 2013, *ApJ*, 771, L45
- Yang, J., Liu, Y., Hu, Y., & Abbot, D. S. 2014, *ApJ*, 796, L22
- Yoder, C. F. 1995, in *Global Earth Physics: A Handbook of Physical Constants*, ed. T. J. Ahrens, 1–31
- Young, P. A., Desch, S. J., Anbar, A. D., Barnes, R., Hinkel, N. R., Kopparapu, R., Madhusudhan, N., Monga, N., Pagano, M. D., Riner, M. A., Scannapieco, E., Shim, S.-H., & Truitt, A. 2014, *Astrobiology*, 14, 603
- Zanazzi, J. J. & Lai, D. 2017, *ArXiv e-prints*
- Zhang, K. & Hamilton, D. P. 2008, *Icarus*, 193, 267